Selenium Redox Cycling;

Isolation and Characterization of a Stimulatory Component from Tissue of Loblolly Pine for Multiplication of Somatic Embryos;

Development of an Assay to Measure L-Phenylalanine Concentration in Blood Plasma

A Thesis
Presented to
The Academic Faculty

By

Veronica DeSilva

In Partial Fulfillment
of the Requirements for the Degree
Doctor of Philosophy in Chemistry

Georgia Institute of Technology

August 2007

Selenium Redox Cycling;

Isolation and Characterization of a Stimulatory Component from Tissue of Loblolly Pine for Multiplication of Somatic Embryos;

Development of an Assay to Measure L-Phenylalanine Concentration in Blood Plasma

Approved

Professor, Sheldon W May, Advisor
(School of Chemistry and Biochemistry)
Georgia Institute of Technology

Professor, James C Powers
(School of Chemistry and Biochemistry)
Georgia Institute of Technology

Professor, Stanley H Pollock
(Pharmaceutical Sciences)
Mercer University

Professor, Nicholas V Hud
(School of Chemistry and Biochemistry)
Georgia Institute of Technology

Professor, Gerald S Pullman
(School of Biology)
Georgia Institute of Technology and
Institute of Paper Science and Technology

Date Approved: July 3, 2007

ACKNOWLEDGEMENTS

I would like to thank the following colleagues: Dr. Sheldon W May and Dr Charlie D. Oldham for their technical assistance, financial support and guidance in design and conduction of experiments; Dr. Gerald S Pullman, Anna Skryabina, Kellie M Chace and the rest of the IPST team (Dregar J, Duncan S, Grabowski J, Gupta R, Halpin J, Howie R, Johns B, Olsen K, Williams LD, Umejiego C and Yang F) for sharing their vast knowledge and expertise in the area of Loblolly Pine somatic embryogenesis; Dr. Richard A Jackson, Dr. Stanley H Pollock, Dr. Rani Singh, Dr. Chunli Yu and Mary J Kennedy for organizing the phenylketonuria metabolic camp and their assistance with statistical analysis of the data collected from the participants of the camp. In addition, I would like to gratefully acknowledge the help of Dr. Gang Bao, Dr. Nicholas V Hud, Andrew Tsourkas and Victoria Mariani in the Molecular Beacon project. I am grateful for the equipment and expertise provided by Dr. Richard F Browner, Dr. Jiri Janata, Dr. Andrew L Lyon, Dr. Laren M Tolbert, Michael Serpe, Luke Roberson and Andy McFadden in the area of portable spectroscopic devices and film – making. I would like to thank Dr. Henry M Neumann, Dr. Michael Furman and Maggie Schwabb for their assistance with creating the MatLab simulation.

I would also like to acknowledge the help of the laboratory staff at Georgia Institute of Technology, in particular that of Nadia Boguslavsky, David Bostiwick, Leslie T Gelbaum, Cameron M Sullards and Steve Woodard. Last but not least I would like to thank the past and present members of the May laboratory for frequently doing their job well: Kristi L Burns, Christina Ellis, Michael S Foster, Michelle M Gill-Woznichak, Paul Hagerdon, Miriam Hojjat, Jennifer D Lane-Overcast, Karin Wikman and Di Wu.

TABLE OF CONTENTS

LIST OF TABLES

LIST OF FIGURES AND SCHEMES

ABBREVIATIONS

AA = Amino Acid

ABA = abscisic acid

AMR = analytical measurement range

APS = ammonium persulfate

Asc = Ascorbate

$AscH^{\cdot}$ = Semi-dehydroascorbate

$AscH_2$ = Reduced ascorbate

BAP = 6-benzylaminopurine

BH_4 = (6R,1R’,2S’)-6-(1’,2’-dihydroxypropyl)-5,6,7,8-tetrahydrobiopterin

CA = cellulose acetate

ClPAESe = 4-chloro phenyl-2-aminoethyl selenide

ClPAESeO = 4-chloro phenyl-2-aminoethyl selenoxide

CNS = central nervous system

Cys = L-cysteine

DABCYL = dimethylaminophenylazobenzoic acid

DβM = dopamine β - monooxygenase

DBS = dried blood spot

DE = diatomaceous earth

DI = deionized

DTPA = diethylenetriamine pentaacetic acid

ECA = enzymatic – colorimetric assay

EDTA = ethylene diamine tetraacetic acid

ESI LC/MS = electron spray ionization liquid chromatography / mass spectrometry

FAB = fast atom bombardment

FG = female gametophyte, megagametophyte

FPAESe = 4-fluoro-phenyl-2-aminoethyl selenide

FPAESeO = 4-fluoro-phenyl-2-aminoethyl selenoxide

FRET = fluorescence resonance energy transfer

FRL = filtering / reflecting layer

FU = fluorescence units

GPx = glutathione peroxidase

GSH = reduced glutathione (γ-L-glutamyl-L-cysteinyl glycine)

GSSG = oxidized glutathione (diglutathione)

H_2O_2 = hydrogen peroxide

HPA = hyperphenylalaninemia

HPLC = high performance liquid chromatography

INT = 2-[4-iodophenyl]-3-[4-nitrophenyl]-5-phenyl-2H-tetrazolium

LP = loblolly pine

L-Phe = L-phenylalanine

L-Trp = L-tryptophan

L-Tyr = L-tyrosine

MB = molecular beacon

MES = N-morpholinoethanesulfonic acid

Met = (D,L) - methionine

MPMS = 1-methoxy-5-methylphenazine methosulfate

MS/MS = tandem mass spectrometry

MTS = 3-(4,5-dimethylthiazol-2-yl)-5-(3-carboxymethoxyphenyl)-2-(4-sulfophenyl)-2H-tetrazolium, inner salt

MTT = 3-[4,5-dimethyl-thiazol-2-yl]-2,5-diphenyl tetrazolium

^{1}H NMR = proton nuclear magnetic resonance

NOS = nitric oxide synthase

$ONOO^-$ / ONOOH / $ONOOH^*$ = oxoperoxynitrate species

PIIxiSG = Protean II xi single - gel

PAA = plasma amino acid analysis

PAD = L-phenylalanine dehydrogenase

PAESe = phenyl-2-aminoethyl selenide

PAESeO = phenyl-2-aminoethyl selenoxide

PAGE = polyacrylamide gel electrophoresis

PAH = L-phenylalanine hydroxylase

PCA = perchloric acid

PCR = polymerase chain reaction

pH 8.6 buffer = 5.4 mM potassium phosphate - 43 mM triethanolamine buffer

PKU = phenylketonuria

PMS = 5-methylphenazinium methyl sulfate

*RM*4 = *Rhodococcus sp.* strain M4

PN = reactive oxoperoxynitrate species

PNS = peripheral nervous system

PRP = platelet rich plasma

SE = somatic embryogenesis

SeCys = L-selenocysteine

SeMet = (D,L) - selenomethionine

(S)-HOMePEASe = (S)-hydroxy-α-methyl-phenyl-2-aminoethyl selenide

(S)-HOMePEASeO = (S)-hydroxy-α-methyl-phenyl-2-aminoethyl selenoxide

SHR = spontaneously hypertensive rats

SL = spreading layer

SME = somatic embryo

SOD = superoxide dismutase

SSP = silver staining protocol

SU = *Sporosarcina ureae*

TBE = Tris borate buffer

TCA = trichloroacetic acid

TEMED = 1,2-Bis(dimethylamino)ethane

TFA = trifluoroacetic acid

TOF = time of flight

ThR = thioredoxin

ThRx = thioredoxin reductase

Tris = tris(hydroxymethyl)amino methane

CHAPTER 1: Selenium redox cycling

1 – 1: SUMMARY

The biological role of selenium is a subject of intense current interest, and the activity of selenoenzymes is now known to be dependent upon redox cycling of selenium within their active sites. Exogenously supplied or metabolically generated organoselenium compounds, capable of propagating a selenium redox cycle, might therefore supplement natural cellular defenses against the oxidizing agents generated during biological activity. Phenylaminoalkyl selenides and sulfides were developed in our laboratory as novel substrate analogs for the enzyme dopamine β-monooxygenase. These selenides were shown to exhibit potent, dose-dependent antihypertensive activity in spontaneously hypertensive rats (SHR). Recently, phenylaminoalkyl selenides were found to protect plasmid DNA and Molecular beacons from oxoperoxynitrate – mediated damage by scavenging this powerful cellular oxidant and forming their respective selenoxides as the sole selenium-containing products. Rate constants were determined for the reactions of the selenoxides with cellular reductants such as GSH at physiological pH at 25^{o}C. The kinetic data obtained in current and previous research was subsequently used in a MatLab simulation, which showed the feasibility of selenium redox cycling by GSH in the presence of a cellular oxidant, oxoperoxynitrate.

1 – 2: INTRODUCTION

Dopamine β-Monooxygenase and Substrates:

The various catecholamines – dopamine, norepinephrine, and epinephrine – are sequentially synthesized from L-tyrosine (L-Tyr). Dopamine β-monooxygenase (DβM, 1.14.17.1) is a key enzyme in catecholamine metabolism, which stereoselectively catalyzes the ascorbate-dependent hydroxylation of dopamine to R-norepinephrine (1).

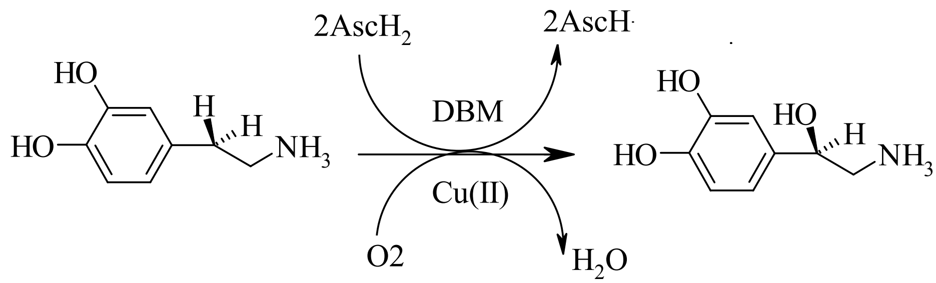

DβM is found in chromaffin vesicles of the adrenal medulla and the sympathetic nerve vesicles of the central and the peripheral nervous systems, CNS and PNS (2, 3, 4). The enzyme exists in both soluble and membrane-bound forms (2). DβM is an ideal target for varying the peripheral adrenergic activity, because inhibition of DβM lowers the available stores of norepinephrine, which in turn diminishes the extent of adrenergic stimulation (4). Phenylaminoalkyl sulfides and selenides were synthesized in our laboratory and were shown to be DβM substrates.

Experimental evidence showed that under standard *in vitro* conditions DβM efficiently catalyzes the ascorbate-dependent oxidation of phenylaminoalkyl sulfides or selenides to the corresponding sulfoxides or selenoxides (5, 6, 7). Biochemical studies revealed that the recycling of the selenoxide product back to the selenide was accomplished at the expense of reduced ascorbate, which formed dehydroascorbate (Asc), a 'dead end' metabolite and therefore lead to the inactivation of the normal ascorbate-dependent DβM activity (5, 6). The equivalent recycling pathway for the sulfoxide product was not observed due to the less easily reducible nature of the sulfoxide moiety when compared to that of the selenoxide.

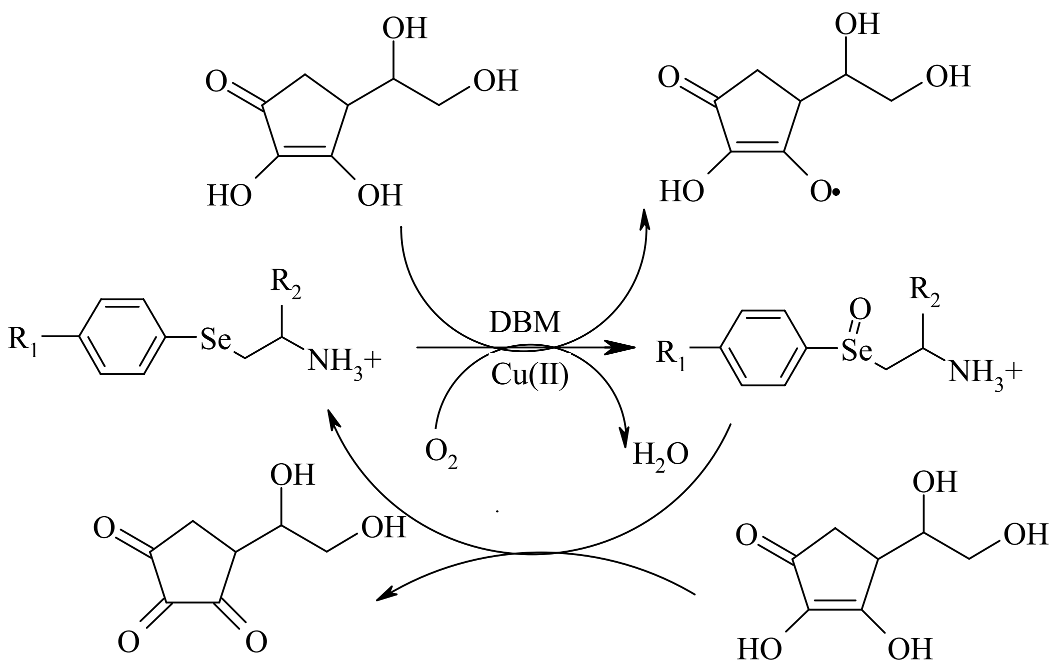

ClPAESe (4-chloro-phenyl-2-aminoethyl selenide): R_1 = Cl, R_2 = H

ClPAESeO (4-chloro-phenyl-2-aminoethyl selenoxide): R_1 = Cl, R_2 = H

FPAESe (4-fluoro-phenyl-2-aminoethyl selenide): R_1 = F, R_2 = H

FPAESeO (4-fluoro-phenyl-2-aminoethyl selenoxide): R_1 = F, R_2 = H

PAESe (phenyl-2-aminoethyl selenide): R_1 = H, R_2 = H

PAESeO (phenyl-2-aminoethyl selenoxide): R_1 = H, R_2 = H

(S)-HOMePEASe [(S)-hydroxy-α-methyl-phenyl-2-aminoethyl selenide]: R_1 = OH, R_2 = CH_3

(S)-HOMePEASeO [(S)-hydroxy-α-methyl-phenyl-2-aminoethyl selenoxide]: R_1 = OH, R_2 = CH_3

MeOPAESe (4-methoxy-phenyl-2-aminoethyl selenide): R_1 = MeO, R_2 = H

MeOPAESeO (4-methoxy-phenyl-2-aminoethyl selenoxide): R_1 = MeO, R_2 = H

Pharmacological testing of (S)-HOMePAESe showed that this compound exhibits restricted CNS permeability and oral dose-dependent antihypertensive activity in spontaneously hypertensive rats (SHR) (7).

Recent experimental evidence has demonstrated that phenylaminoalkyl selenides, in addition to their antihypertensive properties, may also play an important role as scavengers of oxidizing species such as hydrogen peroxide (H_2O_2) and oxoperoxynitrate (PN) (8).

<u>Oxoperoxynitrate ($ONOO^-$/ONOOH):</u>

One of the most predominant cellular oxidants is oxoperoxynitrate ($ONOO^-$) formed from a diffusion-controlled reaction between nitric oxide ($^{\cdot}NO$) and superoxide ($O_2^{\cdot-}$) in endothelial cells, macrophages and neutrophils during pathophysiological conditions involving acute and chronic inflammation, and in ischemia-reperfusion (9 - 14).

$^{\cdot}NO + O_2^{\cdot-} \rightarrow ONOO^-$ $\qquad d[ONOO^-]/dt = k \times [^{\cdot}NO] \times [O_2^{\cdot-}]$

$^{\cdot}NO$ is produced by all three isoforms of nitric oxide synthase [neuronal (nNOS), inducible (iNOS) and endothelial (eNOS)], which under depleted concentrations of L-arginine yield $O_2^{\cdot-}$ as well (15-18). The superoxide radical is also formed through the activity of enzymes such as NAD(P)H oxidases, xanthine oxidase and others (19). The concentration of $O_2^{\cdot-}$ is down regulated by the superoxide dismutase (SOD)-catalyzed reaction of $O_2^{\cdot-}$ to form H_2O_2 and molecular oxygen. $^{\cdot}NO$ is the only biomolecule that can effectively out - compete the SOD-catalyzed dismutation of $O_2^{\cdot-}$, hence resulting in the formation of $ONOO^-$ at a rate of $4 - 20 \times 10^9\ M^{-1}\ s^{-1}$ (20).

$ONOO^-$ is a relatively stable species under alkaline conditions, but upon protonation to peroxynitrous acid (ONOOH) it decays to nitrate with a rate constant of $1.3\ s^{-1}$ at pH 7.4 and 25^oC (21). Oxoperoxynitrate is proposed to react with biological molecules through two main pathways (22). The first pathway involves the direct reaction of $ONOO^-$/ONOOH with the biotarget molecule. The second pathway involves the formation of an activated form of ONOOH, $ONOOH^*$, which exhibits the biological activity of a hydroxyl radical:

$$ONOO^- + H^+ \Leftrightarrow ONOOH \Leftrightarrow ONOOH^* \rightarrow NO_3^- + H^+$$

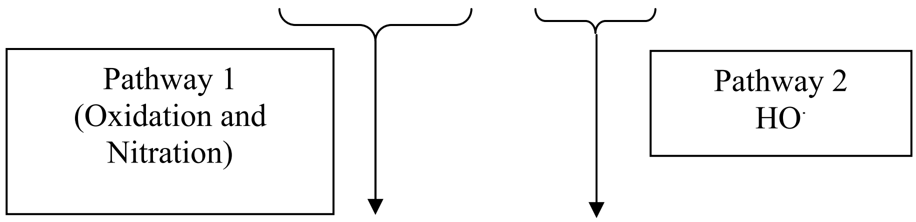

In addition, $ONOO^-$ and carbon dioxide (CO_2) react with a second order rate constant of 5800 $M^{-1}sec^{-1}$ to form the $ONOO^-$ - CO_2 adduct, which can in turn form other reactive intermediates such as $NO_2^{\cdot}$ and $CO_3^{\cdot}$ radicals or the nitrosodioxycarboxylate anion ($O_2NOCO_2^-$) by isomerization (23). The importance of the reactivity of PN towards CO_2 is enhanced by the high *in vivo* concentration of CO_2 (1 to 3 mM in blood plasma) and bicarbonate (HCO_3^-, 12 mM in intracellular fluid and 25 to 30 mM in blood plasma). Reaction of $ONOO^-$ with CO_2 has been shown to enhance nitration reactions but inhibit hydroxylation and oxidation reactions mediated by PN (23, 24).

PN species react with a variety of biological molecules such as lipids, DNA, proteins/peptides, amino acids, thiols and metalloenzymes. For instance, oxoperoxynitrate causes single and double electron oxidations of sulfhydryls and thiols; initiates lipid peroxidation, and oxidizes or nitrates amino acids such as L-phenylalanine (L-Phe), L-methionine (L-Met), L-tryptophan (L-Trp) and L-tyrosine (L-Tyr) (14, 25 – 29). PN induces DNA damage leading to multiple forms of nuclear base modifications, and causes double and single strand breakage in plasmid DNA (30 – 37). The DNA strand breakage has been found to activate a DNA repair enzyme poly(ADP) ribose polymerase (PARP), which causes depletion of NAD^+ pools and can eventually lead to cell death (38). PN was reported to induce apoptosis in a number of cell types such as thymocytes, cortical cells and HL-60 leukaemia cells (39).

Increased formation of PN has been linked to Alzheimer's disease, rheumatoid arthritis, atherosclerosis, lung injury, amyotropic lateral sclerosis and other diseases (40 - 42).

Protection against PN:

There are three physiological and pharmacological strategies for protecting various biological targets from the unwanted effects of PN-mediated reactions: prevention, interception and repair.

Prevention of PN formation involves lowering the concentration of $O_2^{\cdot -}$ and $NO^{\cdot}$ radicals. SOD-mimics, inhibitors of xanthine oxidase and NAD(P)H oxidases inhibit the formation of $O_2^{\cdot -}$ (43). $NO^{\cdot}$ formation can be down-regulated by using NOS inhibitors.

Interception of PN and its reactive intermediates ($ONOOH^{*}$) can be accomplished with various endogenous and exogenously supplied scavengers, which react with this powerful oxidant or its precursors to form harmless products. The effectiveness of an intercepting agent depends on the mechanism, kinetics and thermodynamics of its reaction with the $O_2^{\cdot -}$ and $NO^{\cdot}$ radicals, and PN species. The third strategy is the repair of the PN-mediated damage.

To determine the detoxifying capacity of a given compound for PN, it is useful to consider the rate constant for its reaction with PN, its achievable concentration at site of oxidative stress and the ability of the scavenger to regenerate its active antioxidant form.

Scavengers of PN:

Kinetics, thermodynamics, mechanism of action, regeneration ability and ease of diffusion across various organelle membranes of endogenous and exogenous scavengers of PN have been widely investigated. For instance, various heme proteins (oxyhemoglobin), peroxidases (myeloperoxidase, lactoperoxidase and horseradish peroxidase) and synthetic metalloporphyrins effectively scavenge oxoperoxynitrate by catalyzing its isomerization to nitrite (44 – 48).

The interest in the antioxidative properties of selenium and its derivatives has increased over the years as a number of Se - containing proteins, amino acids and organic compounds were shown to be effective scavengers of PN. Selenomethionine (SeMet) and L-selenocysteine (SeCys) are two major Se - containing amino acids found in the body; SeCys is incorporated into specific protein sites, while SeMet randomly replaces a few L-methionine (Met) residues in proteins (49, 50). There are currently 22 known eukaryotic selenoproteins, which are organized into two distinct selenoprotein groups on the basis of the location and functional properties of SeCys (51). A SeCys-containing enzyme, glutathione peroxidase (GPx), reacts with PN with a second order rate constant of $8.0 \times 10^6\ M^{-1}s^{-1}$ and effectively protects against PN-mediated oxidation and nitration reactions (52, 53). The activity of GPx is catalytically maintained by reduced GSH (52, 53).

Small Se-containing molecules such as SeMet, SeCys and ebselen (2-phenyl-1,2-benzisoselenazol-3(2H)-one) were shown to be effective PN scavengers in *vitro* studies (27, 53, 54). Ebselen exhibits GPx like activity, and reduces PN to nitrite with a second order rate constant of $2 \times 10^6\ M^{-1}s^{-1}$ to yield the corresponding selenoxide as the sole selenium containing product (54, 55). The oxidized product, 2-phenyl-1,2-benzisoselenezol-3(2H)-one-1-oxide, is efficiently reduced back to ebselen either via GSH or thioredoxin reductase (TrxR) (51).

Other scavengers of PN include organotellurium compounds, catecholamines, flavanoids, reduced GSH, zinc - thiolate centers in DNA transcription factors and other antioxidants (51, 56 – 59).

Antioxidative Role of Phenylaminoalkyl Selenides and Sulfides against PN:

Previous research showed that PAESe and PAES derivatives react with PN to form the corresponding selenoxides or sulfoxide with second order rate constants comparable to those of other known Se - and S - containing antioxidants such as SeMet and Met (table 1 - 1) (27, 49, 60). (S)-HOMePAESe is the most effective scavenger of

Table 1 - 1. Second Order Rate constants for PN-Mediated Oxidation of Se - and S - Containing Compounds[a].

Selenium Compounds	k_{ONOO^-} (M^{-1} s^{-1})	Sulfur Compounds	k_{ONOO^-} (M^{-1} s^{-1})
1. Ebselen[b] 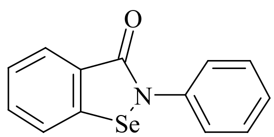	10^6	GSH[d] 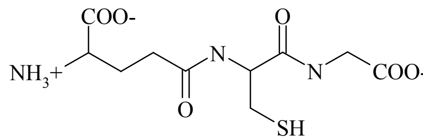	580
2. SeMet[c] 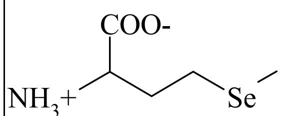	2,400	Met[e] 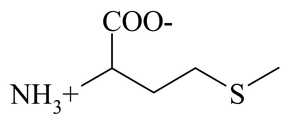	180 ± 8
3. (S)-HOMePAESe 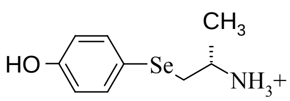	3,010 ± 100	PAES 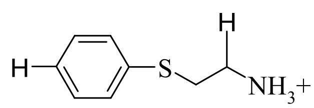	370 ± 10
4. MeOPAESe 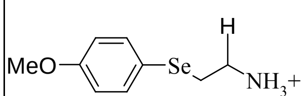	2,310 ± 20		
5. PAESe 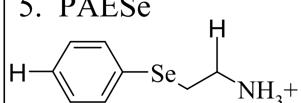	1,790 ± 10		
6. FPAESe 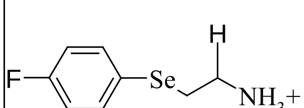	1,070 ± 10		
7. ClPAESe 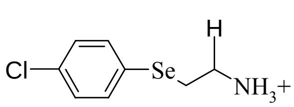	900 ± 10		

[a]Unless otherwise specified, rate constants at pH 7.0 from Woznichak *et. al.* (60)
[b]From Masumoto *et. al.* (54)
[c]Rate constant at pH 7.4, from Padmaja *et. al.* (49)
[d]Rate constant at pH 7.4, from Lee *et. al.* (44)
[e]Rate constant at pH 7.4, from Pryor *et. al.* (27)

PN according to the measured rate constant reported in Table 1 - 1, which is consistent with a proposed bimolecular nucleophilic displacement mechanism for the reaction of PN and selenide (60).

PN has been shown to cause single- and double-strand breakage of supercoiled plasmid pUC19 DNA (41). Hence, we investigated the ability of phenylaminoalkyl selenides and sulfides developed in our laboratory to protect pUC19 plasmid DNA against PN - induced damage (61). In a typical experiment, 0.5 mM PN was incubated with pUC19 (25 ng / µl, pH 7.4) for 3 minutes at 25^{o}C, and the various plasmid forms subsequently separated using agarose gel electrophoresis and quantified by scanning (61). We found that (S)-HOMePAESe, PAESe and SeMet decreased PN - mediated pUC19 DNA damage by as much as 46 % under the experimental conditions, and the selenides were much more effective in this regard than their corresponding sulfur analogs (61). Quantitative HPLC analysis of the reaction mixtures confirmed stoichiometric formation of corresponding phenylaminoalkyl selenoxides or sulfoxides as the sole Se- or S-containing products of the PN-mediated reaction with plasmid DNA (61). This result correlates with the work by Roussyn *et. al.*, who demonstrated that both SeMet and SeCys protect pBluescript II KS DNA from single strand breakage caused by PN more efficiently than Met and Cys respectively (62).

Further experiments were carried out to demonstrate that redox cycling by GSH enhances protection of pUC19 plasmid DNA against PN-induced damage by (S)-HOMePAESe. In the presence of 0.25 mM (S)-HOMePAESe, the amount of DNA damage caused by 0.25 mM PN was reduced by 31% (n = 6), as compared to the level of damage in the absence of any protecting agents (61). Addition of 0.25 mM GSH to the (S)-HOMePAESe / plasmid DNA / PN reaction caused a statistically significant enhancement of protection of up to 14.5%. An ANOVA / Dunnet test (n = 6) was used to confirm that the results of the protection studies were statistically significant (61). Neither (S)-HOMePAESeO nor GSH alone at this concentration provided any protective effects against DNA damage (61). Recycling was confirmed by the observed reduction of (S)-HOMePAESeO in the presence of GSH and the stoichiometric increase in the selenide concentration via HPLC (61).

The current research focused on measuring the rate constants of phenylaminoalkyl selenoxides and sulfoxides with GSH by a spectrophotometric methodology at pH 7.0 and 25^{o}C. The ability of these Se - and S - containing compounds to be catalytically recycled by reducing equivalents such as GSH in the presence of PN was further investigated using a MatLab simulation.

Antioxidative Role of Phenylaminoalkyl Selenides in PN – Mediated Reaction with Molecular Beacons:

Molecular Beacons (MBs) are hybridization probes used for detection of specific nucleic acid sequences (63). MBs are hairpin – shaped molecules with an internally quenched fluorophore whose fluorescence is restored when they bind to a target nucleic acid (63). They are designed in such a way that the loop portion of the molecule is a probe sequence complementary to a target DNA molecule (63). The stem is formed by annealing the complementary arm sequences on the ends of the probe sequence. A fluorescent moiety is attached to the 5' end of one arm and a quenching moiety to the 3' end of the other arm. The stem keeps the two moieties in close proximity to each other, causing fluorescence of the fluorophore to be quenched by energy transfer.

Two forms of energy transfer exist in MBs: direct energy transfer and fluorescence resonance transfer (FRET) (64). The collision between the fluorophore and the quencher distorts the energy level of the excited fluorophore, which causes quenching (64). The quenching moiety dissipates this energy in the form of heat rather than light. In MBs the length of the loop sequence is chosen so that the probe - target hybrid is stable at probing temperature (63, 64). The stem sequence should be strong enough to form the hairpin structure for efficient fluorescence quenching yet still weak enough to be dissociated when a complimentary DNA hybridizes with the loop of MB. Upon binding the target DNA sequence, which is perfectly complimentary to the loop sequence of the MB molecule, the conformational changes open the hairpin, the fluorophore and quencher are separated and fluorescence is turned “on” (64). DABCYL (dimethylaminophenylazobenzoic acid) is used as the quencher at the 3’ end of the sequence and Cy3 is used as the fluorophore at the 5’ end of the sequence in MB used in experiments described in this chapter (63):

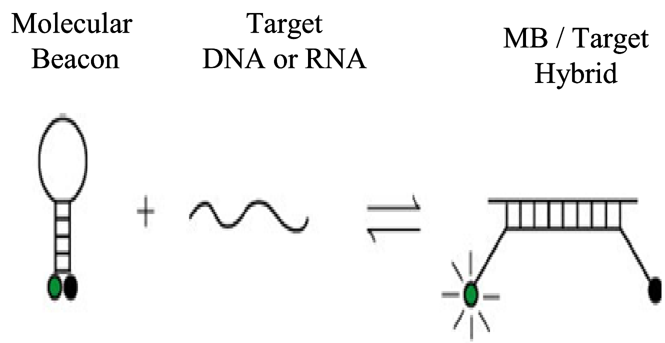

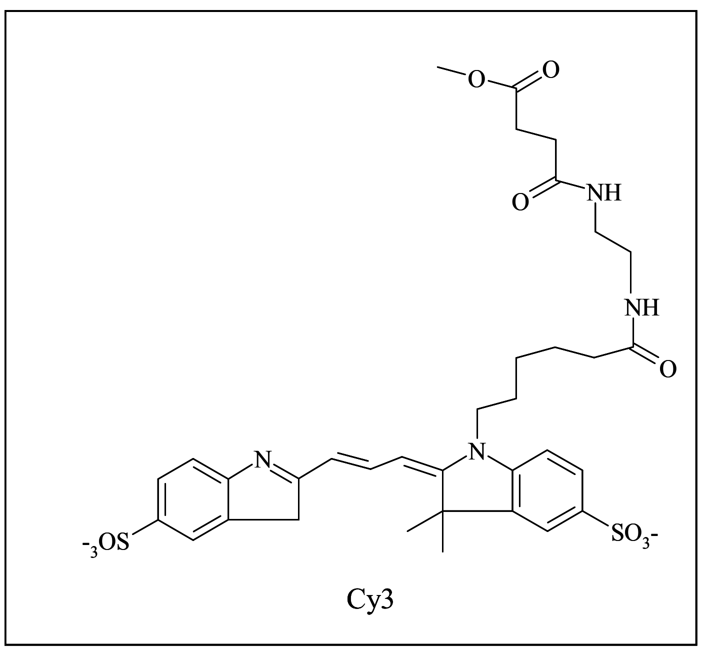

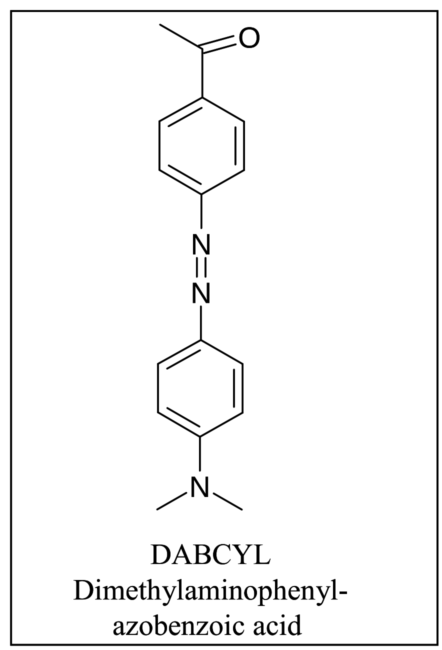

MBs have numerous applications such as real-time monitoring of PCR, spectral gene typing and mutation detection, real-time enzymatic cleavage assays, RNA detection in living cells and others (63, 64). The goal of this study was to investigate the reaction between PN and MB, and demonstrate that phenylaminoalkyl selenides protect MBs from

PN – mediated damage. The products of the reaction between MB and PN were analyzed by denaturing polyacrylamide gel electrophoresis (PAGE).

1 – 3: MATERIALS AND METHODS

Materials:

Boric acid, dibasic potassium phosphate, glacial acetic acid (CH_3COOH), hydroxylamine hydrochloride, H_2O_2 (30 % aqueous solution), HPLC - grade CH_3CN, HPLC – grade trifluoroacetic acid (TFA), methanol (CH_3OH), MnO_2, monobasic potassium phosphate, sodium hydroxide (NaOH), tris(hydroxymethyl)amino methane (Tris base) and urea were purchased from Fisher Scientific (Atlanta, GA). 1,2 - Bis(dimethylamino)ethane (TEMED), diethylenetriamine pentaacetic acid (DTPA), ethylene diamine tetraacetic acid (EDTA), glutathione (GSH) and oxidized glutathione (GSSG) were obtained from Sigma Chemical Co. (St Louis, MO). Acrylamide (99.9 %), ammonium persulfate (APS), bis(N,N'- methylene-bis acrylamide), Nucleic acid sample loading buffer, Protean II xi Single - Gel (PIIxiSG) Alignment card, PIIxiSG Casting Chamber, PIIxiSG comb (15 well, 1.0 mm), PIIxiSG Glass Plates (20 cm), PIIxiSG Power Supply, PIIxiSG 20 cm Slab Cell, PIIxiSG Spacers (1.5 mm), Silver Stain Plus (SSP) Development Accelerator reagent, SSP Fixative Enhancer Solution, SSP Image Development Agent, SSP Reduction Moderator Solution and SSP Silver Staining Solution were purchased from Bio-Rad Laboratories (Hercules, CA, USA). Allsphere Octyl (C8, 250 x 4.6 mm, 5 μm particle size) column, equipped with Alltech guard cartridges (7.5 x 4.6 mm, 5 μm particle size) was obtained from Alltech (Nicholasville, KY). MB 6 (5'-/Cy3/GAGTCCTTCCACGATACCAGGA-CTC/3Dab/-3') was obtained from Integrated DNA technologies Inc.

Synthesis of Phenylaminoalkyl Selenides and Sulfides:

PAESe and PAES were synthesized and characterized by Dr. James E. Colbert as previously described (5, 61). ClPAESe, FPAESe, MeOPAESe, (S)-HOMePAESe were prepared and characterized by Dr. Michelle M. Woznichak as reported in the literature (62).

Synthesis of Phenylaminoalkyl Selenoxides and Sulfoxide:

ClPAESeO, FPAESeO, MeOPAESeO, PAESeO, PAESO and (S)-HOMePAESeO were synthesized by H_2O_2 - mediated oxidation of their corresponding selenides. Briefly, the hydrochloride salt of the selenide was dissolved in 5 ml of DI H_2O and reacted with a 30 % solution of H_2O_2 in a 1:1.2 mol ratio. The reaction was monitored by HPLC (C8 column, UV detection at 236 nm, flow rate of 1.5 ml/min and a mobile phase composed of 80 to 85 % DI H_2O, 20 to 15 % CH_3CN and 0.1 % TFA), once complete it was quenched by the addition of granular MnO_2, filtered and lyophilized overnight.

Synthesis of PN:

PN was synthesized by the autooxidation of 10 mM hydroxylamine in 0.5 M aqueous NaOH containing 0.1 mM DTPA, as previously described (65, 66). Oxygen was bubbled into the 200 ml solution for 3 hours at 25^{o}C. The resulting yellow solution was treated with granular MnO_2 to remove excess H_2O_2, filtered and concentrated by freeze fractionation at -20^{o}C. PN concentration was determined spectrophotometrically at 302 nm (ε_{302} = 1670 $M^{-1}s^{-1}$) in 0.5 M NaOH with a Hewlett Packard Model 8453 diode array spectrophotometer.

Spectrophotometric Determination of Second Order Reaction Rates between Phenylaminoalkyl Selenoxides / Sulfoxide and GSH:

The second order rate constants for the redox reaction between phenylaminoalkyl selenoxides and GSH were determined spectrophotometrically under pseudo-first order conditions using an HP8453 diode-array spectrophotometer equipped with an HP 89090 temperature-control accessory. Selenoxides or PAESO (40 to 50 µM) was combined with GSH (0.35 to 0.6 mM) in 0.1 mM potassium phosphate buffer (final pH 7.0) at 25^{o}C in a quartz cuvette, and the absorbance changes monitored at 0.5 second intervals for a period of 30 seconds. Due to sufficient differences in molar extinction coefficients of reactants and products in the wavelength range of 230 to 300 nm, concentrations of selenide / selenoxide or sulfide / sulfoxide could be determined using the multi-component module of the Biochemical Analysis UV - visible ChemStation software (Figure 1 - 1: Panel A and B). The following data analysis parameters were selected: within spectral processing, the derivative order was set to 1, filter length at 5 and polynomial degree at 3. The wavelength range used was set at 230 to 310 nm with 1 nm intervals and the least squares method of data analysis employed. The pseudo first order rate constants obtained from the concentration versus time plots (Figure 1 - 2, Panel A) were used to determine to second order rate constants for the reaction (Figure 1 - 2, Panel B). Table 1 - 2 lists the second order rate constants for the reaction of phenylaminoalkyl selenoxides and GSH at pH 7.0 and 25^{o}C.

Separation of reactants and products in the selenoxide / GSH reaction mixtures was accomplished on a C8 column (UV detection at 236 nm, flow rate of 1.5 ml/min and a mobile phase composed of 80 to 85 % DI H_2O, 20 to 15 % CH_3CN and 0.1 % TFA). Authentic samples of GSH, GSSG, selenide / selenoxide and sulfide / sulfoxide were used to confirm the identity of the reaction mixtures.

<u>MatLab Kinetic Simulation:</u>

A MatLab simulation was employed to investigate the effectiveness of (S)-HOMePAESe regeneration by GSH in the presence of PN at physiological pH using the second order rate constants for the reactions of (S)-HOMePAESe and PN (3010 $M^{-1}s^{-1}$, table 1 - 1), the selenoxide and GSH (1100 $M^{-1}s^{-1}$), and GSH and PN (580 $M^{-1}s^{-1}$) (60). The apparent 1st order rate constant for the decomposition of PN to nitrite under these conditions was also taken into account (0.5 s^{-1}) in this recycling model (47).

Panel A

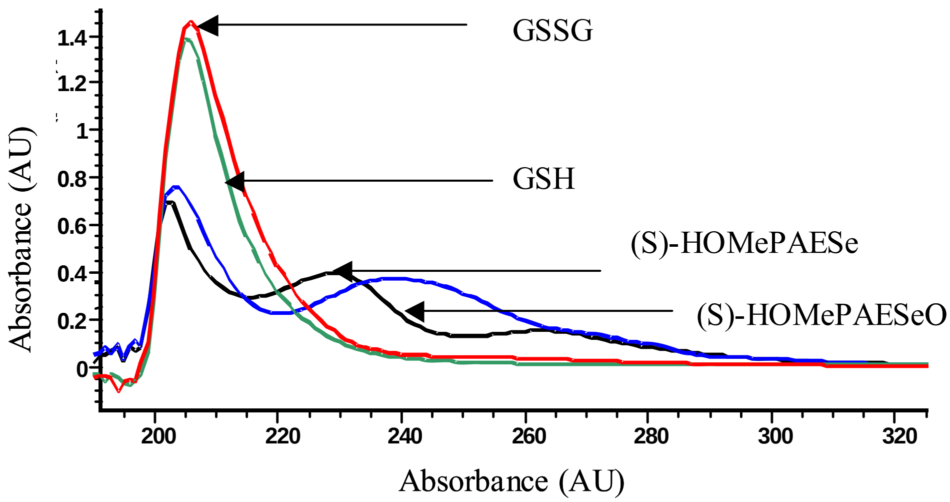

Panel B

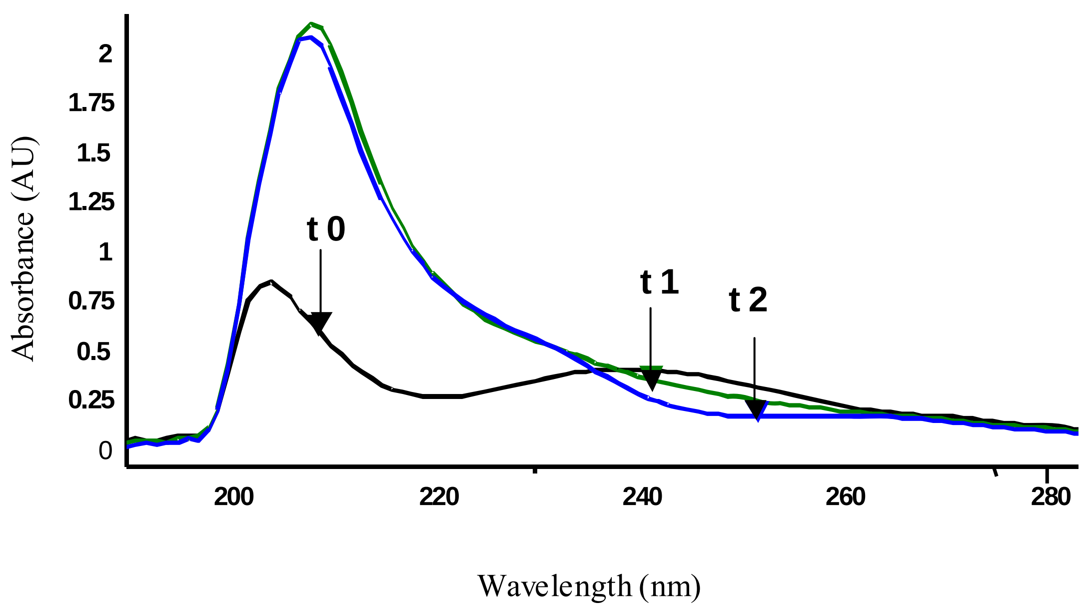

Figure 1 - 1: Panel A: Absorbance spectra of (S)-HOMePAESeO (0.04 mM); (S)-HOMePAESe (0.04 mM); GSH (0.02 mM) and GSSG (0.1 mM) in 100 mM potassium phosphate buffer (pH 7.0). Panel B: Absorbance spectra of the (S)-HOMePAESeO (0.045 mM) and GSH (0.35 mM) reaction mixture in 100 mM potassium phosphate buffer (pH 7.0) after t_0 = 0 sec and t_2 = 6.5 sec (end of reaction).

Panel A

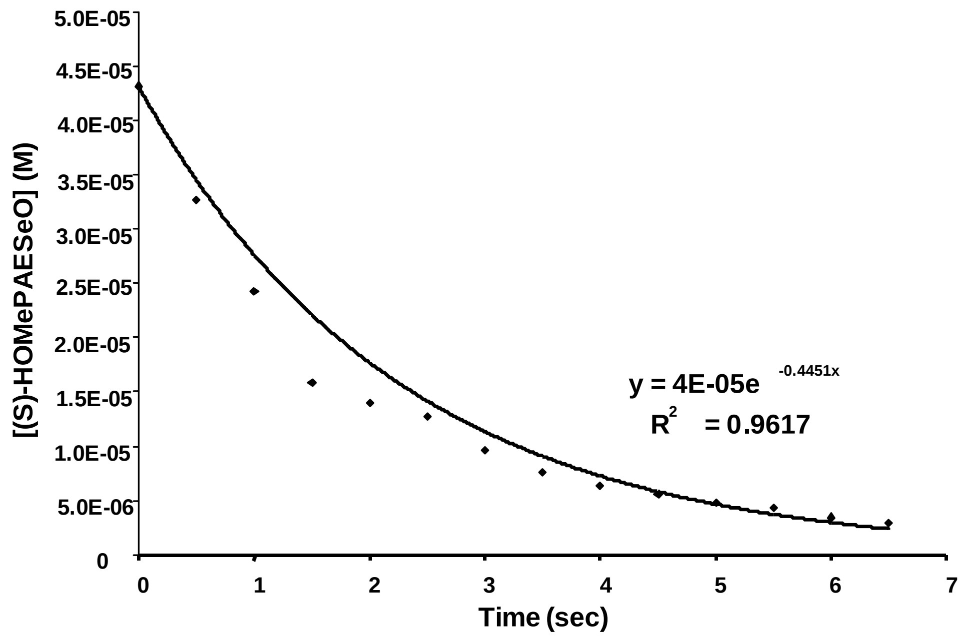

Panel B

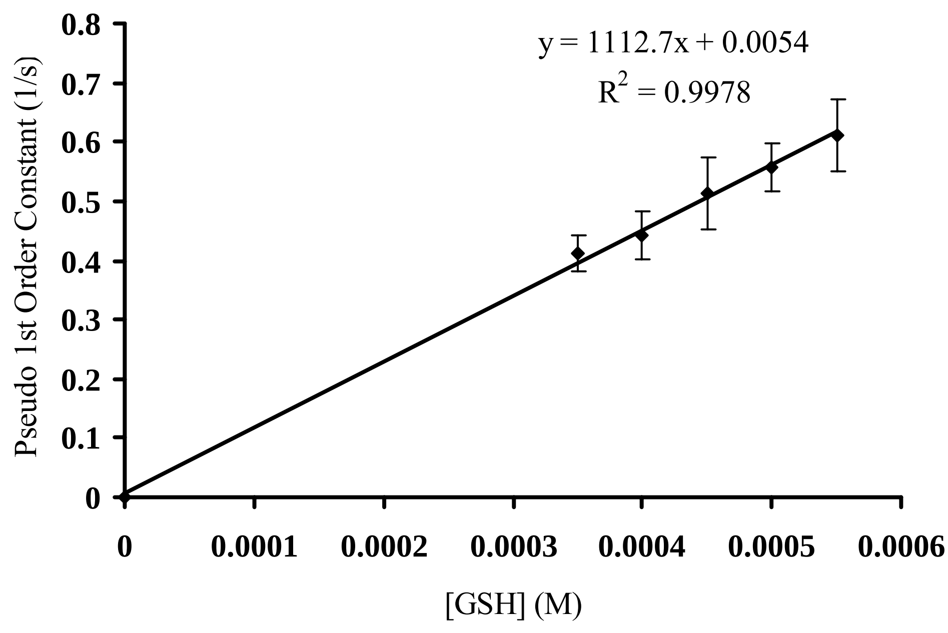

Figure 1 - 2: Panel A: Graph used to determine the pseudo-first order rate constant for the reaction of (S)-HOMePAESeO and GSH. Panel B: Graph used to determine the second order rate constant for the reaction of (S)-HOMePAESeO and GSH.

Table 1 - 2: Second Order Rate constants for GSH-Mediated Reduction of Phenylaminoalkyl Selenoxides and Sulfoxide.

Se- and S- Containing Compound	k_{GSH} (M^{-1} s^{-1}) at pH 7.0 and 25^{o}C
ClPAESeO	4060 ± 20
FPAESeO	3450 ± 20
CH_3OPAESeO	2200 ± 30
PAESeO	1500 ± 20
(S)-HOMePAESeO	1100 ± 30
PAESO	No Reaction

Simulink, a module of MatLab, in conjunction with the kinetic derivations below were used in the simulation:

(S)-HOMePAESe + $ONOO^-$ $\rightarrow$ (S)-HOMePAESeO + NO_2^-

$-\Delta$[(S)-HOMePAESe] / $\Delta t = k_1 \times$ [(S)-HOMePAESe] $\times$ [$ONOO^-$]

2 GSH + $ONOO^-$ $\rightarrow$ GSSG + H_2O + NO_2^-

$-\Delta[ONOO^-] / \Delta t = k_2 \times 2 \times [GSH] \times [ONOO^-]$

2 GSH + (S)-HOMePAESeO $\rightarrow$ (S)-HOMePAESe + GSSG + H_2O

Δ[(S)-HOMePAESeO] / $\Delta t = k_3 \times$ [(S)-HOMePAESeO] $\times$ [GSH]

$ONOO^- + 2\ H^+ \rightarrow H_2O + NO_2^-$

$-\Delta[ONOO^-] / \Delta t = k_4 \times [ONOO^-]$

Mass balance:

$-\Delta$[(S)-HOMePAESe] / $\Delta t = -\ k_1 \times$ [(S)-HOMePAESe] $\times$ [$ONOO^-$] + $k_3 \times$ [(S)-HOMePAESeO] $\times$ [GSH]

$-\Delta[GSH] / \Delta t = -\ 2 \times k_2 \times [GSH] \times [ONOO^-] - k_3 \times$ [(S)-HOMePAESeO] $\times$ [GSH]

Δ[(S)-HOMePAESeO] / $\Delta t = k_1 \times$ [(S)-HOMePAESe] $\times$ [$ONOO^-$] $- k_3 \times$ [(S)-HOMePAESeO] $\times$ [GSH]

$-\Delta[ONOO^-] / \Delta t = -\ k_1 \times$ [(S)-HOMePAESe] $\times [ONOO^-] - k_2 \times [ONOO^-] \times [GSH] - k_4 \times [ONOO^-]$

Investigation of Reactions between MB and PN:

The concentration of MB6 was determined spectrophotometrically on a HP8453 diode - array spectrophotometer using an extinction coefficient (ε_{260nm}) of 253,683 $M^{-1}cm^{-1}$.

```
       C  G  A
     A        T
    C          A
     C         C
      T       C
        T - A
        C - G
        C - G
        T - A
        G - C
        A - T
        G - C
   5' Cy3   Dabcyl 3'
```

Control mixtures were prepared in a polymerase chain reaction (PCR) tube by combining 14 μM MB6 with PN (0.25, 0.7 or 1.4 mM) in 0.2 M potassium phosphate buffer (pH 6.8), gently vortexing the solution and incubating at 25°C for 15 minutes. Note that the pH of the reaction mixtures would differ from each other, due to the presence of different PN concentrations (diluted with 0.5 M NaOH). The background mixture consisted of MB6 in 0.2 M potassium phosphate buffer in the absence of PN. The reaction mixtures were subsequently analyzed on a ABI PRISM 7700 sequence detection system equipped with a built-in thermal cycler, a laser to induce fluorescence, CCD (charge-coupled device) detector, real-time sequence detection software, and TaqMan reagents for the fluorogenic 5' nuclease assay. The control and background mixtures were melted at 95°C, and cooled to 5°C in 1°C increments, with an equilibration time at each temperature of 9.5 minutes and fluorescence measurements in the last 30 seconds at 630 nm. Eight thermocycles were performed and the results collected averaged using the real-time sequence detection software.

Protection of MB from PN – Mediated Damage by (S)-HOMePAESe:

Reaction mixtures were prepared by combining 14 μM MB6 with PN (1.4 mM) and (S)-HOMePAESe (0.7, 0.9 or 1.4 mM) in 0.5 M potassium phosphate buffer (final pH 7.4), gently vortexing the solution and incubating at 25°C or 84°C for 15 minutes. The control mixtures consisted of 8, 10 or 14 μM MB6 incubated with 0.8, 1 or 1.4 mM PN, respectively, under the same conditions as the reaction mixture. The background mixture consisted of 8, 10 or 14 μM MB6 in 0.5 M potassium phosphate buffer (final pH 7.4) in the absence of PN or (S)-HOMePAESe. The reaction, control and background mixtures were subsequently analyzed on a Spectra Max Gemini Dual-Scanning Microplate Spectrofluorometer via end-point analysis and excitation wavelength of 545 nm and emission wavelength of 570 nm. The Spectra Max Gemini Dual-Scanning Microplate Spectrofluorometer is equipped with two holographic diffraction grating monochromators, the dual-scanning capability, a high-powered Xenon flash lamp, temperature control accessory, an auto-mixer and Softmax Pro software.

<u>Analysis of MB and PN Reaction Mixtures by Denaturing PAGE:</u>

Denaturing PAGE gel Preparation and Casting: Thirty % acrylamide / bisacrylamide solution was prepared by dissolving 58.0 g of acrylamide and 2 g of bisacrylamide in 200 ml of DI H_2O and stored in a light-protected container at 4^oC. 10 × TBE (Tris borate buffer) was prepared by dissolving 54.0 g of Tris base, 27.5 g of boric acid and 20.0 ml of 0.5 M EDTA in a total volume of 500 ml, the pH was adjusted to 8.0. Denaturing PAGE gel mixture was prepared by combining 66.7 ml of 30 % acrylamide / bisacrylamide solution with 10 ml of 10 × TBE and 42.04 g of urea, upon complete dissolution, the volume of the solution was adjusted to a total of 100.0 ml with DI water. The mixture was degassed with Argon for 15 to 30 minutes. Five ml of the denaturing PAGE mixture was mixed with 82.5 µl of 10 % APS, 15 µl TEMED, swirled vigorously and poured into a 200 x 200 x 1.5 mm PIIxiSG Slab Cell in a PIIxiSG Casting Chamber. The plug for the gel was allowed to set for a few minutes, in the meantime the remainder of the denaturing PAGE solution was combined with 317 µl APS, 30 µl TEMED and poured on top of the plug, PIIxiSG comb (15 well, 1.0 mm) was placed within the gel. The gel was allowed to set for 45 to 60 minutes.

Preparation of MB and PN Reaction Mixtures: MB6 (14 µM), 1.4 mM PN and 0.9 mM (S)-HOMePAESe were combined together in 0.5 mM potassium phosphate buffer (final pH 7.4) at 25^oC, vortexed gently and allowed to react for 30 minutes. The background reaction mixture consisted of 14 µM MB6 in 0.5 M potassium phosphate buffer (final pH 7.4) and the control mixture contained all reagents with the +exception of (S)-HOMePAESe. The mixtures were all diluted in the same manner such that the final amount of MB6 was 100 ng. The background, control and reaction mixtures were subsequently diluted with an equal volume of the Bio-Rad nucleic acid loading buffer and loaded into the respective wells in the cast denaturing PAGE gel. The PIIxiSG Casting Chamber was then filled with 1 × TBE and ran at constant voltage of 200 V for 30 to 40 minutes.

Silver Staining Protocol for the Denaturing PAGE Gel: After gel electrophoresis, the gel was placed in 400 ml of a SSP Fixative Enhancer Solution for 20 minutes. The SSP Fixative Enhancer solution was prepared by combining 200 ml CH_3OH, 40 ml CH_3COOH, 40 ml SSP Fixative Enhancer Concentrate and 120 ml DI H_2O. The fixative enhancer solution was subsequently decanted and the gel rinsed twice with 400 ml of DI water with gentle agitation. The gel was subsequently stained with a SSP staining solution. The staining solution consisted of 5 ml SSP Silver Complex solution, 5 ml SSP Reduction Moderator solution, 5.0 ml SSP Image Development reagent and 50 ml SSP Development Accelerator solution. The gel was stained for 15 to 20 minutes until the desired degree of staining / contrast was obtained and then transferred to a 5% acetic acid solution for 15 minutes. Afterwards the gel was rinsed with high purity water.

1 – 4: RESULTS

Spectrophotometric Determination of Second Order Rate Constants between Phenylaminoalkyl Selenoxides and GSH:

The antioxidant activity of phenylaminoalkyl selenides is dependent on the efficiency with which they are reduced once oxidized by a biological oxidant such as PN. Hence we were interested in investigating the mechanism of action and kinetics of organoselenium redox cycling. Depending on the intracellular or extra cellular location, GSH is a common reducing agent present in *vivo* in the range of 0.1 to 10 mM, hence it was chosen as the reducing agent in our experiments (69). The second order rate constants at pH 7.0 and 25^{o}C were measured by a spectrophotometric methodology. The stoichiometry of the reactants was 2 molecules of GSH per each molecule of organoselenoxide or sulfoxide, as determined by Overcast JL (70). It was important to keep stoichiometry in mind when selecting the appropriate concentration range of GSH to be used throughout the experiments. GSH was used in excess and the initial rate of phenylaminoalkyl selenoxide reduction measured. The reaction between organoselenoxide and GSH yielded the corresponding selenide and GSSG, respectively, as shown by Overcast (70).

In previous work in this laboratory, the second order rate constants between phenylaminoalkyl selenoxides / sulfoxides and GSH at pH 5.5 and 25^{o}C were measured by HPLC - UV detection (60). The phenylaminoalkyl selenoxide was present in excess and the initial rate of GSH oxidation quantified. Table 1 - 3 shows that the reduction of phenylaminoalkyl selenoxides by GSH is a rapid process and the second order rate of the reaction is less sensitive to the nucleophilic / electrophilic nature of the *para*-substituent, as indicated by the low positive ρ value of 0.133 at pH 5.5 in the Hammett plot by Overcast JL (70).

In order to measure the rate constant between phenylaminoalkyl selenoxides and GSH, 45 to 50 μM organoselenoxide was incubated in 100 mM potassium phosphate at

Table 1 - 3: Second Order Rate Constants for GSH-Mediated Reduction of Phenylaminoalkyl Selenoxides and Sulfoxide at pH 5.5[a] and 7.0 at 25°C Compared.

Se- and S- Containing Compound	k_{GSH} (M^{-1} s^{-1}) at pH 5.5 and 25°C[a]	k_{GSH} (M^{-1} s^{-1}) at pH 7.0 and 25°C
ClPAESeO	230 ± 21	4060 ± 20
FPAESeO	250 ± 12	3450 ± 20
CH_3OPAESeO	290 ± 28	2200 ± 30
PAESeO	300 ± 16	1500 ± 20
(S)-HOMePAESeO	300 ± 28	1100 ± 30
PAESO	No Reaction	No Reaction

[a]Data at pH 5.5 was collected by Overcast (70)

pH 7.0 in a quartz cuvette at 25^{o}C. The reaction was initiated by the addition of 0.35 to 0.65 mM GSH under vigorous stirring and spectrophotometric measurements made in the 230 to 310 nm range at 0.5 second intervals over the course of 30 seconds. It should be noted that in each case the spectrum of the formed selenide was sufficiently different from the parent selenoxide, hence making the accurate estimation of the reactant / product concentration possible over a time course.

Initially a 4 x 4 matrix was used to determine the concentration of phenylaminoalkyl selenide or selenoxide at 4 chosen optimal wavelengths, where maximal change in absorbance was observed for phenylaminoalkyl selenide and selenoxide components. The extinction coefficients of all of the reaction components determined within the concentration range used (with the exception of intermediate / transition species) were used in the calculations. Subsequently, a multi-component module of the Biochemical Analysis UV-visible ChemStation software was used in the calculation of the organoselenide or organoselenoxide concentration over time by employing spectra of the unreacted reactants / products in the appropriate concentration range, as the standards and utilizing the whole wavelength range of interest (230 to 310 nm).

Table 1 - 3 shows that the reaction of ClPAESeO and GSH has the highest second order rate constant at pH 7.0 and 25^{o}C, while the reaction of (S)-HOMePAESeO and GSH has the lowest. The differences between the second order rate constants at pH 7.0 are much more pronounced than those measured at pH 5.5 as shown in table 1 - 3.

<u>Recycling of Phenylaminoalkyl Selenides in the Antioxidant Action against PN:</u>

Previous work showed that phenylaminoalkyl selenides readily react with PN to yield the corresponding selenoxides as the sole Se - containing products, thereby protecting plasmid DNA from PN – mediated base modifications and strand breakage. (S)-HOMePAESe (0.5 mM) reduced the amount of nicked and linear plasmid DNA by as much as 46 % in a typical experiment where 0.5 mM PN was incubated with 25 ng / µl of

DNA, and the DNA plasmid forms separated via agarose gel electrophoresis and quantified.

Current work showed that 1.4 mM PN can also cause irreversible damage to a small biosensor oligonucleotide beacon MB6 (14 μM) at 40^{o}C and alkaline pH as determined using a real-time ABI PRISM 7700 sequence detection system. The level of damage was quantified in terms of fluorescence changes with time at 630 nm, when the PN / MB6 control and background mixtures heated to 95^{o}C were cooled to 5^{o}C in 1^{o}C increments. The melting temperature of MB6's 7-base pair stem is below 95^{o}C, hence MB6 is expected to exhibit the highest fluorescence intensity at this temperature. The increase in fluorescence at 630 nm is due to the complete separation of a quenched fluorophore (Cy3 at the 5' end of the oligonucleotide sequence) from the quenching moiety (DABCYL) at the 3' end, in the absence of a complementary DNA target sequence. Lower PN concentrations of 0.25 mM and 0.7 mM did not yield maximal fluorescence readings below 70^{o}C, indicating that the stem in some MB6 molecules remained intact. The fluorescence intensity was not indicative of the number of MB6 products formed upon reaction with PN, which was further investigated by denaturing PAGE.

(S)-HOMePAESe at a concentration of 0.7, 0.9 or 1.0 mM protected MB6 from reacting with 1.4 mM PN at pH 7.4 and either 25^{o}C or 85^{o}C. For example, both 0.9 and 1.0 mM (S)-HOMePEASe completely inhibited fluorescence emission at 570 nm at 25^{o}C, indicating that the stem remained intact keeping the quencher and fluorophore together. Overall higher end - point fluorescence values at 570 nm were collected at 85^{o}C versus 25^{o}C. Fluorescence readings in control mixtures consisting of MB6 and PN decreased, with decreasing concentration of PN and MB6 (MB concentration varied from 14 μM to 10 μM and finally to 8 μM, while PN concentration was lowered from 1.4 mM to 1.0 mM and then to 0.8 mM). The collected data is summarized in table 1 – 4, but no recycling

Table 1 - 4: End – Point Fluorescence Measurements at 25°C and 85°C in Background, Control and Reaction Mixtures Consisting of MB6 and PN at pH 7.5 and either 25°C or 85°C.

Data Collected at 25°C

Background Reaction	Fluorescence Reading (FU)	Control Reaction	FU	Protection Reaction	FU
14 µM MB6	94	14 µM MB6 1.4 mM PN	837	14 µM MB6 1.4 mM PN 1.0 mM Se	97
10 µM MB6	79	10 µM MB6 1 mM PN	648	14 µM MB6 1.4 mM PN 0.9 mM Se	79
8 µM MB6	72	8 µM MB6 0.8 mM PN	546	14 µM MB6 1.4 mM PN 0.7 mM Se	169

Data Collected at 85°C

Background Reaction	Fluorescence Reading (FU)	Control Reaction	FU	Protection Reaction	FU
14 µM MB6	109	14 µM MB6 1.4 mM PN	987	14 µM MB6 1.4 mM PN 1.0 mM Se	126
10 µM MB6	97	10 µM MB6 1 mM PN	727	14 µM MB6 1.4 mM PN 0.9 mM Se	119
8 µM MB6	91	8 µM MB6 0.8 mM PN	630	14 µM MB6 1.4 mM PN 0.7 mM Se	191

studies with GSH were carried out. The separation of products in MB6 / PN reaction mixture by denaturing PAGE did not yield meaningful results due to problems associated with visualizing the oligonucleotide products via silver staining.

Further experiments were carried out to demonstrate that selenium redox cycling by GSH enhances protection of plasmid DNA from PN-mediated damage. In the presence of 0.25 mM (S)-HOMePAESe, the amount of DNA damage caused by 0.25 mM PN was reduced by 31 % ($n = 6$), as compared to the level of damage in the absence of any protecting agents. Addition of 0.25 mM GSH to the typical reaction mixture containing organoselenide (0.25 mM), PN (0.25 mM) and plasmid DNA resulted in a statistically significant enhancement of protection of up to 14.5 % ($n = 6$, ANOVA/Dunnett test). It should be noted that neither (S)-HOMePAESeO (0.25 mM) or GSH (0.25 mM) provided any protective effects against PN-induced DNA damage. The occurrence of recycling was confirmed by the observed reduction of (S)-HOMePAESeO concentration and the stoichiometric increase in (S)-HOMePAESe concentration via HPLC.

MatLab Kinetic Simulation:

The rate constants measured for the reactions between phenylaminoalkyl selenides and PN, phenylaminoalkyl selenoxides and GSH, PN and GSH, and finally protonation of PN were used to design a model to predict the extent of redox cycling in the antioxidant activity of organoselenides at neutral pH. Keeping in mind that (S)-HOMePAESe is the most efficient scavenger of PN at pH 7.0 and the facility with which PN oxidizes various biological targets, the recycling ability of (S)-HOMePAESe was investigated.

The MatLab simulation (Simulink module) was employed to model the feasibility of (S)-HOMePAESe regeneration from the product selenoxide by GSH in the presence of PN at physiological pH and 25^{o}C. The model used the rate constants for the reaction of (S)-HOMePAESe and PN (3010 $M^{-1}s^{-1}$), (S)-HOMePAESeO and GSH (1100 $M^{-1}s^{-1}$,

Table 1 - 3), GSH and PN (580 $M^{-1}s^{-1}$) and decomposition of protonated PN species (0.5 s^{-1}) at pH 7.0 and 25°C (47, 60, 61). The initial concentrations of the reacting species were the same as those used in the DNA-nicking experiments, but the rate of nicking of the plasmid DNA by PN remains unknown and hence was not taken into account in the simulation.

Figure 1 - 3 shows how the concentrations of (S)-HOMePAESe, (S)-HOMePAESeO, GSH and PN would change with time at physiological pH and 25°C. The degree of recycling (i.e. the fraction of selenoxide converted back to selenide before all PN is consumed) was approximately 25 % when equivalent concentrations (0.25 mM) of GSH, (S)-HOMePAESe and PN were used. Further simulations were carried out using the physiological range of GSH (0.1 – 10 mM), 0.25 mM (S)-HOMePAESe and 0.25 mM PN, and the degree of recycling ranged from 5 to 100 % (69).

The experimental work described in this chapter shows that phenylaminoalkyl selenoxides readily react with reducing equivalents such as GSH to regenerate the corresponding selenides. The MatLab simulation and experimental data demonstrate that the antioxidant activity of phenylaminoalkyl selenides against cellular oxidants, such as PN, is enhanced in the presence of reducing equivalents such as GSH. Therefore, in addition to their potent antihypertensive activity, PAESe and its *para*-substituted derivatives may be of future benefit in supplementing natural cellular defenses against oxidative damage.

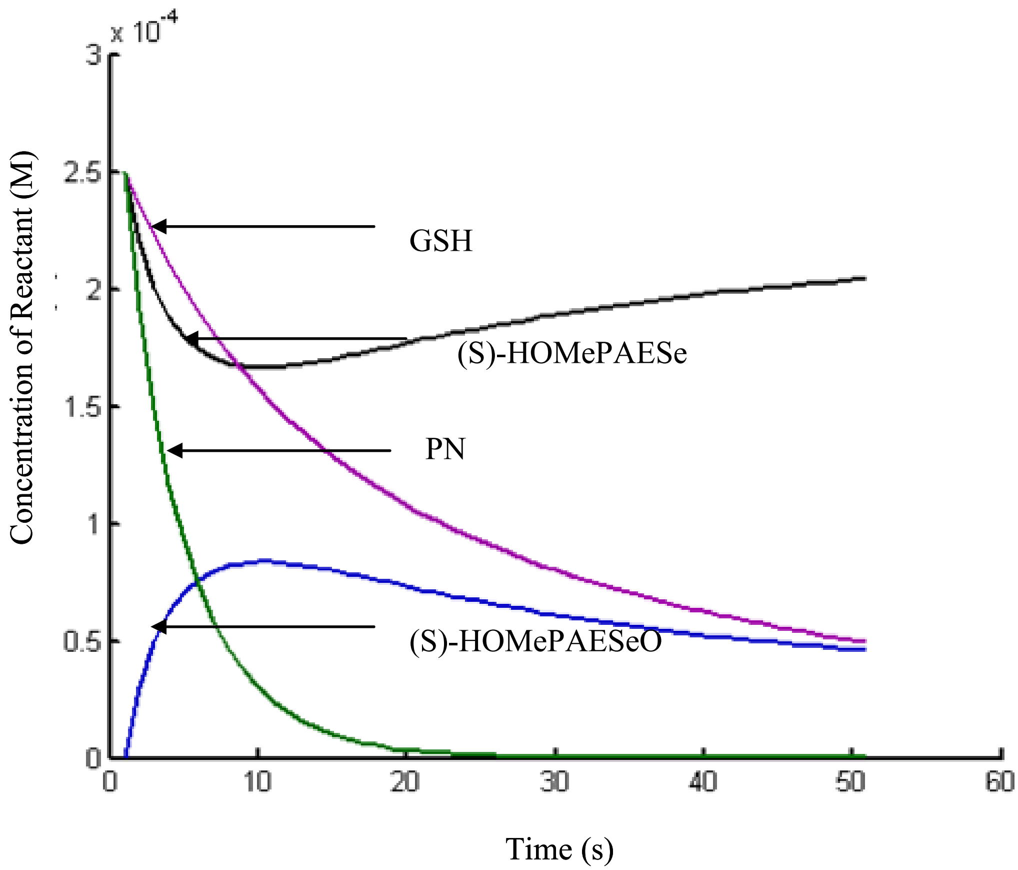

Figure 1 - 3: Predicted changes in concentration of (S)-HOMePAESe, (S)-HOMePAESeO, GSH and PN.

1 – 5: DISCUSSION

The biological role of selenium is a subject that is attracting a great deal of current interest. Selenium has been recognized as an important ‘dietary antioxidant’ and Se deficiency has been linked to various diseases (7). The biochemistry and pharmacology of selenium and its derivatives has been linked with improvement of the following conditions: cancer risk reduction, asthma, atherosclerosis, Dermatitis herpetiformis, heart attack, HIV, infertility (males), phenylketonuria (PKU), rheumatoid arthritis, cardiac arrhythmia, cardiomyopathy, Kashin-Beck disease, depression, diabetes, hypothyroidism, liver cirrhosis, macular degeneration, Osgood Schlatter disease and retinopathy (71). Therefore various synthetic organoselenium compounds have been used as antioxidants, enzyme modulators, anti - tumor, anti - microbial and anti - hypertensive agents (71).

There is an increasing body of information, which shows that selenium and its derivatives play a key role in the cellular antioxidant defense mechanism. A well-studied antioxidant role of Se arises from its presence in the form of a SeCys residue in the glutathione peroxidase (GPx) selenoenzyme family, thioredoxin reductases (TrxR), thioredoxin (TRx), selenoprotein P, selenoprotein W and others (71-73). GPx enzymes efficiently scavenge hydroperoxides and their catalytic activity is maintained by GSH. In addition GPx was shown to effectively reduce PN with a second order rate constant of $8 * 10^6\ M^{-1}s^{-1}$ (52). TrxR, selenoprotein P and W also play a role as antioxidants in the defense mechanisms that minimize the extent of oxidative stress to which the cells are exposed to (71).

Reactive oxygen and nitrogen species such as H_2O_2, hypochlorite, PN and others are formed endogenously during the normal aerobic metabolism and respiration of the cell as well as during pathological conditions associated with chronic infections and diseases. PN is a powerful oxidant formed in *vivo* from nitric oxide ($^{\cdot}NO$) and superoxide ($O_2^{\cdot-}$) with a rate constant of $4 - 20 \times 10^9\ M^{-1}s^{-1}$ (46). It reacts with a number of biological targets such as lipids, DNA, sulfhydryls, proteins and can often cause irreparable damage to cellular components. The biological reactivity of PN has resulted in the association of this species with a number of diseases such as rheumatoid arthritis, Alzheimer's disease, atherosclerosis, lung injury and many others.

Previous research showed that PAESe and its derivatives, developed as novel anti - hypertensive agents in our laboratory, react with PN to form the corresponding selenoxides with second order rate constants comparable to those of other known Se-containing antioxidants such as SeMet (59). The fact that the organoselenides containing an electron - donating substituent such as HO- or MeO- react with PN at a faster rate than those containing an electron - withdrawing substituent such as Cl- or F- in the *para* position is consistent with a bimolecular nucleophilic displacement (SN2) mechanism for the reaction of the selenide with PN. A similar mechanism was postulated by Pryor *et. al.* for the 2 electron oxidation of Met by PN and by Padmaja *et. al.* for the reaction of SeMet with PN (27, 74).

More recently, we found that phenylaminoalkyl selenides protect plasmid DNA from PN-induced damage in a manner comparable to that of SeMet. (S)-HOMePAESe at a concentration of 0.9 mM was inhibitory to the reaction of 14 μM MB6 with 1.4 mM PN at pH 7.4 and 25^{o}C, which resulted in complete separation of the MB stem in the absence of (S)-HOMePAESe. In addition, the extent of plasmid DNA protection was enhanced by the presence of GSH, which functions as a reducing agent of PN and the phenylaminoalkyl selenoxide species, formed from the reaction of the corresponding selenide and PN. Similarly, the addition of GSH resulted in the synergistically enhanced protection by SeMet against the oxidizing action of PN on dihydrorhodamine (DHR, a commonly used fluorescent probe to study PN activity) (75).

The efficiency of a scavenger at preventing PN-mediated reactions depends not only on its reactivity product but also on the ability of its reaction with the oxidant to be catalytically maintained. GSH is a common reducing equivalent present *in vivo* in millimolar concentrations and *in vivo* production of PN is expected to be continuous resulting in a steady state concentration of this oxidant and hence continuous reactivity towards the biological targets. The current project studied the efficiency of redox cycling of phenylaminoalkyl selenides by measuring the second order rate constants of the reactions between phenylaminoalkyl selenoxides and GSH spectrophotometrically and thereafter using the measured rates in a MatLab simulation.

Table 1 - 2 shows that the reduction of phenylaminoalkyl selenoxides by GSH is a rapid process and similar results have been reported with other selenoxides and thiols (76, 77). There was no observable reaction between the sulfoxide (PAESO) and GSH. Table 1 - 3 shows that the reduction of the phenylaminoalkyl selenoxides by GSH to their corresponding selenides is pH dependent and the *para*-substituent effect is less pronounced at pH 5.5 vs. pH 7.0 at 25^{o}C. As expected, the reductant : selenoxide stoichiometry was 2 : 1 and the reaction rate was first order with respect to selenoxide and GSH, respectively.

Chen *et. al.* have proposed a thioselenurane intermediate for the reaction of methylphenyl-selenoxide with GSH and our kinetic data for GSH oxidation is consistent with such an analogous thioselenurane intermediate (Figure 1 - 4, Panel A). In addition Figure 1 - 4, Panel B shows that our ρ value of (+ 0.9 ± 0.2), for rate constants measured at pH 7.0, differs markedly from the large negative ρ values reported for nucleophilic attack of GSH and other thiols on various electrophiles (77). This result is consistent with the rate limiting breakdown of the intermediate, where attack of GSH is not occurring directly on the benzylic “selen-oxy” moiety.

The kinetic data collected by our and other laboratories were then used in a MatLab simulation to confirm the effectiveness of the redox cycling of (S)-HOMePAESe in the presence of GSH and PN. The simulation showed that the extent of recycling was approximately 25 % when equivalent concentrations of GSH, PN and (S)-HOMePAESe (0.25 mM) were used in the recycling model. The extent of recycling is defined as the

Panel A

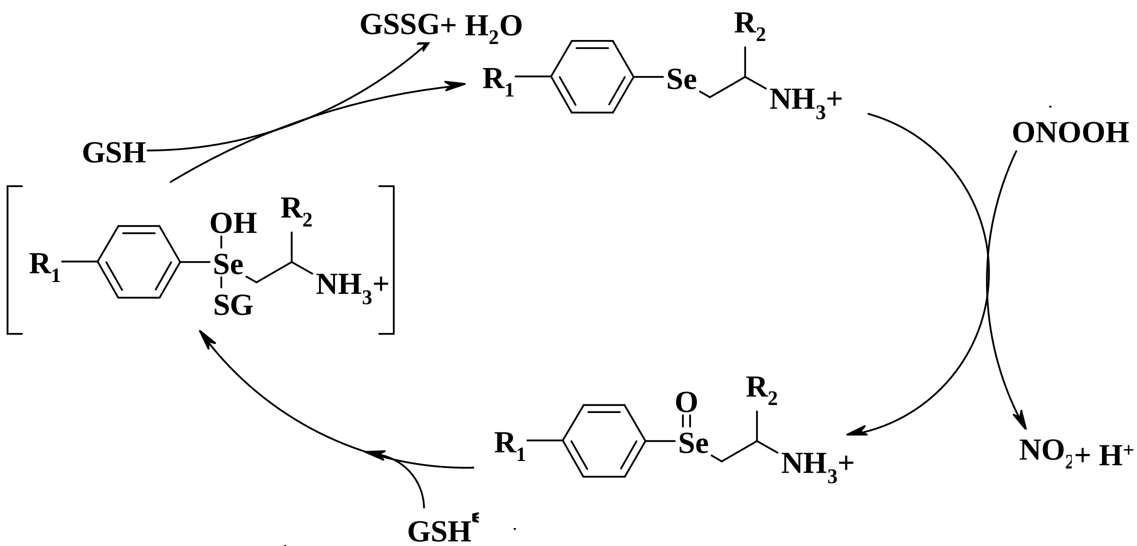

Panel B

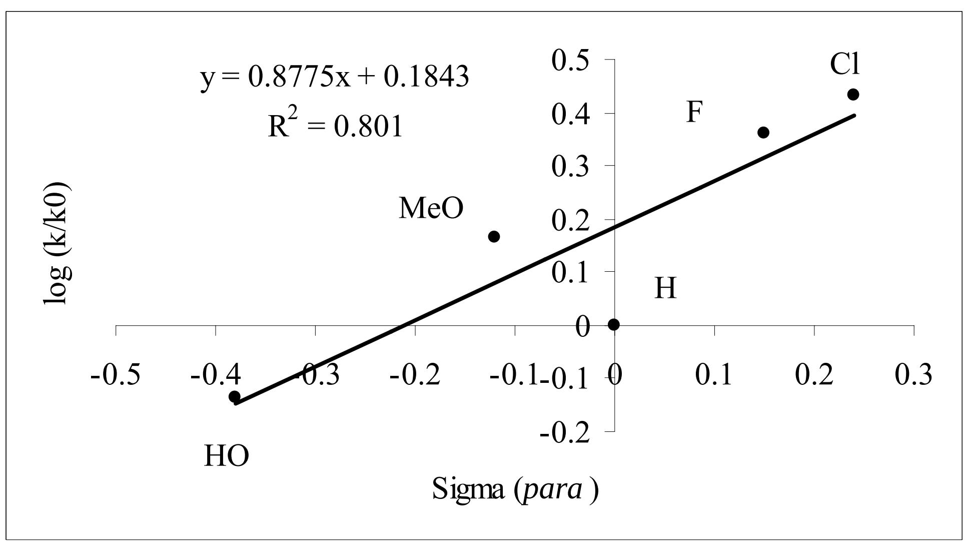

Figure 1 - 4: Panel A: Proposed mechanism of phenylaminoalkyl selenide redox cycling. Panel B: Hammett plot demonstrating the dependence of the second order rate constants for the reaction of phenylaminoalkyl selenoxides with GSH on the nature of the *para*-substituent.

fraction of (S)-HOMePAESeO converted back to its selenide form before all PN is used up in the reaction. Under physiological concentrations of GSH (0.1 to 10 mM) and 0.25 mM concentrations of (S)-HOMePAESe and PN the amount of recycling ranged from 5 to 100 %.

The simulation results agreed with the experimental data, where 0.25 mM PN was incubated with 25 ng / µl pUC19 plasmid DNA for 20 minutes at pH 8.0 and 25°C (61). The supercoiled, nicked and linear forms of the plasmid were subsequently separated by agarose gel electrophoresis and quantified by scanning (ethidium bromide was used to visualize the bands). In the presence of 0.25 mM (S)-HOMePAESe, DNA damage was reduced by 31 % (n = 6), as compared to controls in the absence of the selenide (61). Reverse phase HPLC confirmed stoichiometric formation of the corresponding (S)-HOMePAESeO (approximately 47 µM) during the PN -mediated reactions (61). Neither (S)-HOMePAESeO or GSH alone at a concentration of 0.25 mM protected plasmid DNA from PN-induced damage. However, addition of 0.25 mM GSH to the (S)-HOMePAESe / PN / DNA reaction caused a statistically significant (ANOVA/Dunnett test [n = 6]) enhancement of protection of up to 14.5 % (61). The occurrence of recycling was confirmed by the stoichiometric reduction in the selenoxide concentration using HPLC. The results are once again consistent with the theory of catalytic cycling of the selenoxide back to the selenide form by GSH in the DNA nicking assay.

Conclusion:

The results of this study provide further evidence that, in addition to their antihypertensive properties, phenylaminoalkyl selenides may also play an important role as antioxidants against powerful oxidizing species such as PN. The maintenance of the catalytic activity of phenylaminoalkyl selenides such as (S)-HOMePAESe by GSH as PN scavengers GSH was supported by kinetic studies, MatLab simulation, the results from the DNA nicking assays in the presence of (S)-HOMePAESe, GSH and PN, and the HPLC analysis of the corresponding reaction mixtures.

1 – 6: REFERENCES

1. DeSilva V (2001). The protective role of phenylaminoalkyl selenides against peroxynitrite-mediated reactions. Master's thesis, Georgia Institute of Technology.

2. Corcoran JJ, Wilson SP, Kirshner N. Flux of catecholamines through chromaffin vesicles in cultured bovine adrenal medullary cells. J Biol Chem 1984;259:6208-14.

3. Lagercrantz H. On the composition and function of large dense cored vesicles in sympathetic nerves. Neuroscience 1976;1:81.

4. Winkler J, Westhead E. The molecular organization of adrenal chromaffin granules. Neuroscience 1980;5:1803-23.

5. May SW, Herman HH, Roberts SF, Ciccarello MC. Ascorbate depletion as a consequence of product cycling during dopamine β-monooxygenase catalyzed selenoxidation. Biochem 1987;26:1626-33.

6. Wimalasena K, Herman HH, May SW. Effects of dopamine β-monooxygenase substrate analogs on ascorbate levels and norepinephrine synthesis in adrenal chromaffin granule ghosts. J Biol Chem 1989;264:124-30.

7. May SW, Pollock SH. Selenium-based antihypertensives. Drugs 1998;56:959-64.

8. Woznichak MW, Overcast JD, Robertson K, Neumann HM, May SW. Reaction of phenyaminoethyl selenides with peroxynitrite and hydrogen peroxide. Arch Biochem Biophys 2000;379:314-20.

9. Lee J, Hunt JA, Groves JT. Rapid decomposition of peroxynitrite by manganese porphryn-antioxidant redox couples. Bioorg Med Chem Lett 1997;7:2913-8.

10. Pryor WA, Squadritto GL. The chemistry of peroxynitrite: a product from the reaction of nitric oxide with superoxide. Am J Physiol 1995;268:L699-722.

11. Beckman JS, Koppenol WH. Nitric oxide, superoxide, and peroxynitrite: the good, the bad and the ugly. Am J Physiol 1996;271:C1424-37.

12. Kooy NW, Royall JA. Agonist-induced peroxynitrite production from endothelial cells. Arch Biochem Biophys 1994;310:352-9.

13. Ischiropoulos H, Zhu L, Beckman JS. Peroxynitrite formation from macrophage-derived nitric oxide. Arch Biochem Biophys 1992;298:446-51.

14. Carreras MC, Paramagnet GA, Cat SD, Padres J, Bovril A. Kinetics of nitric oxide and hydrogen peroxide production and formation of peroxynitrite during the respiratory burst of human neutrophils. FEBS Letters 1994;341:65-8.

15. Hobbs AJ, Fukutoku JM, Ignarro LJ. Formation of free nitric oxide from L-arginine by nitric oxide synthase: direct enhancement of generation by superoxide dismutase. Proc Natl Acad Sci USA 1994;91:10992-6.

16. Vasquez-Vivar J, Kalyanaraman B, Martasek P, Hogg N, Masters BSS, Karoui H. Superoxide generation by endothelial nitric oxide synthase: the influence of cofactors. Proc Natl Acad Sci USA 1998;95:9220-5.

17. Xia Y, Dawson VL, Dawson TM, Snyder S, Zweier JL. Nitric oxide synthase generates superoxide and nitric oxide in arginine-depleted cells leading to oxoperoxynitrate-mediated cellular injury. Proc Natl Acad Sci USA 1996;93:6770-4.

18. Xia Y, Zweier JL. Superoxide and peroxynitrite generation from inducible nitric oxide synthase in macrophages. Proc Natl Acad Sci USA 1997;1997:6954-8.

19. Patel RP, Mc Andrew J, Sellak H, White RC, Hanjoong J, Freeman BA, Darley-Usmer VM. Biological aspects of reactive nitrogen species. Biochim Biophys Acta 1999;1411:385-400.

20. Kissner R, Nauser T, Bugnon P, Lye PG, Koopenol WH. Formation and properties of peroxynitrite as studied by laser flash photolysis, high-pressure stopped-flow technique and pulse radiolysis. Chem Res Toxicol 1997;101:1285-92.

21. Koppenol WH, Moreno JJ, Pryor WA, Ischiropoulos H, Beckman JS. Peroxynitrite, a cloaked oxidant formed by nitric oxide and superoxide. Chem Res Toxicol 1992;5:834-42.

22. Squadritto GL, Pryor WA. Oxidative chemistry of nitric oxide: the roles of superoxide, peroxynitrite, and carbon dioxide. Free Rad Biol Med 1998;25:392-403.

23. Denicola A, Freeman BA, Trujillo M, Radi R. Peroxynitrite reaction with carbon dioxide/bicarbonate: kinetics and influence on peroxynitrite-mediated oxidations. Arch Biochem Biophys 1996;333:49-58.

24. Lermercier J-N, Padmaja S, Cueto R, Squadritto GL, Uppu RM, Pryor WA. Carbon dioxide modulation of hydroxylation and nitration of phenol by peroxynitrite. Arch Biochem Biophys 1997;345:160-70.

25. Quijano C, Alvarez B, Gatti RM, Augusto O, Radi R. Pathways of peroxynitrite oxidation of thiol groups. Biochem J 1997;322:167-73.

26. Van der Vliet A, O'Neill CA, Halliwell B, Cross CE, Kaun H. Aromatic hydroxylation and nitration of phenylalanine and tyrosine by peroxynitrite: evidence of hydroxyl radical involved? Free Radic Res 1994;29:71-82.

27. Pryor WA, Lin X, Squadritto GL. One- and two electron oxidations of methionine by oxoperoxynitrate. Proc Natl Acad Sci USA 1994;91:11173-7.

28. Alvarez B, Rubbo H, Kirk M, Barnes S, Freeman BA, Radi R. Peroxynitrite-dependent tryptophan nitration. Chem Res Toxicol 1996;9:390-6.

29. Ischiropoulos H. Biological tyrosine nitration: a pathophysiological function of nitric oxide and reaction oxygen species. Arch Biochem Biophys 1998;356:1-11.

30. Yermilov V, Rubio J, Becchi M, Frieson MD, Pignatelli B, Oshima H. Formation of 8-nitroguanine by the reaction of guanine with peroxynitrite in *vivo*. Carcinogenesis 1995;16:2045-50.

31. Douki J, Cadet J. Peroxynitrite-mediated oxidation of purine bases of nucleosides and isolated DNA. Free Radic Res 1996;24:369-80.

32. Epe B, Ballmier D, Roussyn I, Brivibia K, Sies H. DNA damage characterized with DNA repair enzymes. Nucleic Acids Res 1996;24:4105-10.

33. Groves JT, Maria SS. Peroxynitrite-induced DNA strand scission mediated by a manganese porphryn. JACS 1995;117:9578-79.

34. Salgo MG, Stone K, Squadritto GL, Battista JR, Pryor WA. Peroxynitrite causes DNA nicks in plasmid pBR322. Biochem Biophys Res Commun 1995;210:1025-30.

35. Tamir S, Burney S, Tannenbaum SR. DNA damage by nitric oxide. Chem Res Toxicol 1996;9:821-27.

36. Zingarelli B, O'Connor M, Wong H, Salzman AL, Szabo C. Peroxynitrite-mediated DNA strand breakage activates poly-adenosine diphosphate ribosyl synthase and causes cellular energy depletion in macrophages stimulated with bacterial lipopolysaccharide. J Immunol 1996;156:350-8.

37. Salgo MG, Bemudez E, Squadritto GL, Battista JR, Pryor WA. DNA damage and oxidation of thiols peroxynitrite causes in rat thymocytes. Arch Biochem Biophys 1995;322:500-5.

38. Bonfoco E, Krainc D, Ankarcrona M, Nicotera P, Lipton SA. Apoptosis and necrosis: two distinct events induced, respectively, by mild and intense insults with N-methyl-D-aspartate or nitric oxide/superoxide in cortical cell cultures. Proc Natl Acad Sci USA 1995;92:7162-66.

39. Lin KT, Xue JY, Nomen M, Spur B, Wong PY. Peroxynitrite-induced apoptosis in HL-60 cells. J Biol Chem 1995;270:16487-90.

40. Haddad IY, Pataki G, Hu P, Galliani C, Beckman JC, Matalon S. Quantitation of nitrotyrosine levels in lung sections of patients and animals with acute lung injury. J Clin Invest 1994;94:2407-13.

41. Szabo C, Ohshima H. DNA damage induced by peroxynitrite: subsequent biological effects. Nitric Oxide Biol Chem 1997;1:373-85.

42. Buttery LD, Springall DR, Chester AH, Evans TJ, Standfield EN, Parums DV, Yacoub MH, Polak JM. Inducible nitric oxide synthase is present within human atherosclerotic lesions and promotes the formation and activity of peroxynitrite. Lab Invest 1996;75:77-85.

43. Matheis G, Sherman MP, Buckberg GD, Haybron DM, Young HH, Ignarro LJ. Role of L-arginine-nitric oxide pathway in myocardial reoxygenation injury. Am J Physiol 1992;262:H616-20.

44. Schmidt K, Klatt P, Mayer B. Reaction of peroxynitrite with oxyhemoglobin: interference with photometrical determination of nitric oxide. Biochem J 1994;301:645-7.

45. Alayash AI, Ryan BA, Cashon RE. Peroxynitrite-mediated heme oxidation and protein modification of native and chemically modified hemoglobins. Arch Biochem Biophys 1998;349:65-73.

46. Floris R, Piersma SR, Yang G, Jones P, Wever R. Interaction of myeloperoxidase with peroxynitrite. A comparison with lactoperoxidase, horseradish peroxidase and catalase. Eur J Biochem 1997;215:767-75.

47. Lee J, Hunt JA, Groves JT. Rapid decomposition of peroxynitrite by manganese porphryn-antioxidant redox couples. Bioorg Med Chem Lett 1997;7:2913-8.

48. Stern MK, Jensen MP, Kramer K. Peroxynitrite decomposition catalysts. J Am Chem Soc 1996;118:8735-6.

49. Padmaja S, Squadritto GL, Lemercier JN, Cueto R, Pryor WA. Rapid oxidation of D,L-selenomethionine by peroxynitrite. Free Rad Biol Med 1996;21:317-22.

50. Asahi M, Fuji J, Takao T, Kuzuya T, Hori M, Shimonishi Y, Taniguchi N. The oxidation of selenocysteine is involved in the inactivation of glutathione peroxidase by nitric oxide donor. J Biol Chem 1997;272:19152-7.

51. Nogueira CW, Zeni G, Rocha JBT. Organoselenium and organotellurium compounds: toxicology and pharmacology. Chem Rev 2004;104:6255-85.

52. Sies H, Sharov VS, Klotz LO, Brivibia K. Glutathione peroxidase protects against peroxynitrite-mediated oxidations: a new function for selenoproteins as peroxynitrite reductase. J Biol Chem 1997;272:27812-7.

53. Brivibia K, Kissner R, Koppenol WH, Sies H. Kinetic study of the reaction of glutathione peroxidase with peroxynitrite. Chem Res Toxicol 1998;11:1398-401.

54. Masumoto H, Kissner R, Koppenol WH, Sies H. Kinetic study of the reaction of ebselen with peroxynitrite. FEBS Lett 1996;398:179-82.

55. Sarma BK, Mugesh G. Glutathione peroxidase (GPx)-like antioxidant activity of the organoselenium drug ebselen: unexpected complications with thiol exchange reactions. J Am Chem Soc 2005;127:11477-85.

56. Haenen GRMM, Paquay JBG, Korthouwer REM, Bast A. Peroxynitrite scavenging by flavanoids. Biochem Biophys Res Commun 1997;236:591-3.

57. Pannala AS, Rice-Evans CA, Halliwell B, Singh S. Inhibition of peroxynitrite-mediated tyrosine nitration by catechin polyphenols. Biochem Biophys Res Commun 1997;232:164-8.

58. Sies H. Glutathione and its role in cellular functions. Free Radic Biol Med 1999;27:916-21.

59. Brivibia K, Tamler R, Klotz L-O, Engman L, Cotgreave IA, Sies H. Protection of organotellurium compounds against peroxynitrite-mediated oxidation and nitration reactions. Biochem Pharmacol 1998;55:817-23.

60. Woznichak MM, Overcast JD, Robertson K, Neumann HM, May SW. Reaction of phenylaminoethyl selenides with peroxynitrite and hydrogen peroxide. Arch Biochem Biophys 2000;379:314-20.

61. DeSilva V, Woznichak MM, Burns KL, Grant KB, May SW. Selenium redox cycling in the protective effects of organoselenides against oxidant-induced DNA damage. J Am Chem Soc 2004;126:2409-13.

62. Roussyn I, Brivibia K, Masumoto H, Sies H. Selenium-containing compounds protect DNA from single-strand breaks caused by peroxynitrite. Arch Biochem Biophys 1996;330:216-8.

63. http://www.molecular-beacons.org/Introduction.html

64. Fang X, Li JJ, Perlette J, Tan W. Molecular beacons: novel fluorescent probes. Anal Chem 2000;1:747-53.

65. Benton DJ, Moore P. Kinetics and mechanism of the formation and decay of peroxynitrous acid in perchloric acid solutions. J Chem Soc 1970;3179-82.

66. Brivibia K, Roussyn I, Sharov VS, Sies H. Attenuation of oxidation and nitration reactions of peroxynitrite by selenomethionine, selenocysteine, and ebselen. Biochem J 1996;319:13-15.

67 May SW, Phillips RS. Asymmetric sulfoxidation by dopamine beta-monooxygenase, an oxygenase heretofore considered specific for methylene hydroxylation. J Am Chem Soc 1980;102:5981-3.

68. Woznichak MM. Investigation of the biochemical activity of phenylaminoethyl selenide compounds, synthetic substrate analogs for dopamine beta-monooxygenase. Ph D Dissertation in Chemistry and Biochemistry, Georgia Institute of Technology, Atlanta, GA 1999.

69. Anderson ME. Glutathione and glutathione delivery compounds. Adv Pharmacol 1997;38:65-78.

70. Overcast JD. Hemodynamic effects of novel selenium antihypertensive agents; Biocatalysis in organic and mixed solvents; Biotechnological production of polyesters. Ph. D Dissertation in Chemistry and Biochemistry, Georgia Institute of Technology, Atlanta, GA 2001.

71. Soriano-Garcia M. Organoselenium compounds as potential therapeutic and chemopreventive agents: a review. Curr Medic Chem 2004;11:1657-69.

72. Arscott LD, Gromer S, Schirmer RH, Becker K, Williams CH. The mechanism of thioredoxion reductase from human placenta is similar to the mechanisms of lipoamide dehydrogenase and glutathione reductase and is distinct from the mechanism of thioredoxin reductase from Escherichia Coli. Proc Natl Acad Sci USA 1997;94:3621-6.

73. Zhong L, Arner ES, Holmgren A. Structure and mechanism of mammalian thioredoxin reductase: the active site is a redox-active selenolthiol / selenenylsulfide formed from the conserved cysteine-selenocysteine sequence. Proc Natl Acad Sci USA 2000;97:5854-9.

74. Padmaja S, Squadritto GL, Lemercier JN, Cueto R, Pryor WA. Rapid oxidation of D,L-selenomethionine by peroxynitrite. Free Rad Biol Med 1996;21:317-22.

75. Assman A, Brivibia K, Sies H. Reduction of methionine selenoxide to selenomethionine by glutathione. Arch Biochem Biophys 1998;349:201-3.

76. Akerboom TPM, Sies H, Ziegler DM. The oxidation of ebselen metabolites to thiol oxidants catalyzed by liver microsomes and perfused rat liver. Arch Biochem Biophys 1995;316:220-6.

77. Chen WJ, Graminski GF, Armstrong RN. Dissection of the catalytic mechanism of isozyme 4-4 of glutathione S-transferase with alternate substrates. Biochem 1988;27:647-54.

CHAPTER 2:

Isolation and Characterization of a Stimulatory Component from Tissue of Loblolly Pine for Multiplication of Somatic Embryos

2 – 1: SUMMARY

Loblolly pine (LP, *Pinus taeda*) is the primary commercial species in southern forests covering 11.7 million hectares. Somatic embryogenesis (SE) is an effective technique to implement clonal tree production of high value genotypes from various breeding and genetic engineering programs. SE is a multi-step process, which includes initiation of somatic embryo (SME) growth from parent tree tissue, maintenance and multiplication of early stage SMEs and the maturation/germination phase. In this work, we isolated a substance from stage 2 or 3 LP female gametophyte (FG) tissue that stimulates early stage SME growth, and we then characterized this stimulatory substance as citric acid on the basis of ^{1}H NMR and mass spectrometry. We then demonstrated that topical application of citric acid to SMEs stimulates embryo colony growth at $p = 0.05$ for a combination of 3 of the 5 genotypes tested. Moreover, we find that there is a good correlation between the amount of citric acid isolated from FG tissue (65 nmoles per stage 2-3 FG) and the amount of citric acid that stimulates colony growth (25 to 50 nmoles) when applied topically to SMEs. This unique approach of isolating and characterizing a molecule from plant tissue, and investigating its role on SE processes can provide valuable information about the importance of various biological molecules at different stages of SME initiation, multiplication, development and germination.

2 – 2: INTRODUCTION

Loblolly pine (LP, *Pinus taeda*):

In the Plantae kingdom, the seed producing organisms belong to the division Pinophyta (1). Gymnosperms are a group of vascular plants whose seeds are not enclosed by a ripened ovary (fruit) (1). The Gymnosperms are further divided into orders such as Pinales (1). In North America, the order Pinales contains commercially important families such as pines (Pinaceae), cypress (Cupressaceae), etc. Forestry-associated products are the second most valuable agricultural product in USA. Loblolly pine (LP, *Pinus taeda*) is the primary commercial species in southern forests with 1-1.5 billion LP seedlings planted a year (2). Somatic embryogenesis (SE) and organogenesis are effective means to implement clonal tree production of high value genotypes from various breeding and genetic engineering programs (3 - 6).

Reproduction in Gymnosperms:

In temperate climates pines have a 3-year reproduction cycle. A mature pine tree develops both male and female organs; microsporangia (catkins) and megasporangia (conelets), respectively, in separate strobili (cones) on the same tree in late summer (1). Pollination occurs in spring, where the microsporangia are shed, while the small megasporangiate cones persist in development into mid- to late- summer, when the growth of the pollen tube and ovule stops and resumes the following spring (1). Fertilization occurs that spring and seeds mature by fall. The quality of the seed crop and their germination potential depends on temperature; light intensity and length of photoperiod; nutrition and physiology (balance of bioregulators). Under proper conditions the seed germinates and develops into a seedling, it passes through a juvenile phase and becomes again a mature pine tree capable of bearing cones and producing seeds.

Generally, the male strobili are located predominantly on the lower and side branches of the pine tree and consist of an axis on which microsporophylls are borne. On the underside of each microsporophyll, are two microsporangia that open during spring and discharge vast quantities of pollen. The pollen grain has an air sac or bladder attached to it on each side. The female strobili are typically located on the upper part of the crown and consist of an axis upon which ovuliferous scales are arranged. The ovules are encased by a nucellus and a seed coat with a distinct micropylar and chalazel ends (1).

At the time of pollination, the scales of the female strobili are slightly separated and the pollen grain comes in contact with the nucellus tissue through the micropyle end, at which point the pollen tube begins to grow into the tissue (1). During the first cell division of the nucellus, the number of chromosomes is reduced by half giving rise to the female gametophyte tissue (FG) also called the endosperm, which has a haploid number of chromosomes. Almost a year after pollination, 2 to 6 archegonia are formed at the micropylar end of the endosperm, each containing an egg cell and large cells filled with cytoplasm and lipoprotein-packed vacuoles (1). After a period of winter rest, the pollen tube finally reaches the FG tissue and fertilization takes place. The resulting zygote has a diploid number of chromosomes, half from the sperm nucleus of the pollen tube and half from the ovule nucleus (1). There are several archegonia within the FG tissue containing more ovules susceptible to fertilization, which could result in polyembryony (production of several embryos per seed). In addition, more embryos can be produced by a process referred to as cleavage polyembryony, where the embryonal mass within an archegonium gives rise to 4 separate embryos. In reality, only 1 or 2 of these embryos actually develop to maturity (1).

Embryo Development in Gymnosperms:

Embryo development in gymnosperms can be divided into several stages; the first stage is proembryogenesis, which is the time prior to the formation of the suspensor system (7). The second stage is termed early embryogenesis, which involves suspensor elongation and formation of the root meristem (7). Finally, the third stage is called late embryogenesis, which involves the formation of the polar meristems of the root and shoot (7). Scheme 2 - 1 shows a further classification system, developed by Pullman and Webb (1994), where LP embryogenesis was subdivided into nine distinct stages based on morphological characteristics of the embryo (8).

During the proembryogenesis stage, the proembryo is nourished by the egg cytoplasm through the suspensor system (7). The proembryo consists of four tiers of cells, the uppermost tier, two embryonal tiers and finally the suspensor tier. The cells of the uppermost tier are closest to the micropyle end of the archegonium and have no cell walls on the upper side, which is contiguous with the egg cytoplasm. The cells of the embryonal tiers divide to form a conspicuous mass of cells while the cells of the suspensor tier elongate (7).

In the two later stages of the embryo development, the nourishment is provided by the FG, which contains various cellular metabolites (starch, proteins etc.). During the second stage of embryogenesis, proliferation and elongation of the suspensor cells takes place, embryonal call mass continues to grow and the protoderm is established (7). In these early stages of embryo development, the whole embryo-suspensor complex is an intertwined mass of tubular and isodiametric cells.

During the late embryogenesis phase, cellular differentiation in the embryonal mass takes place such that a maturing zygotic embryo consists of a shoot apical meristem, embryonic cortex, epidermis, embryonic pith, procambium, root cap and root meristem. Initially, a clear demarcation between the cells of the proximal apex and the suspensor region is established. The cells of the proximal region to the micropyle are the forerunners of the root cap, while the cells of the distal region become the hypocotyl, shoot apex and cotyledons.

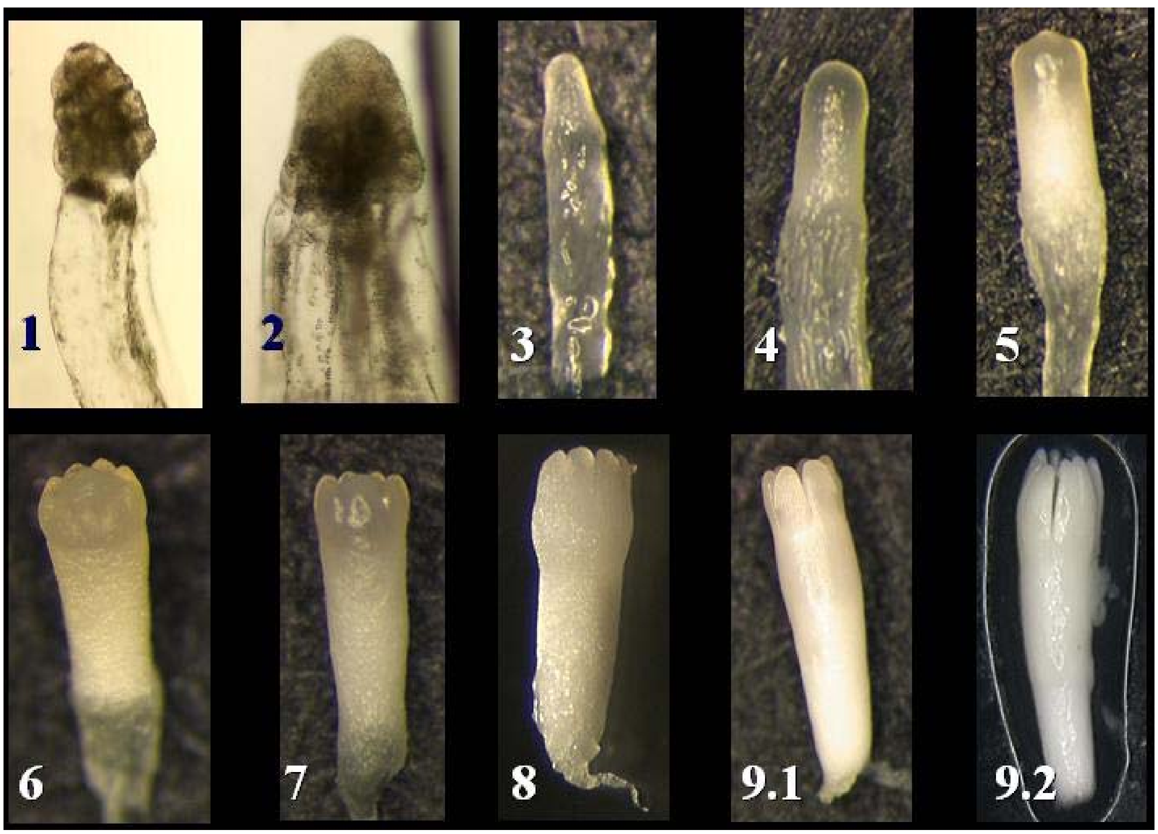

Scheme 2 - 1: LP Zygotic Embryogenesis – Stages 1 through 9.2.

The pith is one of the first tissues in the hypocotyl-shoot axis region to be defined, and is surrounded by dividing cells, which become the origin of the procambium before cotyledons are established (7). The apical meristem subsequently gives rise to the cotyledons and to the epicotyl. Further development of the embryo subsequently involves increase in size and tissue differentiation. The primary meristems are precursors of the basic plant organization: epidermal tissue is derived from the protoderm; primary conducting tissue is formed from procambium, and fundamental tissue (parenchyma, sclerenchyma and collenchyma) originates from the ground meristem (1). The cells of permanent tissues can again become capable of division, giving rise to secondary meristems: vascular cambium (bark), cork cambium and phellogen (1).

LP Somatic Embryogenesis:

SE is a technique of producing embryos asexually in tissue culture, where somatic embryos (SMEs) develop into structures resembling zygotic embryos through a characteristic embryogenesis process but in the absence of gamete fusion. SE is a multi-step process, which includes initiation of SME growth from parent tree tissue, maintenance and multiplication of stage 1 to 2 SMEs; the development and maturation phase and the germination phase (8 - 11). Scheme 2 - 2 shows the morphological changes in the structure of the somatic embryo as it goes through various stages of the development process.

In pines, the initiation step includes selection of an explant, such as a female gametophyte (FG) containing zygotic embryo(s), from a female pollinated cone (12). In LP the megagametophyte (FG) containing one or more zygotic embryos is used as the explant, where an embryogenic mass containing at least one SME extrudes from the micropylar end of FG in successfully initiated tissue culture systems (11). The plant growth regulators, auxin (2,4-dichlorophenoxyacetic acid [2,4-D]) and cytokinin (N6-benzyladenine) are usually present in the LP initiation medium.

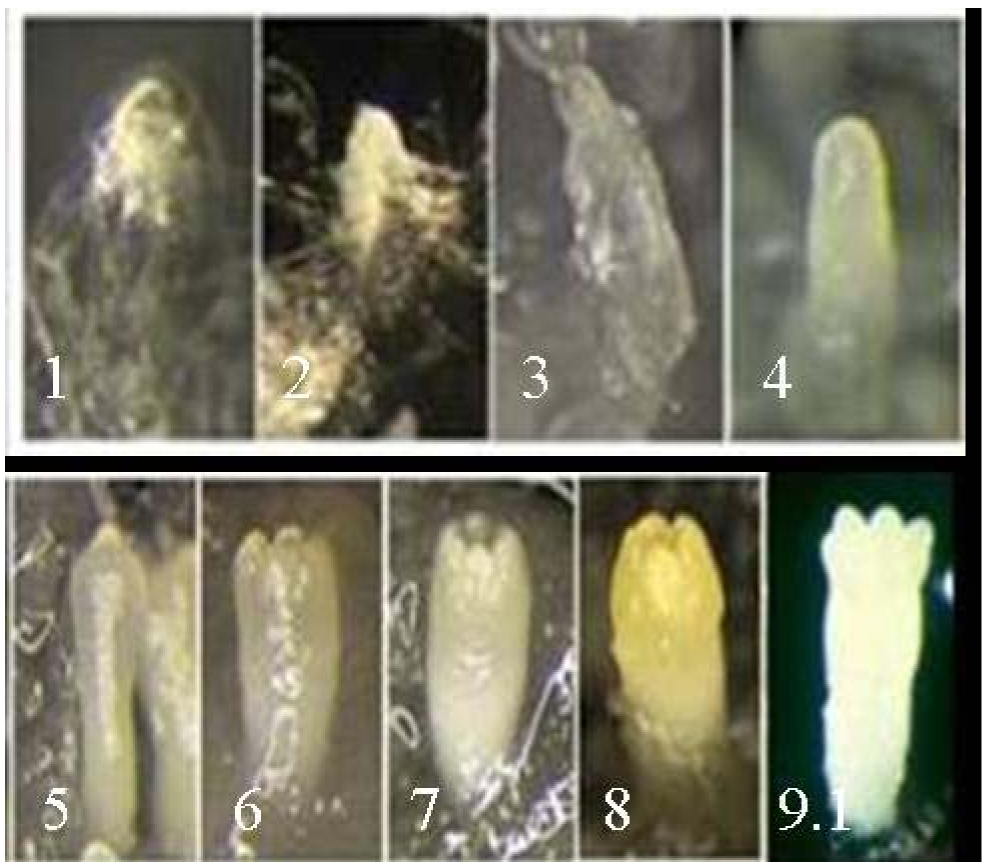

Scheme 2 - 2: LP Somatic Embryogenesis – Stages 1 through 9.1.

The importance of concentration of plant growth hormones in explant tissues, as well as the nature, ratio and level of plant growth regulators (such as auxins, cytokinins, gibberellins, abscisic acid, ethylene, brassinosteroids and polyamines) in the initiation medium, has been underscored by research reported by various laboratories (13).

The initiation phase is followed by the maintenance and multiplication step, which ensures that numerous early stage SMEs can be produced from the previously initiated culture. Maintenance media can be liquid or semi-solid and the former demonstrated higher multiplication rates, ease of manipulation of SE cultures and the added advantage of continuous mixing of reagents that SMEs are exposed to.

During the development and maturation phase, SMEs are induced to develop into late stage embryos capable of germination. Maturation of SMEs is typically achieved on a semi-solid medium over 3 to 6 weeks. Unfortunately many of the embryos do not develop beyond stage 9.1 and hence exhibit no or low germination (5). The germination assay involves the transfer of mature embryos on a basal medium for 6 to 8 weeks under a 16 hour light / 8 hour dark photoperiod. At the end of the growth period the root and shoot growth are quantified.

<u>Usefulness of SE in LP:</u>

Forestry products are widely used in the paper making industry, construction, as a source of energy and other ways. There are a number of ways to increase the yield of favorable tree genotypes including breeding programs of preferred trees, plant cutting, micro propagation, mass control pollination and, finally, clonal forestry, where either superior tree genotypes or genetically engineered trees are mass produced. Depending on the intended use of the preferred tree genotype or transgenic tree, desirable tree characteristics that are propagated from generation to generation include disease resistance, increased growth rates, insect resistance, favorable lignin to cellulose ratio for minimizing the cost of paper making etc.

The technique of SE is currently used to mass produce industrially and environmentally important tree families such as Eucalyptus and Populus. Mass production of favorable LP genotypes by the process of SE has lagged behind that of the formerly mentioned families. Factors that limit commercialization of LP SE include low initiation rates, low culture survival, the inability of SMEs to fully develop and germinate, and recalcitrance of favored genotypes over time. Additional concerns with LP SE are plant tissue maintenance (resources and labor costs), time consuming field trials and other factors. Improvements in the various phases of LP SE processes are therefore needed (14).

Bottlenecks in SE of Loblolly Pine:

Numerous improvements in the preparation of initiation, multiplication, maturation and basal culture media for LP SE and organogenesis have been made over the years via supplementation with metal ions, endogenous and chemically synthesized plant growth regulators, amino acids, vitamins, organic acids, activated charcoal, carbohydrates and other additives (5, 6, 11, 15-21). The changes in composition of initiation, multiplication and maturation media for SE were based either on a trial and error methodology, or more systematically on analyses of FG and zygotic embryo tissue from various stages of development. In previously published work FG and zygotic embryo tissue from different stages of development, obtained from several tree sources, was analyzed for organic acid content and key elemental composition by gas chromatography / mass spectrometry (GC/MS) and inductively coupled emission spectroscopy, respectively (5, 14). Based on the changes in concentration of the analytes across stages in development, the appropriate SE growth media were supplemented with specific amounts/ratios of organic acids, vitamins and / or elements. For example, altering the concentrations of boron, calcium, potassium, and iron in the maturation media resulted in an increase in LP cotyledonary embryo yields. However, the stage to which SMEs matured and the germination potential of the embryos were not changed by these media changes (19). Supplementation of SE initiation media with various combinations of Vitamin B12 and E, α-ketoglutaric, succinic and pyruvic acids resulted in increases in initiation of LP SMEs (17).

Recent studies have shown that a water extract from LP FG tissue of stage 2 or 3 promotes growth of early stage LP SMEs in a statistically significant manner as shown in figure 2 - 1. Therefore, the aim of this study was to isolate, characterize and quantify the stimulatory material present in LP FG tissue of stages 2 and 3. We report herein that the stimulatory material in water-extracted FG tissue was isolated by a protocol involving HPLC fractionation as shown in scheme 2 - 3 and then characterized as citric acid on the basis of ^{1}H NMR and mass spectrometry (MS). The amount of citric acid in FG tissue of stage 2 or 3 was quantified via HPLC, and topical application of the appropriate citric acid concentration to the surface of early stage SMEs was found statistically stimulatory to embryo colony growth for a combination of 3 out of the 5 genotypes tested. This unique approach of isolating and characterizing a molecule from plant tissue that exerts a desired effect on one or more stages of the SE processes can be used with plant species other than LP. Investigations of this nature not only improve the effectiveness of SE media but also provide valuable information about the importance of various biological molecules at different stages of SME initiation, multiplication, development and germination.

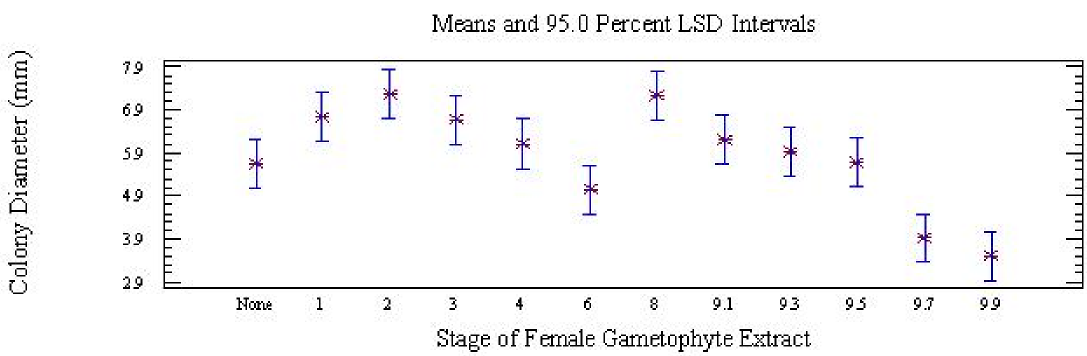

Figure 2 - 1: The effect of FG Extract from Various Stages on the Multiplication of SMEs, see "MATERIALS AND METHODS" for further details.

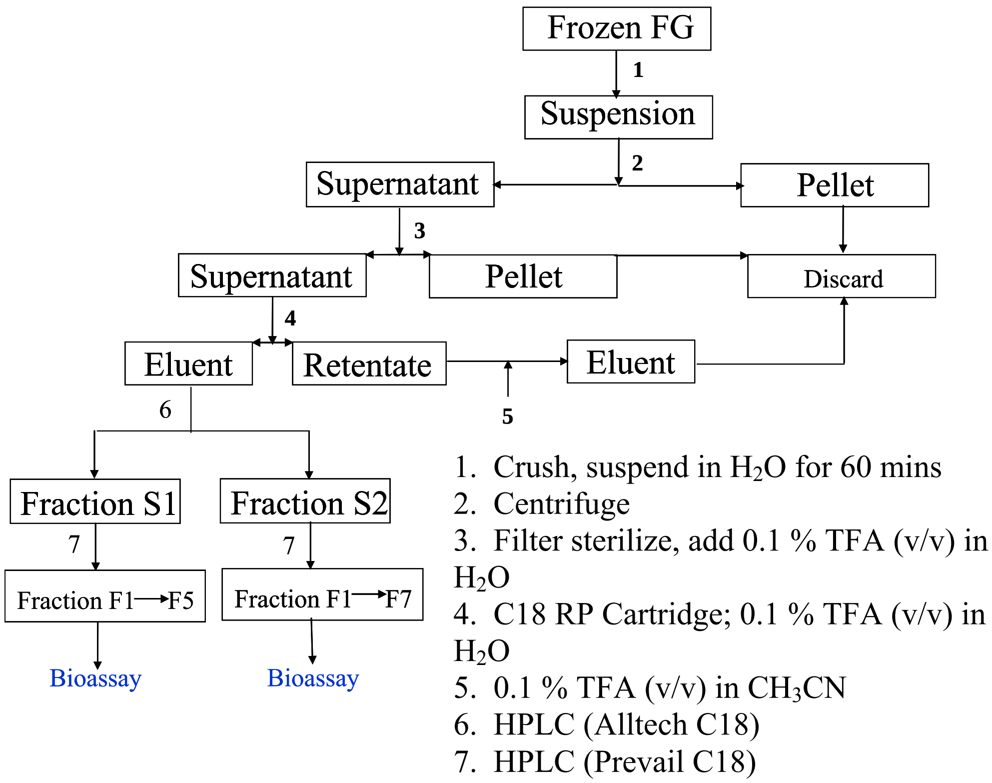

Scheme 2 - 3: Overall Purification Protocol of Stage 2 and 3 FG Material

2 – 3: MATERIALS AND METHODS

Materials:

Abscisic acid (ABA), N-(4-aminobenzoyl)-glycine, ammonium nitrate, 6-benzylaminopurine (BAP), biotin, boric acid, calcium nitrate tetrahydrate, cobalt chloride hexahydrate, copper sulfate pentahydrate, folic acid, Gelrite, glutamine, glycine, iron sulfate heptahydrate, kinetin, magnesium chloride hexahydrate, magnesium nitrate hexahydrate, magnesium sulfate heptahydrate, manganese sulfate heptahydrate, N-morpholinoethanesulfonic acid (MES), myo-inositol, nicotinic acid, *m*-nitrobenzyl alcohol, potassium iodide, potassium hydroxide, thiamine hydrochloride and zinc sulfate heptahydrate were obtained from Sigma Aldrich (St Louis, MO, USA). Citric acid, Corning Costar Cell culture plates, HPLC grade CH_3OH, CH_3CN, H_2SO_4 and trifluoroacetic acid (TFA) were obtained from Fisher Scientific (Pittsburgh, PA, USA). Casamino acids were purchased from Beckton Dickinson (Franklin Lanes, NJ, USA). 2,4-Dichlorophenoxyacetic acid was purchased from Chem Service (West Chester, PA, USA). DL-isocitric acid was obtained from Acros Organics (Morris Plains, NJ, USA). Potassium dihydrogen phosphate, potassium hydrogen phosphate, potassium nitrate, sodium EDTA and sucrose were obtained from JT Baker (Phillipsburg, NJ, USA). Prevail C18 column (250 x 4.6 mm, 5 μm particle size) and Prevail guard cartridges (4 x 3 mm) were purchased from Waters Corporation (Milford, MA, USA). Allsphere semi-prep C18 column (250 x 10 mm, 5 μm particle size) was obtained from Alltech (Deerfield, IL, USA). C18 guard cartridges (4 x 3 mm) were purchased from Phenomenex (Torrance, CA, USA). Vydac C18 column (150 x 0.3 mm, 3 μm particle size) was obtained from Grace Vydac (Hesparia, CA, USA). Nexus C18 solid phase extraction cartridges were obtained from Varian (Palo Alto, CA, USA). Acrodisc syringe filter (0.2 μm HT Tuffryn membrane, low protein binding and non-pyrogenic) was purchased from Pall Life Sciences (East Hills, NY, USA).

Plant Material:

Loblolly pine (LP, *Pinus taeda*) cones were collected from open – pollinated mother trees, UC5-1036 (Union Camp located in a seed orchard near Belville, GA, USA) and S4PT6 (seed orchards located in LA and TX, USA). The cones were received within 24 to 48 hours after the collection period and stored at 4^{o}C. Cones were pried open, and the female gametophyte (FG) extracted from seeds cracked open with a hemostat. FG was slit open, and the dominant embryo(s) removed and examined under the dissecting microscope in order to determine the stage of the embryo. Twenty embryos of the same stage were collected in a vial, frozen under liquid nitrogen and stored at –70^{o}C. The corresponding FGs (20) were similarly stored. The embryos were staged using the system of Pullman and Webb (1994). Typically stages 2 to 3 occurred in mid-June, approximately 4 weeks after estimated fertilization.

FG Tissue Extraction:

FG frozen tissue (from stage 2 or 3) was crushed into a fine powder using a mortar and pestle under liquid nitrogen. The resulting powder was extracted with deionized (DI) water (2 ml per 20 FGs) by stirring the suspended FG tissue at 4^{o}C for 60 minutes. The mixture was subsequently centrifuged at 20,000 × g and 25^{o}C for 5 minutes and the supernatant collected. The pellet was washed with minimal DI water, centrifuged and the wash combined with the supernatant. FG extract was filter-sterilized through a 0.2 μm membrane and treated with a 0.1 % (v/v) aqueous TFA solution for 10 minutes at 0^{o}C. The resulting mixture was centrifuged using a bench top Damon/IEC centrifuge at approximately 10,000 × g and 25^{o}C for 5 minutes, the pellet discarded, the supernatant collected and lyophilized to dryness. The resulting lyophil was dissolved in 1 ml of 0.1 % (v/v) aqueous TFA solution, applied onto a Varian Nexus solid-phase cartridge and the flow-through collected. The cartridge was eluted with 1 ml of 0.1 % (v/v) TFA and the eluent combined with the previously collected flow - through, which was lyophilized to dryness.

HPLC Fractionation of FG Extract:

The first HPLC fractionation was carried out on a Waters LC Module I Plus HPLC equipped with Millenium chromatography manager software (Milford, MA, USA) and using an Allsphere ODS-2 column with a Phenomenex ODS-2 guard cartridge. Lyophilized FG extract was dissolved in 200 µl of DI water and one-half was fractionated in each of the two separate HPLC runs, the fractionation was carried out under linear gradient elution with CH_3OH (0.1 % [v/v] TFA) (A) / H_2O (0.1 % [v/v] TFA) (B) mobile phases: 0 to 12 mins (3% A / 97 % B), 12 to 25 mins (3% A / 97% B to 14% A / 86 %B), 25 to 45 mins (14% A / 86% B to 25% A / 75% B) with UV detection at 215 nm and a flow rate of 4.7 ml min^{-1}. Fractions S1 through S6 were collected and lyophilized to dryness, retention times are listed in Table 2 - 1.

The next HPLC fractionation was performed on the same apparatus using a Prevail C18 column with a corresponding Prevail C18 guard cartridge. Fraction S2 was dissolved in 200 µl of DI water and injected in two separate aliquots onto the column, fractionation was carried out under isocratic elution conditions with aqueous 0.1 % (v/v) TFA (UV detection at 215 nm and a flow rate of 0.7 ml min^{-1}). Fractions S2-1 through S2-7 were collected and lyophilized to dryness; corresponding retention times are listed in Table 2 - 2.

Preparation of maintenance and multiplication media (1133 and 1250):

Plant Tissue Culture:

Media components and concentrations (1133 and 1250) are listed in Table 2 - 3. Typically the media were prepared by combining all the reagents with the exception of abscisic acid (ABA), glutamine and citric acid in DI water, adjusting the pH to 5.7 with 1 N KOH and autoclaving the resulting mixture in absence (1133) or presence (1250) of Gelrite using the liquid cycle (highest temperature of 121°C). ABA, glutamine and sometimes citric acid were filter-sterilized through a 0.2 µm membrane, added to the media mixture and 2 ml poured into each well of a cluster plate.

Table 2 - 1: Effect of fractionated FG extract on early-stage SME growth (HPLC fractionation #1).

Fraction (treatment in bioassay)	Retention time (min)	Change in colony diameter (mm) (2 bioassays)
S1	2 to 3.7	0.10, *2.25
S2	3.7 to 4.5	*0.90, *2.10
S3	4.5 to 5	0.61, *1.37
S4	5 to 7	0.06, 0.26
S5	12.5 to 14.5	- 0.02, 0.44
S6	23.5 to 27	- 0.15, 0.38

*Represents a statistically significant change in mean colony diameter (95% LSD intervals) of FG-extract-treated SMEs compared to the control treatment.

Table 2 - 2: Effect of fractionated FG extract on early-stage SME growth (HPLC fractionation #2).

Fraction (treatment in bioassay)	Retention time (min)	Change in colony diameter (mm) (2 bioassays)
S2-1	3.5 to 5.5	- 0.37, 0.11
S2-2	6.0 to 8.0	0.03, - 0.01
S2-3	8.0 to 10.0	0.62, - 0.76
S2-4	10.0 to 13.0	0.32, - 0.58
S2-5	14.5 to 15.0	- 0.12, - 0.30
S2-6	15.5 to 17.0	*1.81, *3.19
S2-7	17.0 to 18.5	- 0.15, - 0.75

*Represents a statistically significant change in mean colony diameter (95% LSD intervals) of FG-extract-treated SMEs compared to the control treatment.

Table 2 - 3: Maintenance and Multiplication Media Components

Media Components	1133 (mg/L) Maintenance Medium	1250 (mg/L) Multiplication Medium
NH_4NO_3	603.8	603.8
KNO_3	909.9	909.9
KH_2PO_4	136.1	136.1
$Ca(NO_3)_2.4H_2O$	236.2	236.1
$MgSO_4.7H_2O$	246.5	246.5
$Mg(NO_3)_2.6H_2O$	256.5	256.5
$MgCl_2.6H_2O$	101.7	101.7
KI	4.15	4.15
H_3BO_4	15.5	15.5
$MnSO_4.H_2O$	10.5	10.5
$ZnSO_4.7H_2O$	14.4	14.4
$Na_2MoO_4.2H_2O$	0.125	0.125
$CuSO_4.5H_2O$	0.125	0.125
$CoCl_2.6H_2O$	0.125	0.125
$FeSO_4.7H_2O$	6.95	9.95
Na_2EDTA	9.33	9.33
Sucrose	30,000	30,000
Myo-inositol	1,000	1,000
Casamino Acids	500	500
L-Glutamine	450	450
Thiamine.HCl	1.0	1.0
Pyridoxine HCl	0.5	0.5
Nicotinic Acid	0.5	0.5
Glycine	2.0	2.0
MES	-	250
Biotin	-	0.05
Folic Acid	-	0.5
2,4-D	1.1	1.1
BAP	0.45	0.45
Kinetin	0.43	0.43
Abscisic Acid	1.3	1.3

LP SME Multiplication Assay:

SME of stage 1 or 2 was isolated from liquid maintenance medium 1133 and placed on approximately 2 ml of 1250 medium. Lyophils from HPLC fractions were dissolved in 2 ml of 10 mM MES (pH 5.7), pH adjusted to 5.7 with KOH if necessary and filter-sterilized through a 0.2 μm membrane. 50 μl of each fraction (equivalent to material from half a FG) was applied to each SME previously placed on medium 1250 (4 replicates of 10 embryos per treatment) and allowed to grow in the dark at 23-25^{o}C for 4 to 6 weeks. The control experiment (treatment 0) consisted of 40 embryos with no extract applied to them. At the end of the growth period the embryogenic tissue diameter was measured with a dissecting microscope (typically a single stage embryo is on average 1.0 mm in size and will grow to form an embryogenic mass 5 to 9 mm in diameter). The data was evaluated by multifactor analysis of variance, significant differences between treatment means were determined by the Multiple Range Test at 95 % or 90 % level of significance using Statgraphics Plus Version 4.0.

Characterization of S2-6 via MS and ^{1}H NMR:

Experiment 1: Electron spray ionization liquid chromatography / mass spectrometry (ESI LC/MS) protocol:

The LC-MS system was comprised of an Applied Biosystems QSTAR-XL quadrupole / time – of - flight tandem mass spectrometer (TOF MS MS) interfaced with capillary LC pumps, autosampler, and a micro switching device. LC fractionation of S2 was carried out on a Vydac C18 column at a flow rate of 4 μL min^{-1} and UV detection at 210 nm using gradient elution with 98:2 H_2O:CH_3CN (0.05 % [v/v] TFA) (A) / 20:80 H_2O:CH_3CN (0.04 % [v/v] TFA) (B) mobile phases. The elution protocol consisted of a 1 minute column pre-equilibration with 100% A, followed by 5 μL sample injection, a 5 minute sample load and wash with 100% A, a 45 minute linear gradient to 100% B, and a 5 minute hold at 100% B. The capillary HPLC was directly connected to the QSTAR-XL where subsequent dispersal and desolvation of the eluent occurred. The turbo ion spray needle was held at –3500 V and the declustering and focusing potentials were held low at -40 V and -200 V, respectively to prevent ions from fragmenting at the source. Subsequently formed ions were detected using negative ion TOF MS acquisitions from 200 to 2000 atomic mass units (AMU).

Experiment 2: Fast Atom Bombardment (FAB) MS Analysis of fraction S2-6 and citric acid:

FAB MS was carried out on the VG-70 SE two sector mass spectrometer equipped with an AUF axis photomultiplier detector (8 KV acceleration voltage). Exact mass of fraction S2-6 was determined to be 191.0197, corresponding to molecular weight of citric acid within 2.5 ppm (in negative mode). *m*-Nitrobenzyl alcohol (employed as the matrix) and N-(4-aminobenzoyl)-glycine were used as low and high molecular weight calibrators respectively.

Experiment 3: ^{1}H NMR of S2-6 and citric acid were determined on a 500 MHz Bruker DRX instrument. ^{1}H NMR chemical shifts in D_2O of citric acid were δ 2.96 (d, 2H), δ 2.78 (d, 2H) and of S2-6 in D_2O were δ 2.88 (d, 2H), δ 2.73 (d, 2H), respectively.

<u>HPLC quantitation and further analysis of S2-6:</u>

The amount of citric acid present in S2-6 was quantified using 0.5 to 10 mM citric acid calibration curve obtained on the Prevail C18 column equipped with the Prevail C18 guard cartridge under isocratic elution conditions with 0.1 % (v/v) aqueous TFA and UV detection at 215 nm. S2-6 fraction spiked with citric acid was then further analyzed under three isocratic elution conditions with 99:1 H_2O (0.1 % [v/v] TFA):CH_3OH (0.1% [v/v] TFA) (MP1), H_2O (0.1 % [v/v] TFA) (MP2) and H_2SO_4 (pH 1.5) (MP3).

<u>Effect of Citric Acid and Other Additives on LP SME Multiplication Assay:</u>

Experiment 1: Dependence of SME growth on concentration of topically applied citric acid

A 50 μl aliquot of 0.05 mM, 0.1 mM, 0.5 mM, 1.0 mM or 2.0 mM citric acid in 10 mM MES (pH 5.7), filter sterilized through a 0.2 μm membrane, was applied to each stage 1-2 SME of genotype 500 on medium 1250 (4 replicates of 10 embryos per treatment) and allowed to grow in the dark at 23-25^{o}C for 4 to 6 weeks. In treatment 0 (control) no extract was applied to the early stage SMEs. Additional experiments showed that higher concentrations of citric acid (greater than 2 mM) are not stimulatory to SME at $p = 0.05$ (data not included).

In control experiments, 50 µl of 10 mM MES buffer (pH 5.7) or 50 µl of 10 mM MES buffer with an appropriate amount of KOH necessary to neutralize 0.5 mM citric acid (pH 6.0) or 1.0 mM citric acid (pH 6.3), filter sterilized through a 0.2 µm membrane, was added to individual embryos of genotype 500 on medium 1250.

In additional control experiments 50 µl of 0.5 mM or 1.0 mM glutaric acid in 10 mM MES (pH 5.7), filter sterilized through a 0.2 µm membrane, was applied to each stage 1-2 SME of genotype 500 on medium 1250.

Experiment 2: Comparison of 3 different methods of application of citric acid on SME growth:

50 µl of 0.5 mM or 1 mM citric acid in 10 mM MES buffer (pH 5.7), filter sterilized through a 0.2 µm membrane, was added to each stage 1-2 SME of genotype 500 on medium 1250 (4 replicates of 10 embryos per treatment) or stage 1-2 SMEs were placed on medium 1250 containing 0.0125 mM or 0.025 mM citric acid (added to 1250 medium before or after autoclaving). The control experiment consisted of 40 embryos grown in the absence of citric acid.

Experiment 3: Effect of topically applied 0.5 mM and 1 mM citric acid on SME growth of 3 genotypes.

50 µl of 0.5 mM or 1.0 mM citric acid in 10 mM MES (pH 5.7), filter sterilized through a 0.2 µm membrane, was applied to each stage 1-2 SME of 3 different genotypes placed on medium 1250 (4 replicates of 10 embryos of a single genotype per treatment) and allowed to grow in the dark at 23-25^{o}C for 4 to 6 weeks. The control experiment (treatment 0) consisted of 40 embryos with no extract applied to them.

2 – 4: RESULTS

Isolation of Stimulatory Material from Early Stage LP FG Tissue:

Studies carried out by Pullman *et. al.* (2007) have shown that a water extract from FG tissue of stage 2 or 3 is stimulatory to growth of an early stage SME as compared to control experiments where no FG extract is applied to the embryos. Therefore, a protocol involving HPLC with aqueous-organic gradient and isocratic elution profiles was developed to isolate the stimulatory component present in FG tissue. The final procedure for isolating the stimulatory material from early stage FG material (trees S4PT6 and UC5-1036) entailed initial water extraction from crushed tissue for an hour at 4^{o}C, removal of proteins by TFA precipitation, and further purification of FG extract using a Nexus Varian extraction cartridge. The TFA - eluted fraction from the cartridge was further fractionated on a C18 column with gradient aqueous / organic elution. Fractions S1 (2 to 3.7 min), S2 (3.7 to 4.5 min) and S3 (4.5 to 5 min) were found to be stimulatory at $p = 0.05$ to early stage SME growth of genotype 500 as compared to the control treatment, where no fractionated FG material was applied to the embryos (Figure 2 - 2 and Table 2 - 1). Subsequently, only fraction S2 was found to be consistently stimulatory at $p = 0.05$ to early stage SME growth, where the mean colony diameter increased by 0.90 mm (bioassay 1) and 2.10 mm (bioassay 2) as compared to the control treatments. Hence one can conclude that fractions S1 and S3 likely contain molecules stimulatory to early stage SME growth that are more sensitive to concentration changes than the compounds present in fraction S2.

ESI LC/MS analysis indicated that S2 contains several other components, which were further fractionated on a Prevail C18 column under isocratic elution conditions with an aqueous acidic mobile phase (Figure 2 - 2, inset). The sixth fraction, S2-6 (15.5 to 17 min), was found to be stimulatory to multiplication of early stage SMEs of genotype 500

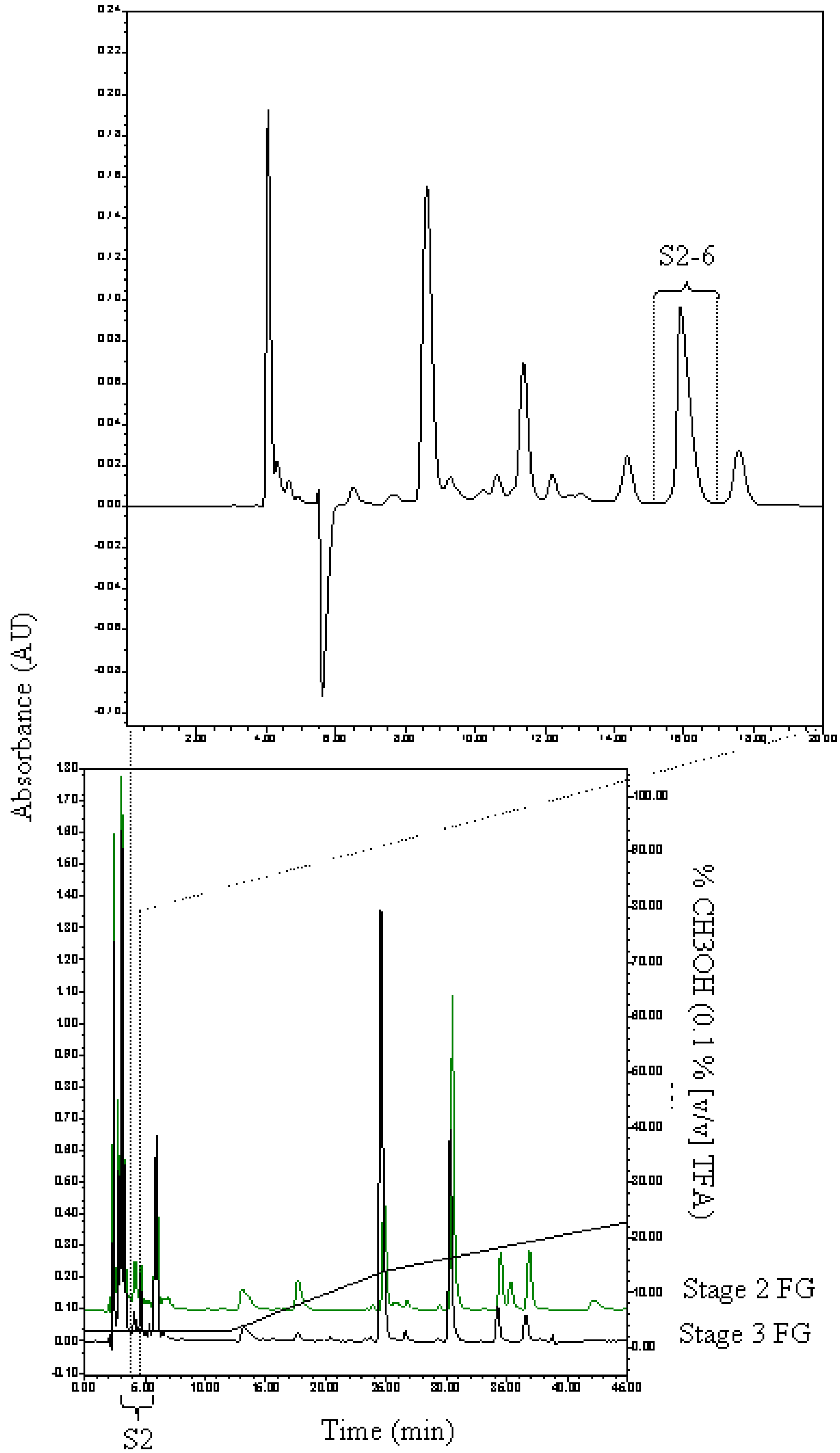

Figure 2 - 2. HPLC fractionations of stage 2 or 3 FG tissue extracts performed as described in the MATERIALS AND METHODS section. See tables 2 - 1 and 2 - 2 for further details.

compared to the control at $p = 0.05$ in two separate bioassays. The mean embryo colony diameter increased by 1.81 mm (bioassay 1) and 3.19 mm (bioassay 2) as compared to the controls where early stage SMEs grew in the absence of S2-6 (Table 2 - 2). Fraction S1 was also further fractionated under identical elution conditions but none of the separated components were found to be consistently stimulatory at $p = 0.05$ to early stage SME growth (data not shown).

Characterization of Stimulatory Material from Early Stage LP FG Tissue:

Fraction S2-6 was subsequently analyzed using FAB MS in negative mode. A peak at 191 (m/z) was observed in the spectrum, which at an exact molecular weight of 191.01965 matched a compound of a molecular formula ($C_6H_7O_7$) within 2.4 ppm (Figure 2 - 3). To conclusively characterize the structure of S2-6, the fraction was analyzed by ^1H NMR and found to consist of citric acid. Further HPLC analysis of S2-6 spiked with citric acid under three different elution conditions supported the conclusion that the only component in this fraction was citric acid (Figure 2 - 4, panel A). It should be noted that citric and isocitric acids (structural isomers) have different retention times under the same elution conditions as depicted in Figure 2 - 4, panel B.

The amount of citric acid in S2-6 from different experiments was quantified using HPLC as described in the experimental section. On the average, 20 FGs from stage 2 or 3 were found to contain 1.30 μmoles of citric acid, which corresponds to 32.5 nmoles in half a megagametophyte. Therefore, citric acid in the range of 25 to 50 nmoles was used in the treatment of a single early stage SME in the growth assay. This is in good agreement with a previous report where the amount of citric and isocitric acids in FG tissue from various stages of development was quantified by GC/MS and found to be 33.3 nmoles in half a FG of stage 3 (14).

Further bioassays to identify the concentrations of citric acid that would be most stimulatory to early stage SME colony growth were carried out. It was found that

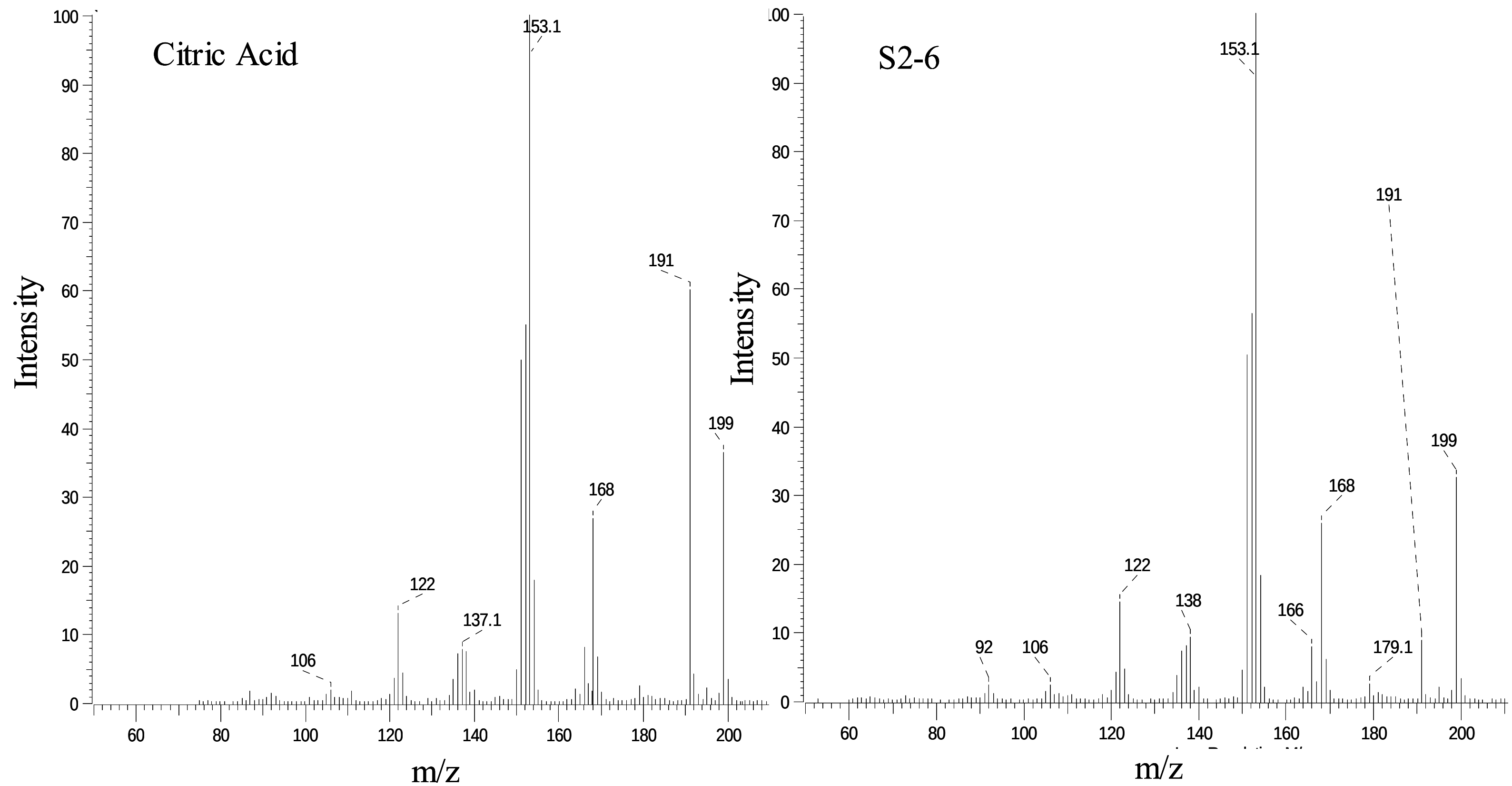

Figure 2 - 3. FAB mass spectra of citric acid and S2-6.

Panel A

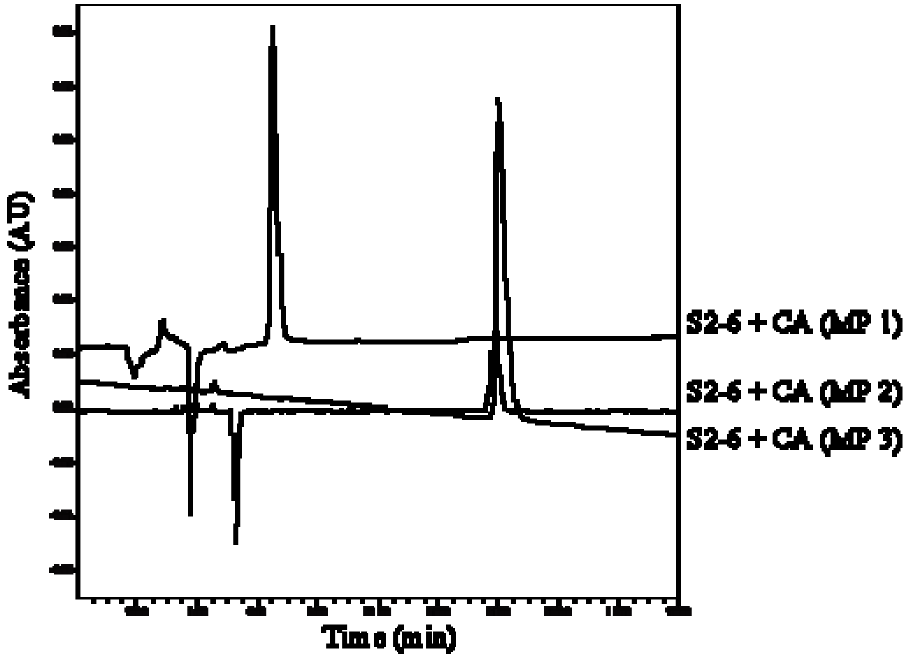

Panel B

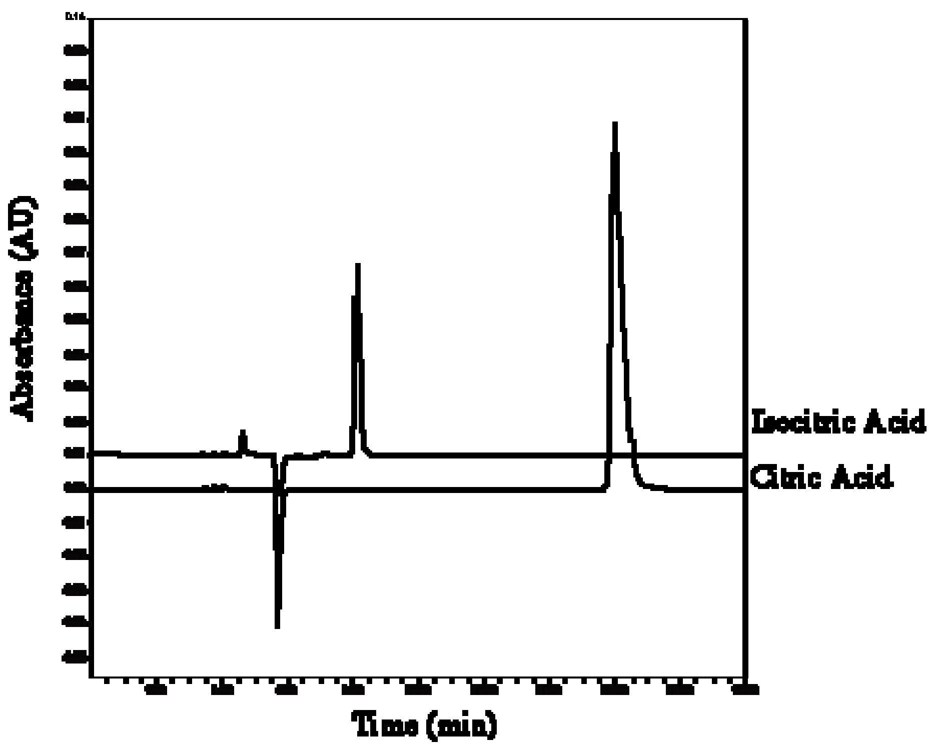

Figure 2 - 4. Panel A: Overlaid chromatograms of S2-6 spiked with citric acid using 3 different mobile phases (MP1, MP2 and MP3), see MATERIALS AND METHODS section. Panel B: Overlaid chromatograms of citric and isocitric acids using elution with MP2.

concentrations of 0.5 mM (25 nmol per SME) to 1 mM (50 nmol per SME) were consistently stimulatory at p = 0.05 to SME multiplication of genotype 500 as compared to the control treatments when applied directly to the surface of the embryo (Figure 2 - 5 and Table 2 - 4). When the same amounts of citric acid were added to the multiplication medium before or after autoclaving, it was found that the stimulatory effect on SME growth of genotype 500 was less pronounced than when citric acid was applied topically. For example, promotion of SME growth of genotype 500 was statistically significant in all bioassays only when 0.5 mM citric acid was added topically to the embryo surface but not when the same amount (0.0125 mM) was added to the medium before autoclaving (Figure 2 - 5, panel B and Table 2 - 4). When citric acid at concentrations of 0.0125 mM or 0.025 mM was added to the multiplication medium after autoclaving, it was found that colony growth of genotype 500 was increased compared to the control but not in a statistically significant manner at p = 0.05. This observation may be explained by the fact that citric acid is more readily available to the growing SME when placed on the surface of the embryo versus within the medium, where it has a longer exposure to components of growth medium 1250 at a higher temperature. Hence the amount of citric acid available to growing SMEs would depend on the concentration and oxidation state of reacting/chelating species within the multiplication medium, growth rate of SME, duration of bioassay, pH fluctuations and temperature. Dalton *et. al.* (1983) demonstrated that approximately 45% of the iron present in Murashige and Skoog medium precipitated as iron phosphate after ferrous EDTA rapidly oxidized to ferric EDTA (23). Previous investigations by van Winkle (2001) showed that Fe (III) precipitation as phosphate or hydroxide was reduced by addition of 10 μM citrate to the Norway spruce initiation medium, thus increasing its availability (24).

Additional experiments using 2 different combinations of 3 LP genotypes were subsequently carried out. Table 2 - 5 shows that 0.5 mM citric acid applied topically to SMEs of genotypes 500, 351 and 60 was stimulatory to colony growth at p = 0.05. The

Panel A:

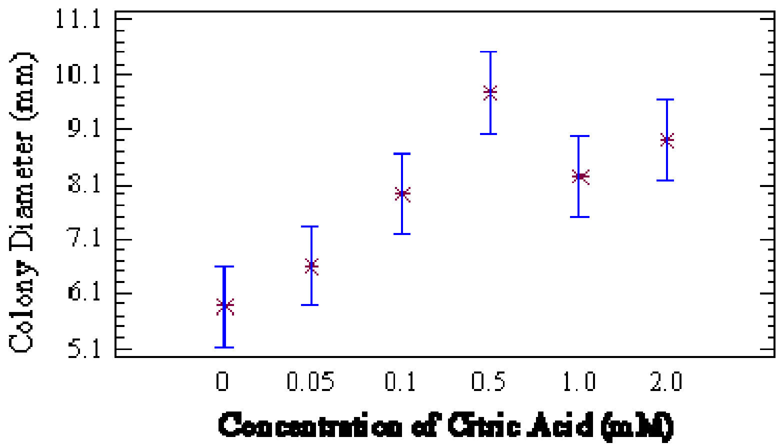

Panel B:

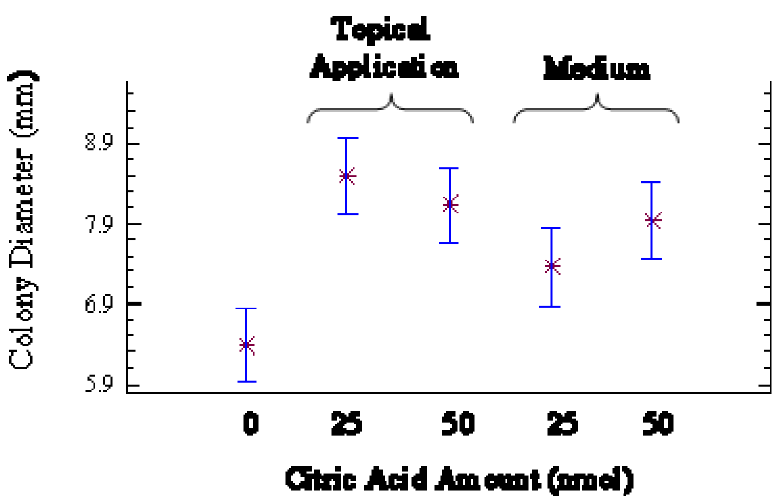

Figure 2 - 5. Panel A: Effect of different citric acid concentrations on growth of early stage SMEs. Panel B: Topical application of citric acid compared to direct addition of citric acid prior to autoclaving to medium 1250 on SME growth.

Table 2 - 4: Effect on SME growth of three different methods of application of various citric acid concentrations.

[Citric Acid] mM	Change in Colony Diameter (mm) (1 to 3 bioassays)
$0.0125^{+,\Omega}$	$^{*}0.97^{+}$, 1.13^{+}, 0.16^{Ω}
$0.025^{+,\Omega}$	$^{*}1.55^{+}$, $^{*}1.74^{+}$, 0.37^{Ω}
0.05^{Ψ}	0.74^{Ψ}
0.10^{Ψ}	$^{*}2.07^{\Psi}$
0.50^{Ψ}	$^{*}3.90^{\Psi}$, $^{*}2.11^{\Psi}$, $^{*}2.83^{\Psi}$
1.00^{Ψ}	$^{*}2.4^{\Psi}$, $^{*}1.74^{\Psi}$, $^{*}2.34^{\Psi}$
2.00^{Ψ}	$^{*}3.06^{\Psi}$

$^{+}$Citric acid added to medium 1250 before autoclaving (genotype 500 SMEs). $^{\Omega}$ Citric acid added to medium 1250 after autoclaving (genotype 500 SMEs). $^{\Psi}$Citric acid applied to the surface of SMEs (genotype 500) on medium 1250. *Represents a statistically significant change in mean colony diameter (95% LSD intervals) of SMEs grown in the presence of citric acid compared to the control treatment.

Table 2 - 5: Topical application of optimal citric acid concentrations on early-stage SMEs of different genotypes.

	Change in colony diameter (mm)	
	Genotypes	Genotypes
[Citric acid] (mM)	500, 351 and 60	500, 112 and 146
0.50	$^{*}0.98$	0.72
1.00	- 0.16	- 0.02

*Represents a statistically significant change in mean colony diameter of SMEs grown in the presence of citric acid compared to the control treatment at p = 0.05.

effect of the same amount of citric acid was stimulatory to SME growth of genotypes 500, 112 or 146 only at $p = 0.1$.

A possible concern with above experiments was the effect of 10 mM MES buffer and different amounts of KOH used to maintain citric acid solutions at pH 5.7 on SME growth assay. Control bioassays showed that neither MES nor additional KOH had a statistically significant effect at $p = 0.05$ on colony growth. In addition, we found that topical application of a biologically inactive chemical osmoticant, glutaric acid at 0.5 mM or 1.0 mM concentration, was not stimulatory to colony growth at $p = 0.05$.

2 – 5: DISCUSSION

In previous work, improvements in LP SE media were made using either a trial and error approach or a more systematic methodology, where molecules found or suspected to be present in nutritive FG tissue surrounding the LP zygotic embryo within the seed were used as supplements (5, 6, 11, 15-21). For example, the concentrations of organic acids present in FG and zygotic tissues at various stages of development were profiled using GC/MS (14). It was found that α-ketoglutaric, pyruvic and succinic acids have a stimulatory effect on LP SME multiplication ($p = 0.05$) and initiation ($p = 0.1$ to 0.14) at certain concentrations, when used alone or in combination (17).

In this paper we report the results of a more direct approach for improving the composition of medium 1250 used in LP SE. Here, we isolated a substance from early stage LP FG tissue that promotes SME growth; we then characterized this stimulatory substance as citric acid on the basis of ^{1}H NMR and MS. Finally, we demonstrated that topical application of 0.5 mM citric acid to early stage SMEs indeed stimulates colony growth for three genotypes at $p = 0.05$. Moreover, we find that there is a good correlation between the amount of citric acid actually isolated from FG tissue (65 nmoles per stage 2 or 3 FG) and the amount of topically applied citric acid that stimulates colony growth (25 to 50 nmoles per SME). The fact that an equivalent consistent stimulation of SME growth at $p = 0.05$ was not observed when 25 or 50 nmoles of citric acid was added directly to 1250 medium before or after autoclaving can be likely attributed to increased availability of iron to the growing embryogenic colony (24).

In previous work, the amount of citric and isocitric acids in LP FG tissue was profiled by GC/MS and found to increase from stage 1 to 3, peak in mid-development and subsequently decrease from stage 7 onwards. One FG of stage 3 was found to contain approximately 67 nmoles of these acids, which is in good agreement with our HPLC quantitation of citric acid in stage 2 or 3 FG (14). Other research groups have investigated the role of citric acid in plant SE processes. Nichol *et. al.* (1991) reported that pre-treatment of RA-3 alfalfa callus with optimum concentrations of organic acids (K^+- citrate [20 mM], K^+-malate [60 mM], K^+-succinate [less than 50 mM], K^+- tartarate [70 mM] or K^+-oxalate [10 mM]) improved the yield and morphology of SMEs during the induction process without inducing embryogenesis per se (25). Nichol *et. al.* (1991) found that substitution of citric acid by an appropriate chemical amount of other chelating or buffering reagents such as EGTA (ethylene glycol-bis(2-aminoethylether-N,N,N',N'-tetraacetic acid), EDTA or MES in the pre-treatment medium had no statistically significant effect on SME yield. Hence he postulated that the mechanism by which these organic acids stimulated SE of RA-3 alfalfa was not dependent on buffering or chelation effects (25). On the other hand, Malabadi and van Staden (2005) found that pre-treatment with or incorporation into initiation medium of different ratios and combinations of citric and ascorbic acids, or tri-potassium citrate and citric acid caused a reduction in surviving cultures of three genotypes of *Pinus patula* and the number of SMEs produced (26). Anthony *et. al.* (2004) carried out a similar study by adding tri-potassium citrate and citric acid (0.01 % [w/v]) to induction medium of *Conostephium pendulum* after autoclaving and found that although the tissue necrosis was reduced, the treatment had no significant effect on the number of SMEs formed (27).

There are a number of possible mechanisms by which citric acid could stimulate early stage SME growth. In order to participate in the biochemical pathways of the rapidly growing SME, citric acid could enter the plant cell and various organelles within via the tricarboxylate electroneutral transporter or an organic acid carrier (28). A proportion of citric acid that enters the somatic embryo cell is expected to participate in the mitochondrial citric acid cycle, which in turn has a direct impact on the energy production in the growing embryogenic mass. The flow of citric acid through in the glyoxylate pathway of the glyoxisome is also plausible, which impacts the supply of C4 molecules involved in nitrogen assimilation, gluconeogenesis, photo-respiration, fatty acid biosynthesis and other biologically important pathways in the cell (29). Citric acid could also participate in the production of cytosolic isocitrate via aconitate hydratase, and thereby affect production of glutamate and glutamine via 2-oxoglutarate. Cytosolic NADPH produced during this process has a direct impact on the activity of various dehydrogenase enzymes and hence important biosynthetic pathways of SME.

The direct involvement of citric acid as a source of energy to the growing early stage SMEs is supported by the fact that other acids from the citric acid cycle – pyruvic, succinic and α-ketoglutaric at respective concentrations of 0.52 mM, 0.125 mM and 0.68 mM in the media - were all found to be stimulatory to SME colony growth of 3 genotypes at $p = 0.05$ (17). In addition, in our hands, glutaric acid, which is structurally similar to α-ketoglutaric acid, but is not an intermediate in the citric acid cycle, was found to be non-stimulatory to SME growth at the two concentrations tested ($p = 0.05$).

Citric acid is a multi-functional molecule, whose presence at different concentrations could change the transport of various chemical osmoticants across plant outer and inner organelle membranes, affect plant metabolism and hence synthesis / degradation of biologically important molecules, alter the ratio of metal ions available outside and inside of SME via chelation and in general have a direct effect on the charge balance of the medium and SME. The fact that only specific concentrations of citric acid are stimulatory at $p = 0.05$ to SME growth suggests that there is a delicate balance of anions/cations, metabolites, chemical osmoticants and metal ions that would be stimulatory to early stage SME growth.

2 – 6: REFERENCES

1. Mirov NT (1967). The Genus Pinus. The Ronald Press Company, New York, USA.

2. Schultz RP. Loblolly - the pine for the twenty-first century. New For 1999;17:71-88.

3. Attree SM, Fowke LC. Embryogeny of gymnosperms: advances in synthetic seed technology of conifers. Plant Cell Tiss Org Cult 1993;35:1-35.

4. Becwar MR, Pullman GS (1995). Somatic embryogenesis in Loblolly pine (*Pinus taeda* L.). In: Jain JS, Gupta PK, Newton, RJ (eds) Somatic embryogenesis in woody plants – gymnosperms, vol 3, Kluwer, Dordrecht, pp 287-301.

5. Pullman GS, Buchanan M. Loblolly pine (*Pinus taeda* L.): Stage-specific elemental analyses of zygotic embryo and female gametophyte tissue. Plant Sci 2003;164:943-54.

6. Tang W, Guo Z. In vitro propagation of loblolly pine via direct somatic organogenesis from mature cotyledons and hypocotyls. Plant Growth Reg 2001;33:25-31.

7. Raghavan V, Sharma KK (1995). Zygotic embryogenesis in Gymnosperms and Angiosperms. In: Thorpe TT (ed) In vitro embryogenesis in plants, Kluwer, Dordescht, pp 73-115.

8. Pullman GS, Webb DT (1994). An embryo staging system for comparison of zygotic and somatic embryo development. In: Proc TAPPI Biol Sci Symp. TAPPI Press, pp 31-34.

9. von Arnold S, Sabala I, Bozkhov P, Dyachok J., Filonova L. Developmental pathways of somatic embryogenesis. Plant Cell Tiss and Org Cult 2002;69:233-49.

10. Handley LW, Becwar MR, Chesick EE. Research and development of a commercial tissue culture system in Loblolly pine. TAPPI J 1998;78:169-75.

11. Pullman GS. United States Patent 6,893,873 (2005). Methods for improving conifer embryogenesis.

12. Becwar MR, Nagmani R, Wann SR. Initiation of embryogenic cultures and somatic development in Loblolly pine (*Pinus taeda*). Can J For Res 1990;20:810-7.

13. Jimenez VM. Involvement of plant hormones and plant growth regulators on in vitro somatic embryogenesis. Plant Growth Reg 2005;47:91-110.

14. Pullman GS, Buchanan M. Identification and quantitative analysis of stage-specific organic acids in Loblolly pine (*Pinus taeda* L.) zygotic embryo and female gametophyte. Plant Sci 2006;170:634-47.

15. Li XY, Huang, HF, Gbur EE. Effect of basal medium, growth regulators and Phytagel concentration on initiation of embryogenic cultures from immature zygotic embryos of Loblolly pine (*Pinus taeda* L.). Plant Cell Rep 1998;17:298-301.

16. Li XY, Huang HF, Murphy JB, Gbur Jr EE. Polyethylene glycol and maltose enhance somatic embryo maturation in Loblolly pine. *In Vitro* Cell Dev Biol 1998;34:22-6.

17. Pullman GS, Chopra R, Chase KM. Loblolly pine (*Pinus taeda* L.) somatic embryogenesis: Improvements in embryogenic tissue initiation by supplementation of medium with organic acids, Vitamins B12 and E. Plant Sci 2006;170:648-58.

18. Pullman GS, Johnson S, Peter G, Cairney J, Xu N. Improving Loblolly pine somatic maturation: comparison of somatic and zygotic embryo morphology, germination, and gene expression. Plant Cell Rep 2003;21:747-58.

19. Pullman GS, Montello P, Cairney J, Xu N, Feng X. Loblolly pine (*Pinus taeda* L.) somatic embryogenesis: maturation improvements by metal analyses of zygotic and somatic embryos. Plant Sci 2003;164:955-69.

20. Pullman GS, Namjoshi K, Zhang Y. Somatic embryogenesis in Loblolly pine (*Pinus taeda* L.): improving culture initiation with abscisic acid and silver nitrate. Plant Cell Rep 2003;22:85-95.

21. Silveira V, Floh EIS, Handro W, Guerra MP. Effect of plant growth regulators on the cellular growth and levels of intracellular protein, starch and polyamines in embryogenic suspension of Pinus taeda. Plant Cell Tiss and Org Cult 2004;76:53-60.

22. Pullman GS, Zhang Y, Skryabina A. Loblolly pine female gametophyte contains bioactive agents that alter embryo growth and development *in vitro*. Plant Cell Rep 2007, unpublished work.

23. Dalton CC, Iqbal K, Turner DA. Iron phosphate precipitation in Murashige and Skoog media. Physiol Plant 1983,57:472-6.

24. van Winkle S (2001). The effect of activated carbon on the organic and elemental composition of plant tissue culture medium. Dissertation, Institute of Paper Science and Technology.

25. Nichol JW, Slade D, Viss P, Stuart DA. Effect of organic acid pretreatment on the regeneration and development (conversion) of whole plants from callus cultures of alfalfa, *Medicago sativa* L. Plant Sci 1991;79:181-92.

26. Malabadi RB, van Staden J. Role of antioxidants and amino acids on somatic embryogenesis of *Pinus Patula*. *In Vitro* Cell Dev Biol 2005;41:181-6.

27. Anthony JM, Senaratna T, Dixon KW, Sivasithampram K. The role of antioxidants for initiation of somatic embryos with *Conostephium pendulum* (Ericaceae). Plant Cell Tiss Org Cult 2004;78:247-52.

28. Siedow JN, Day AA. Respiration and photorespiration. In: Buchanan BB, Gruiseem W, Jones RL (eds) Biochemistry and molecular biology of plants, Amer Soc Plant Phys, Rockville, pp 676-729.

29. Popova TN, Punheiro de Carvalho MAA. Citrate and Isocitrate in plant metabolism. Biochim. *et* Biophys Acta 1998;1364:307-25.

CHAPTER 3

Development of an Assay to Measure L-Phenylalanine Concentration in Blood Plasma

3 – 1: SUMMARY

Phenylketonuria (PKU) is an autosomal recessive disorder caused by an impaired conversion of L-phenylalanine (L-Phe) to L-tyrosine (L-Tyr) typically resulting from a deficiency in activity of a hepatic enzyme L-phenylalanine hydroxylase. The disease is characterized by an increased concentration of L-Phe and its metabolites in body fluids. A novel assay based on enzymatic-colorimetric methodology was developed in order to detect elevated concentrations of L-Phe in undeproteinized plasma of PKU patients via continuous spectrophotometric detection. We report here on a comparison of L-Phe concentrations in undeproteinized plasma measured using the enzymatic-colorimetric assay with those in deproteinized plasma obtained on an amino acid analyzer, and in derivatized dried blood spot eluates measured by HPLC and MS/MS, respectively. Pearson correlation coefficients of 0.951, 0.976 and 0.988 were obtained when amino acid analyzer-measured L-Phe concentrations were compared with the enzymatic-colorimetric -, HPLC - and MS/MS - measured values, respectively. A Bland and Altman analysis revealed that mean L-Phe concentrations determined on an amino acid analyzer were on average 0.067 mM lower than values measured by our enzymatic-colorimetric assay and 0.14 mM and 0.1 mM higher than values measured by MS/MS and HPLC analyses, respectively. Therefore, L-Phe concentrations determined by our enzymatic-colorimetric assay method are indeed comparable to those determined on an amino acid analyzer for a broad range of plasma L-Phe levels.

3 – 2: INTRODUCTION

L-Phenylalanine Hydroxylase (PAH):

The PAH gene (on chromosome 12) contains 13 exons and spans 90 kbases (1); and is known to code for a 2.4 kbase *m*RNA. PAH from *Homo Sapiens* (*HS*) consists of 452 amino acids (AAs) and exists as homotetramers (2). PAH is a mononuclear non-heme iron (II)-containing enzyme composed of an N-terminal regulatory, a catalytic and a C-terminal tetramerization domains (2-4). PAH converts L-phenylalanine (L-Phe) to L-tyrosine (L-Tyr) in the presence of an essential (6R,1R',2S')-6-(1',2'-dihydroxypropyl)-5,6,7,8-tetrahydrobiopterin (BH_4) co-factor and O_2 as shown in Scheme 3 - 1. BH_4 is recycled back to its reduced form by the action of dihydropteridine reductase with NADH as a co-factor or formed via dihydrofolate reductase from quinoid 7,8-dihydrobiopterin. *HS* PAH is activated by Fe (III) to Fe (II) reduction, binding of substrate and phosphorylation of Ser 16 (regulatory domain) by cAMP-dependent protein kinase (5).

X-Ray crystallography data, mutagenic, radio-label and spectral studies reveal some insight into PAH mechanism of action, which is still poorly understood (5). A plausible mechanism based on cumulative data from various research groups is depicted in Scheme 3 - 2 (5, 6). Initially, the active site iron (II) atom has six coordinates in a square-pyramidal coordination to 3 H_2O molecules, His290, His285 and Glu330 residues. An active site conformation shift occurs when BH_4, L-Phe are bound near Fe (II), with a subsequent displacement of 2 H_2O molecules. Next, the last H_2O molecule is displaced by molecular O_2 with subsequent formation of a 4-peroxy-BH_4 intermediate. In the following step a heterolytic cleavage of the O-O bond in 4-peroxy-BH_4 takes place with a concomitant formation of 4-hydroxy-BH_4 and an activated oxygen intermediate. In the final step of catalysis, L-Tyr and 4-hydroxy-BH_4 are released, the latter rapidly dehydrates in aqueous environment to quinoid 7,8-dihydrobiopterin.

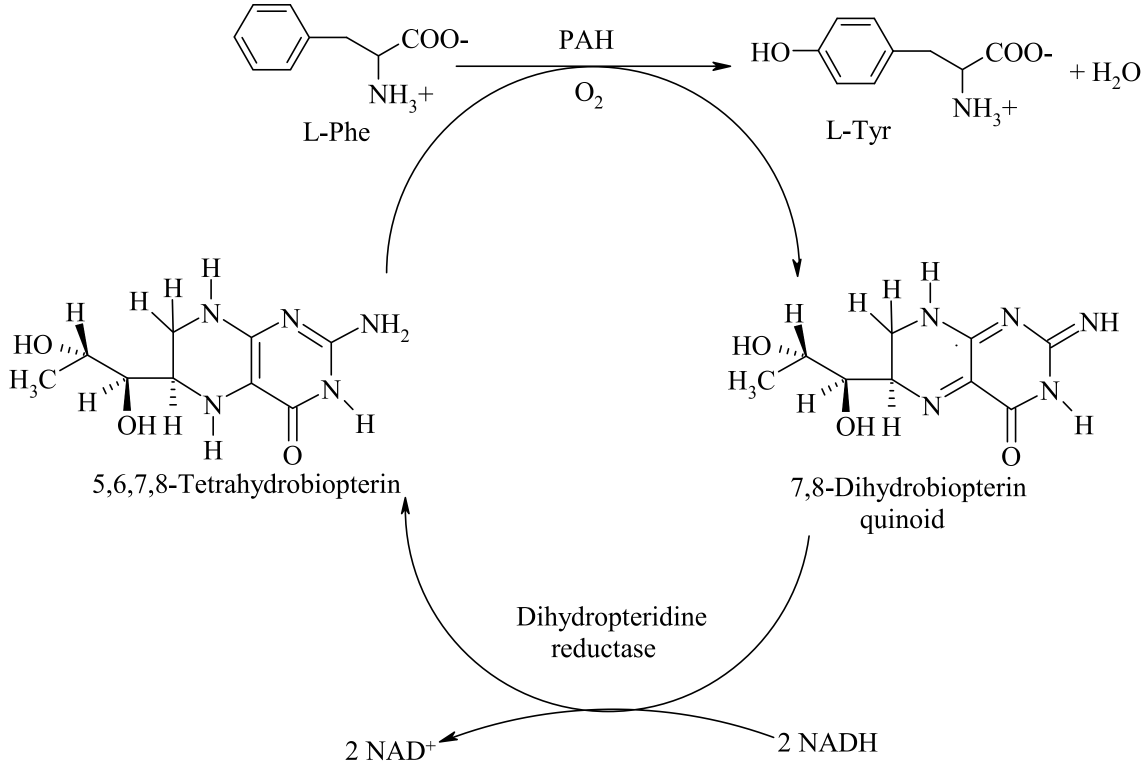

Scheme 3 - 1: Hepatic PAH Function

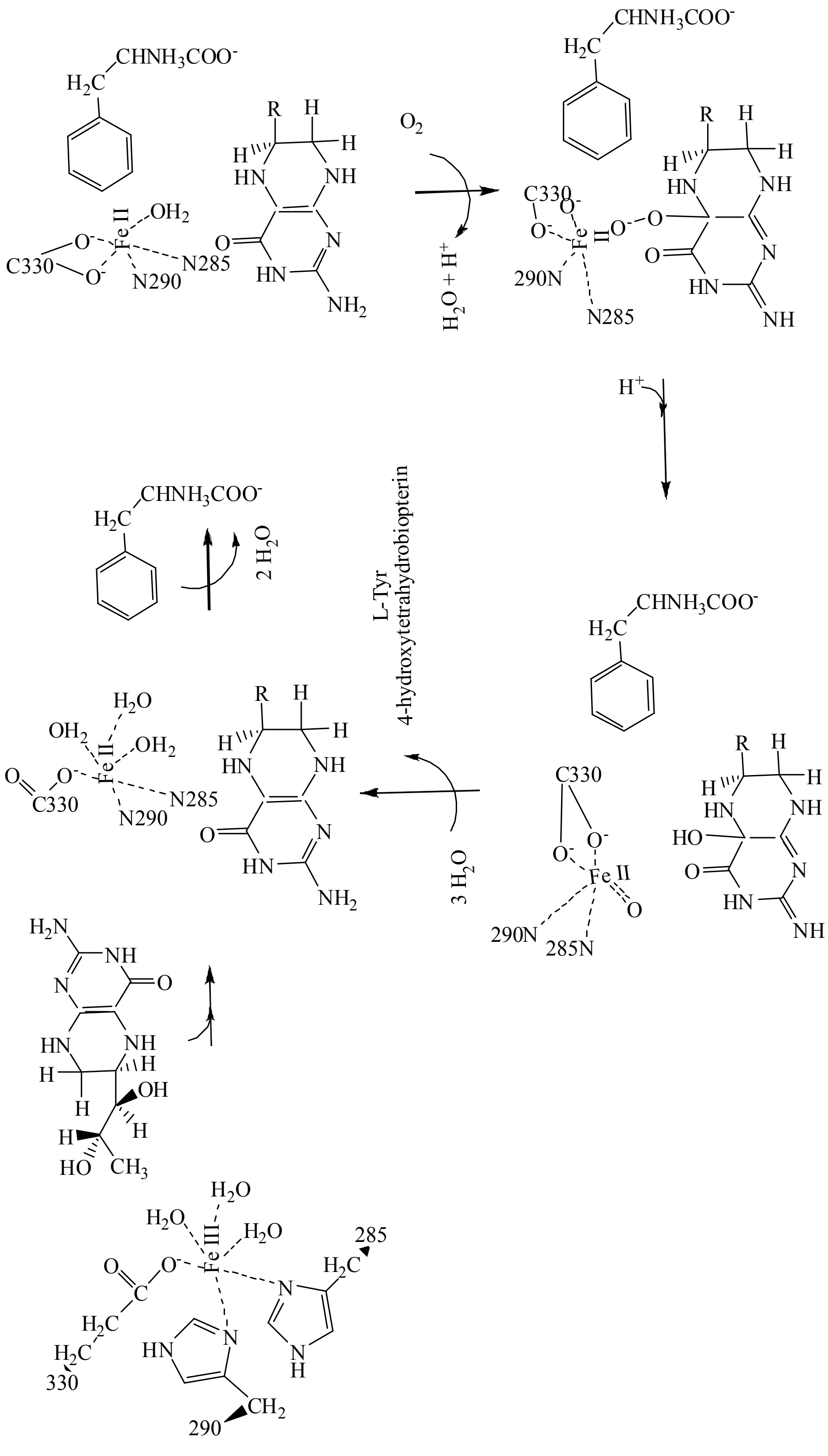

Scheme 3 - 2: Plausible PAH Mechanism (5, 6)

PKU Background:

Hyperphenylalaninemia (HPA) is an autosomal recessive disorder resulting from an impaired conversion of L-Phe to L-Tyr, PAH is responsible for the disposal of approximately 75 % of L-Phe in the body. In addition, tyrosine hydroxylase and tryptophan hydroxylase localized in brain tissue and adrenal glands can hydroxylate L-Phe to L-Tyr but with a different catalytic efficiency to PAH (5). HPA can be caused by a number of possible mutations (over 400) in the gene that encodes PAH (7). This disorder is characterized by an increased concentration of L-Phe and its metabolites (phenylpyruvate, phenyllactate, phenylethylamine and phenylacetate) in bodily fluids (8). Scheme 3 - 3 shows the normal pathway of L-Phe catabolism via L-Tyr and the alternate route of phenylketone formation, which is a direct result of elevated L-Phe plasma concentrations.

Persons with classic PKU show very high elevations of blood L-Phe levels frequently exceeding 20 mg/dL or 1.2 mM (9). Affected individuals tolerate less than 20 mg of dietary L-Phe per kg of weight a day in order to maintain plasma L-Phe concentrations at a safe level of 0.12 to 0.3 mM. A partial deficiency in PAH activity results in non-PKU HPA, a lower concentration of blood L-Phe that occurs without phenylketone accumulation and is characterized by a tolerance for higher dietary L-Phe levels (10). PKU, if left undiagnosed and untreated, results in mental retardation, microcephaly, delayed speech, seizures, eczema, impaired pigmentation, behavior abnormalities and other negative symptoms (11). The accumulation of L-Phe in the blood is suspected to cause competitive inhibition of transport of other large, neutral AAs required for protein and neurotransmitter synthesis across the blood brain barrier, reduced synthesis and increased degradation of myelin and inadequate formation of dopamine, epinephrine and norepinephrine as shown in Scheme 3 - 4 (12, 13). But the relationship between clinical phenotype and genotype is not always constant (9).

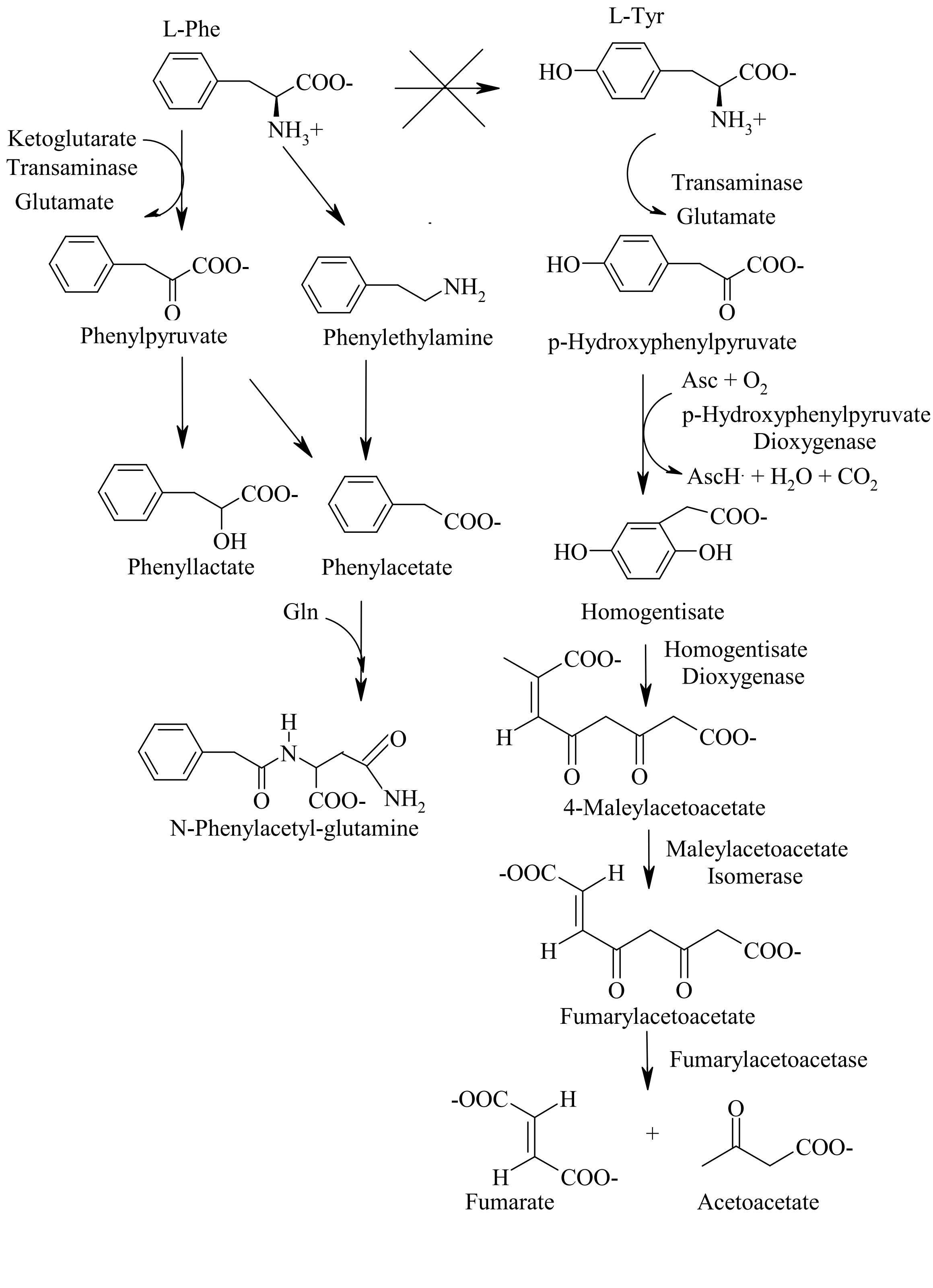

Scheme 3 - 3: Catabolism of L-Phe Under Normal and Elevated L-Phe Concentrations

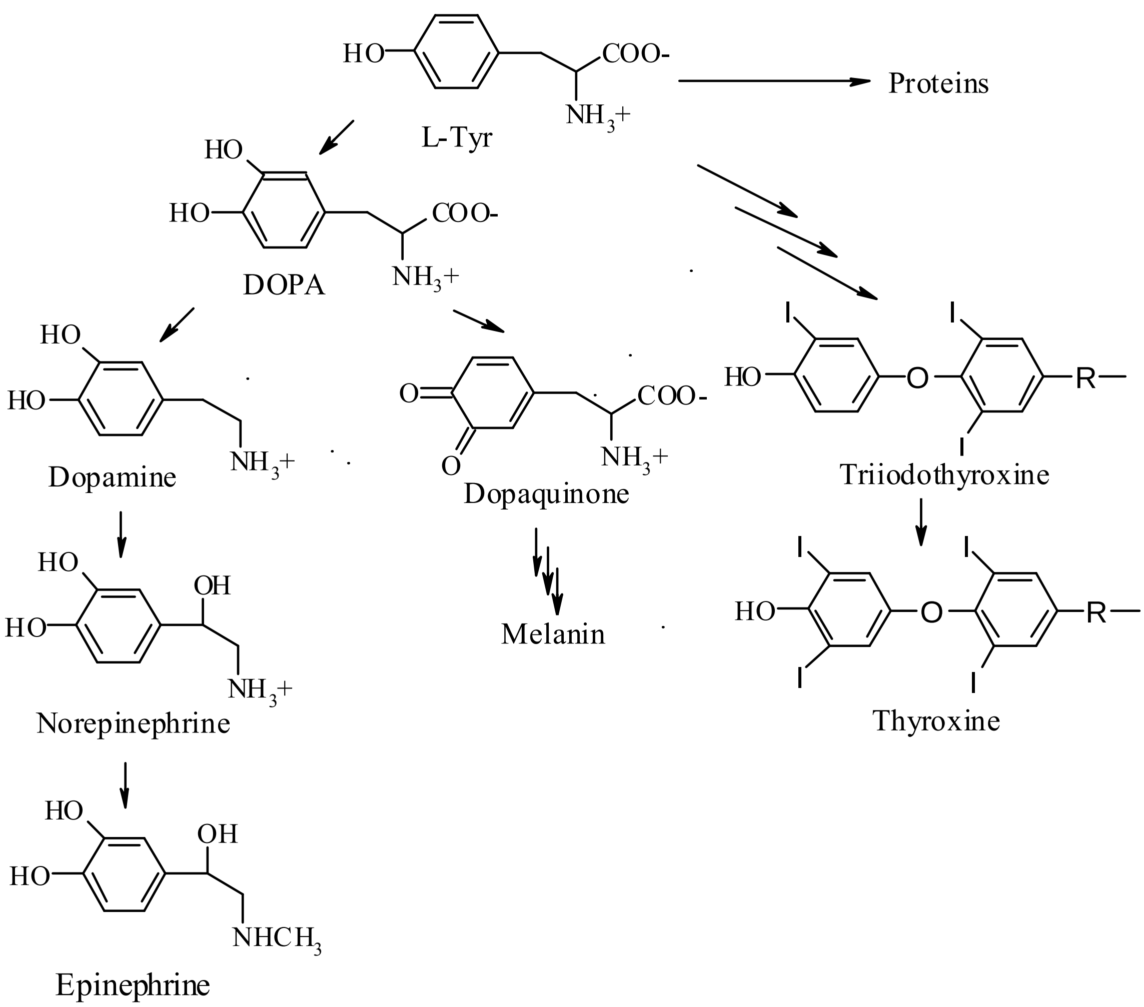

Scheme 3 - 4: Metabolism of L-Tyr

Methods to Quantify L-Phe Concentrations in Bodily Fluids of PKU patients:

In the USA, newborn screening for PKU has been underway for nearly 40 years. According to the NIH Consensus Statement (NIHCS), approximately 1 out of 15,000 neonates is born with PKU every year, while for non-PKU HPA the yearly incidence is 1 out of 48,000 births (10). In order to prevent the severe mental and physical symptoms associated with PKU, diagnosis and initiation of dietary treatment must occur before the child is 3 weeks of age. Several PKU screening methodologies are widely used currently: the Guthrie card bacterial inhibition assay, an inexpensive and semi-quantitative test (14); fluorometric analysis (15,16); amino acid analysis (PAA) (17); MS (18,19); HPLC (20); and enzymatic-colorimetric assays (ECA) (21-34). Initial screening tests for elevated L-Phe typically yield significant numbers of false positive results, which could be due to improper dried blood spot (DBS) preparation, liver immaturity, protein overload and other factors. Therefore, abnormal L-Phe and / or L-Tyr levels are confirmed using quantitative analysis of AAs and BH_4 determination. Further molecular genetic tests (mutation, sequence and linkage analyses; as well as mutation scanning) are then performed to distinguish infants with complete PAH deficiency from those with an impaired activity of PAH (HPA) (7, 10). In 1 to 2 % of cases impaired PAH activity could be caused by abnormalities in biosynthesis and metabolism of BH_4, termed malignant PKU. Other experimental techniques developed to measure plasma Phe levels include NADH-detecting biosensor (35); capillary electrophoresis / ESI MS (36) and LC-MS (37), the latter two methods can detect and quantify underivatized Phe. Preliminary studies have been carried to evaluate the feasibility of non-invasive PKU / HPA diagnosis by measuring concentrations of L-Phe and creatine in urine photometrically and by a kinetic method, respectively, and correlating these to corresponding plasma L-Phe levels (38).

Treatment of HPA / PKU:

The generally accepted goal of treatment of PKU and HPA is normalization of the blood L-Phe and L-Tyr levels and thus prevention of the severe symptoms associated with this disorder. Dietary therapy is the current most commonly used method to establish metabolic control over L-Phe levels. The response to medical therapy is monitored at specialized metabolic centers at varying frequencies depending on the age of the patient and individual policy. Limited studies have demonstrated that age at treatment initiation for PKU and the level of metabolic control influence intellectual, cognitive and behavioral outcomes of individuals suffering from PKU (10). Hence the development of a reliable home monitoring testing method is recommended (10).

ECAs Used to Measure Blood L-Phe Concentrations:

ECA has proven to be a reliable, easily automated, and sensitive method for measuring L-Phe in deproteinized plasma and dried blood spot (DBS) eluates of PKU patients (21-34) as shown in table 3 - 1. Wendel *et. al.* (1989, 1990 and 1991) used PAD from *Rhodococcus* sp. Strain M4 (*RM*4) to formulate an enzymatic assay coupled with an intermediate electron acceptor system (2-[4-iodophenyl]-3-[nitrophenyl]-5-phenyl-2H-tetrazolium [INT] / diaphorase) to accurately quantify plasma or DBS L-Phe levels within a broad concentration range of 0.03 to 1.2 mM. Other research groups (24, 29) similarly employed PAD / co-factor coupled with various tetrazolium dyes and either enzymatic or chemical mediators to diagnose and monitor PKU or HPA. Next, Porton Cambridge launched a commercial kit (Quantase) for neonatal PKU screening in DBS and plasma samples (25, 28, 30-32). The Quantase assay requires a 30-minute pre-incubation step of the eluted DBS or deproteinized plasma sample with enzyme / co-enzyme mixture, prior to addition of colorimetric reagents and end point spectrophotometric measurements (25, 28, 30-32). The currently used enzymatic / colorimetric assays require deproteinization of plasma samples or elution and /or deproteinization of DBS, which takes 8 to 60 minutes as shown in Table 3 - 1.

Table 3 – 1: Summary of ECAs Developed in Other Laboratories

Ref	Enzyme source/ co-factor	Colorimetric Assay Constituents	Spectroscopic Method; λ of Detection	Blood Sample Type; n; Patient type	Deproteinization and / or Elution Instrument Used	AMR, Comparison, R or Bland and Altman
21	*RM4* PAD / NAD^+	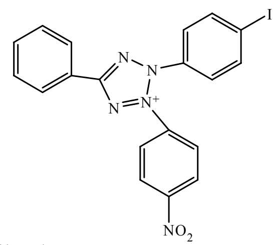 + diaphorase	λ = 492 nm Kinetic Assay (30 mins)	Plasma; n = 41 Treated PKU	PCA Beckman DU-8 Spectrophotometer	0.03 to 1.2 mM); PAA, R=0.998
22	*RM4* PAD / NAD^+	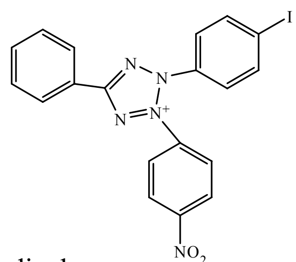 + diaphorase	λ = 492 nm Kinetic Assay (30 mins)	DBS; n = 16; Treated PKU	H_2O + boil (60 mins) Titertee Microplate Reader	0.015 to 1.2 mM; PAA, R=0.996
23	*RM4* PAD / NAD^+	None	λ = 340 nm End Point (10 mins)	Plasma; n = 120 Treated PKU	PCA	0.05 to 2 mM; PAA, R=0.987
24	Undisclosed PAD / NAD^+	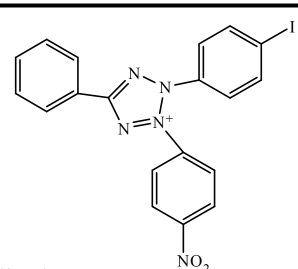 + diaphorase	λ = 492 nm Kinetic Assay	DBS; n = 199 Neonates	H_2O (10 mins) Cobas Bio Centrifugal Analyzer	up to 2.5 mM; Fluorometric Auto Analyzer, R=0.872
25	Quantase, Undisclosed PAD / NAD^+	Tetrazolium salt / Intermediate electron acceptor	λ = 570 nm End Point	Plasma, n = 30 DBS, n = 54	PCA (15 mins) TCA (30 mins) Cobas Fara (Roche)	0.2 to 1 mM; HPLC, R = 0.995 HPLC, R = 0.983

Table 3 – 1: Summary of ECAs Developed in Other Laboratories (Continued)

26	*RM4* PAD / NAD^+	None	λ = 340 nm End Point	Plasma; n = 70 Treated HPA	PCA Cobas Fara II Centrifugal Analyzer	0.05 to 1.5 mM PAA, R = 0.996
27	Undisclosed PAD / NAD^+	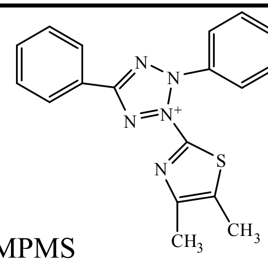 + MPMS	λ = 570 nm End Point (2 mins)	DBS; n = 50	TCA (30 mins); LabSystems Multiscan Plus Microtiter Plate Reader	0.036 mM to 2 mM HPLC (PCA), R=969
28	Quantase, Undisclosed PAD / NAD^+	Tetrazolium salt / Intermediate electron acceptor	λ = 570 nm End Point (2-5 mins)	DBS; n = 50 non-PKU	TCA (30 mins)	0.025 and up
29	Undisclosed PAD / NAD^+	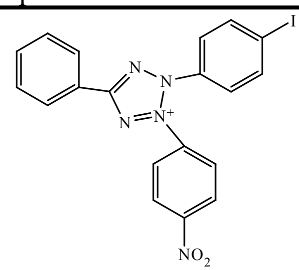 + Diaphorase	λ = 500 nm End Point (6.5 minutes)	DBS; n = 208; PKU and Non-PKU	H_2O (8 mins); Cobas MIRAS analyzer	0.01 to 3.75 mM PAA, R = 0.982
30	Quantase (Shield Diagnostics)	Undisclosed	Undisclosed	Plasma; n = 48	TCA	0.4 mM to 1.7 mM; Fluorescence
31	Quantase Enzyme / Co-Enzyme	Undisclosed	λ = 570 / 690 nm	DBS; n = 190	TCA (60 mins)	0.055 to 1.65 mM; Fluorescence, -ve bias of 0.018 mM
32	Quantase Undisclosed PAD / NAD^+	Undisclosed	λ = 570/690 nm End Point (2 mins)	DBS; Plasma; n = 423,773	TCA PCA Multiscan MCC 349	0.043 to 1.08 mM; ESI MS/MS, PAA

For instance, a standard protocol for sample preparation using the Quantase kit requires a 60-minute elution and deproteinization of DBS with 3 % (v/v) TCA (25, 28, 31 and 32). In 1994, a laboratory in Baden-Wurttemberg (Germany) changed from BIA to ECA methodology to screen neonate blood L-Phe levels. Schulze *et. al.* (2002) used the PAD-based ECA to screen 423,773 neonate samples for HPA, non-PKU or PKU during a 6-year period and found the number of false positives to be 0.23 % with no false negatives reported.

This chapter describes the development of a novel ECA for measuring L-Phe concentrations in undeproteinized plasma samples. The methodology described here relies on the L-phenylalanine dehydrogenase (EC: 1.4.1.20; PAD)-mediated oxidative deamination of L-Phe to phenylpyruvate with a concomitant reduction of NAD^+ to NADH. The amount of NADH produced is quantified via continuous spectrophotometric detection (a kinetic assay), where 3-(4,5-dimethylthiazol-2-yl)-5-(3-carboxymethoxyphenyl)-2-(4-sulfophenyl)-2H-tetrazolium (MTS) is reduced to its water-soluble formazan product in the presence of NADH and an electron mediator, 5-methylphenazinium methyl sulfate (PMS) as depicted in Scheme 3 - 5.

<u>Formulation of Home-Monitoring Device:</u>

A simple robust device for the determination of plasma L-Phe, which could be used by the patient at home, would greatly facilitate the ability of the patient, in consultation with his or her physician, to control the tissue L-Phe concentrations. In the last decades analytical and clinical chemistry developed to a point where many useful analytical measurements can be made using relatively simple and inexpensive instrumentation, the most common example being the quantitative glucose measurement for diabetics (39).

The present work describes the progress being made towards the formulation of a novel test strip for analysis of plasma L-Phe levels. Preliminary studies have been carried out to employ a modified thin film format methodology similar to that of

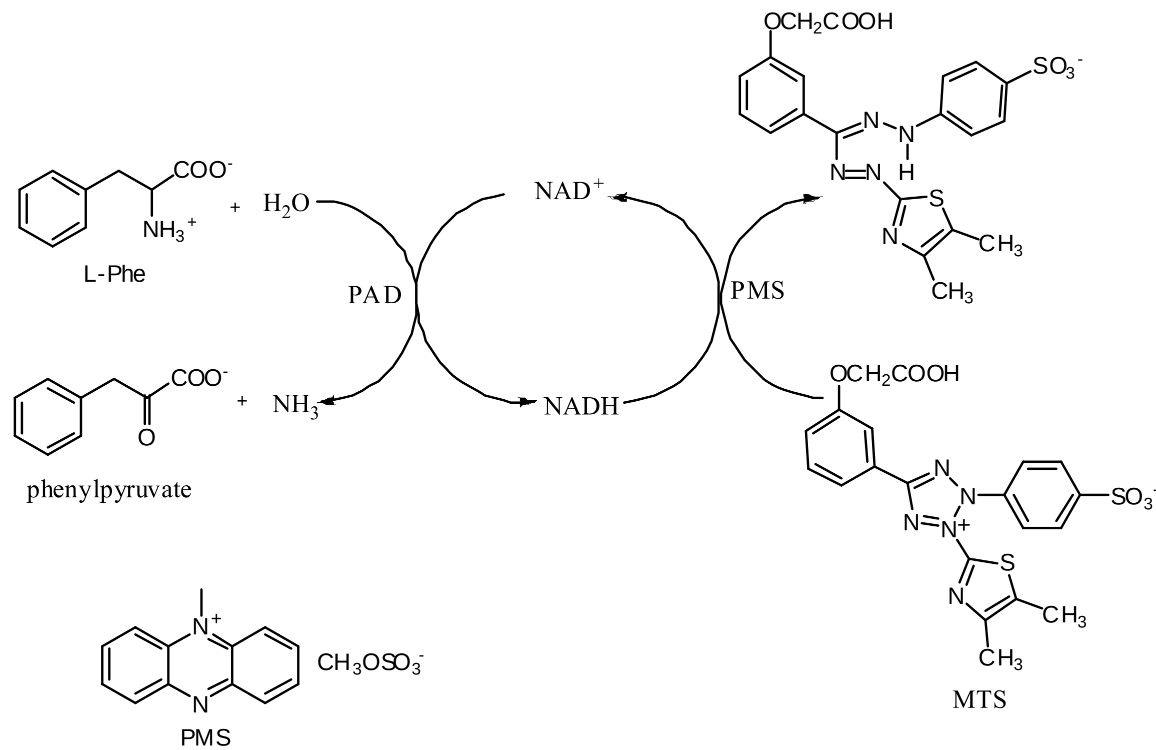

Scheme 3 - 5. ECA shows PAD-catalyzed conversion of L-Phe to phenylpyruvate with a concomitant production of NADH, recycled back to NAD^+ by MTS-PMS assay.

Przybylowicz *et. al.* (1976), as the basis for making a home-monitoring device (40). The test strip is proposed to consist of two or three super-imposable layers in liquid contact with each other on a solid support as shown in Scheme 3 - 6. The reagent layer would contain appropriate concentrations of immobilized ECA reagents buffered at an optimal pH, such that in the presence of detectable L-Phe concentrations the signal could be measured and quantified. The spreading and / or reflecting layer would assist in uniform spreading of the analyte, penetration towards ECA layer, filtering of red blood cells (RBCs) and serve as the reflection surface in order to enable the quantitation of signal via reflection densitometry.

The device should enable the patient suffering from PKU to adjust the diet accordingly once he or she has measured the plasma L-Phe levels.

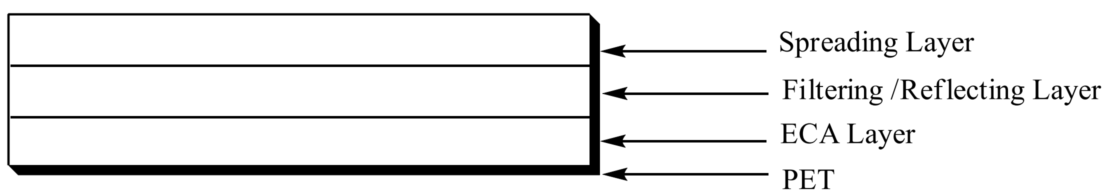

Scheme 3 - 6. Multi-layer film for L-Phe quantitation.

3 – 3: MATERIALS AND METHODS

Materials:

MTS was purchased from Promega (Madison, WI, USA). 3,5-Dibromo-L-tyrosine monohydrate; cellulose acetate; [$^2H_4$]-phenylalanine; HPLC-grade CH_3CH_2OH, CH_3CN, CH_3OH; [$^2H_4$]-tyrosine; human serum (Type A/B); Hyflo Super Cel diatomaceous earth; L-Phe; L-Tyr; methylene blue, NAD^+; NADH; *n*-butanolic HCl; PMS; S-aminoethylcysteine (SAEC); sulfosalicylic acid (SSA), teleostean gelatin (Type A), TiO_2 powder (particle size of less than 5 μm) and Triton X-100 detergent were purchased from Sigma Aldrich (St Louis, MO, USA). PAD from *Sporosarcina urea (SU)* was purchased either from Sigma Aldrich or ICN Biomedicals (Irvine, CA, USA). Acetone, CH_2Cl_2, D_2O, Fisherfinest Premium Microscope Slides Plain (2.54 × 2.54 × 0.10 cm), glycine and xylenes were purchased from Fisher Scientific (Atlanta, GA, USA). TiO_2 (particle size of 30 nm) was obtained from Alfa Aesar (Ward Hill, MA, USA). Monobasic potassium phosphate, TiO_2 anatase powder (200 nm particle size) and triethanolamine were obtained from Acros Organics (Norcross, GA, USA). Quality control DBS standards (QCS spotted with 0.0025, 0.005, 0.01, 0.02 and 0.08 mM L-Phe or L-Tyr) were obtained from the Center for Disease Control (CDC) (Atlanta, GA, USA). AccQ-Fluor reagent kit and AccQ-Tag column (150 × 3.9 mm) were purchased from Waters (Milford, MA, USA). Schleicher & Schuell 903 (S&S 903) filter paper was obtained from Schleicher & Schuell, Inc. (Keene, NH, USA). Beckmann Coulter's Lithium buffers A, B, D, E and F; Beckmann high performance cation exchange column (0.4 × 10 cm), and ninhydrin were obtained from Beckmann Coulter (Fullerton, CA, USA). Bird type film applicators (4 and 8 mil), Gardco wire-wound rods (40 and 80 mil) and Leveling Drawdown Plate were purchased from Paul N. Gardner Inc. (Pompano Beach, FL, USA). Polyethylene terephthalate (PET) was obtained from Goodfellow Corporation (Oakdale, CA, USA). Aluminum mold was manufactured at the Georgia Tech Machine Shop. USB2000-FLG Spectrofluorometer (380 to 1050 nm), tungsten halogen light source (360 nm to 0.002

mm), reflection / backscattering probes and RPH-1 probe holder were purchased from Ocean Optics (Dunedin, FL, USA). Spin coater WS-400B-6NPP-LITE was from Laurell Technologies (North Wales, PA).

PAD Enzyme Activity Assay:

In a 3 mL quartz cuvette 10 mM L-Phe, 3 mM NAD^+ and 0.002 to 0.008 units of PAD were combined together at 30^{o}C in 192 mM glycine buffer (pH 10.5) and changes in absorbance at 340 nm (ΔA_{340}) monitored using an HP 8453 diode array spectrophotometer equipped with an HP 8909 temperature-control accessory (n = 3). The assay procedure was repeated in the absence of PAD (n = 3). Initial ΔA_{340} was calculated using the kinetics module of the Biochemical Analysis UV-visible ChemStation software. The enzyme activity in U/mL was calculated as follows, when a 0.1 mL aliquot of PAD was added to give a final volume of 3 mL:

U/mL PAD = [(ΔA_{340} w/ PAD - ΔA_{340} w/o PAD) × 3 × DF] / (6.22 × 0.1), where DF = dilution factor of PAD and 6.22 is the millimolar extinction coefficient (ε_{340}) of NADH.

Investigation of ECA:

All subsequent experiments were conducted at 25^{o}C unless otherwise indicated.

Experiment 1: Effect of MTS and PMS on ECA

0.06 mM MTS or 0.04 mM PMS, 0.06 mM L-Phe, 0.75 mM NAD^+ and 0.1 U/mL PAD were combined together in pH 8.6 buffer and ΔA_{340} monitored. A control assay was performed in the absence of MTS and / or PMS.

Experiment 2: Effect of pH on NADH Oxidation by MTS and PMS

0.06 mM MTS; 0.04 mM PMS, and 0.012 mM, 0.03 mM or 0.06 mM NADH in 198 mM glycine buffer (pH 10.5) were combined together and ΔA_{340} and ΔA_{550} monitored. A control assay was performed in the absence of NADH. The observed shift in λ_{max} of the formazan product from 490 to 550 nm is due to the pH change in ECA.

Experiment 3: Determination of the Rate-Limiting Step in the ECA

Enzymatic Assay: 0.012 mM, 0.06 mM or 0.12 mM L-Phe; 0.75 mM NAD^+, and 0.1 U/mL PAD were combined together in 5.4 mM potassium phosphate / 43 mM triethanolamine buffer (pH 8.6 buffer) and production of NADH monitored at 340 nm. A control assay was performed in the absence of PAD.

Colorimetric Assay: 0.06 mM MTS, 0.04 mM PMS and 0.06 mM NADH were combined together in pH 8.6 buffer, and NADH and formazan production monitored at 340 nm and 490 nm, respectively. A control assay was performed in the absence of NADH.

Experiment 4: Effect of L-Tyr and Phenylpyruvate on ECA (0 to 0.3 mM L-Phe)

0.3 mM MTS; 0.15 mM PMS; 0.75 mM NAD^+; 0.05, 0.15 or 0.3 mM L-Phe, 0.1 mM L-Tyr and 0.17 U/mL PAD were combined together in pH 8.6 buffer and ΔA_{490} monitored. A control assay was performed in the absence of L-Tyr. It should be noted that L-Tyr at appropriate concentrations can function as a substrate of *SU* PAD at pH 8.6 (41). However, when the enzymatic reaction is coupled to the colorimetric assay, we find that 0.1 mM L-Tyr does not compete with oxidation of L-Phe. The procedure above was repeated except that L-Phe was used at a concentration of 0.125 mM or 0.275 mM and L-Tyr was substituted with 0.004 mM or 0.02 mM phenylpyruvate.

Experiment 5: ECA in 0 to 0.3 mM L-Phe Concentration Range

0.3 mM MTS, 0.15 mM PMS, 0 to 0.3 mM L-Phe, 0.75 mM NAD^+ and 0.17 U/mL PAD were combined together in pH 8.6 buffer and ΔA_{490} monitored. A control assay was performed in the absence of L-Phe. Two measurements for each L-Phe concentration were made per run, and each run repeated over 3 days. Initial ΔA_{490} (over 60 seconds) was calculated and plotted against L-Phe concentration to obtain a calibration curve of $y = 0.0017$ (0.0014 to 0.0019) + 0.02 (0.019 to 0.021) × x with n = 39, R = 0.98, standard deviation of residuals (S_R) = 0.00042 and limit of quantitation (LOQ) = 0.069 mM. Linear regression analysis was performed using Microsoft Excel

(2003), where values in parentheses represent lower and upper limits of either slope or intercept values at $p = 0.05$. LOQ was calculated as shown: LOQ = $3.3 \times S_R$ / slope of regression equation.

Experiment 6: Compare Effects of Serum and Plasma on ECA

0.3 mM MTS; 0.15 mM PMS; 0.075, 0.125 or 0.2 mM L-Phe - spiked serum or plasma sample; 0.375 mM NAD^+, and 0.17 U/mL PAD were combined in pH 8.6 buffer and ΔA_{520} monitored. A control assay was performed in the absence of L-Phe - containing serum or plasma sample.

<u>Measurement L-Phe Concentrations in Plasma Samples of PKU Patients Using a Microplate Reader:</u>

Patient Selection: Twenty five and 22 samples, respectively, of whole blood were collected in heparinized containers from patients at the beginning (6/21/04) and end (6/26/04) of "PKU camp" held at Emory University School of Medicine (Atlanta, GA). The methodology for blood collection was carried out in accordance with ethical standards of the Responsible Committee in Human Experimentation. All participants in the camp were females, diagnosed with PKU. Twenty participants were in the 12 to 18 years age - group and 5 participants were in the 18 to 48 years age - group.

DBS Preparation: DBS were prepared by the finger-prick method, where each S & S 903 filter paper was saturated with whole blood from a patient and air-dried at ambient temperature.

Calibration Curve: Fifty µL of ECA mixture was combined with 50 µL of L-Phe-spiked serum and ΔA_{510} monitored using a Molecular Devices Thermomax microplate reader. The final concentrations of reagents were as follows 0.2 mM MTS; 0.025 mM PMS; 0.37 mM NAD^+; 0.23 U/mL PAD; and 0.06, 0.1, 0.15, 0.2, 0.25, 0.3 L-Phe in 2.7 mM potassium phosphate / 21.4 mM triethanolamine buffer (pH 8.6). Five to 7 measurements for each concentration were performed per run and each run was repeated on 4 different days. Initial ΔA_{510} (over the first 300 seconds) was plotted against L-Phe concentration to obtain a calibration curve with a typical equation of y = 0.00019 (0.00018 to 0.00021) + 0.00064 (0.0006 to 0.00068) × x with n = 42, R = 0.98, S_R = 0.000025 and LOQ = 0.13 mM.

Each blood sample was centrifuged for 5 minutes at ambient temperature using a table-top IEC-HS centrifuge. Platelet-rich plasma (PRP) was separated from red blood cell mass, and either analyzed by ECA or stored at – 20°C. Three to 7 measurements for each fresh or frozen / thawed plasma sample were made in each run and the accompanying calibration curve obtained on that day was used to determine the sample L-Phe level. Several runs were carried out to determine pre- and post- "PKU camp" L-Phe concentrations. Depending on sample L-Phe concentration, 15 to 50 μL of PKU plasma was required for a single measurement.

<u>L-Phe Concentration Determination in Deproteinized Plasma by PAA:</u>

400 μL plasma sample was deproteinized with an equal volume of 6 % (v/v) SSA, centrifuged and the supernatant diluted with 500 μL of Lithium B buffer and 100 μL of 0.25 mM SAEC (17). PAA (AMR [Analytical Measurement Range]: 0.00625 mM to 2.00 mM) was performed on a Beckman 6300 AA analyzer equipped with an in-line colorimetric detector. The sample was applied onto a Beckman column and AAs separated using a combination of Beckman Coulter's Lithium buffers A, D, E and F (pH range: 2.9 - 3.9). The eluent was mixed with ninhydrin and absorbance measured at 570 nm and 440 nm, respectively. The Beckman Gold analysis software was used to identify and quantify AAs based on retention time and absorbance values with respect to that of calibration standards. One measurement was performed for each plasma sample and pre- and post- "PKU" specimen were analyzed on two separate days.

<u>L-Phe Concentration Determination in DBS by HPLC:</u>

A 3 mm diameter circle was punched out from the center of DBS on S&S 903 filter paper from a PKU patient or a QCS and eluted with 50 μL of 70 % (v/v)

CH_3CH_2OH containing 5 μM $(Br)_2$ L-Tyr for 20 minutes via sonication (42-44). After centrifugation, 20 μL of the supernatant was derivatized with AccQ-Fluor reagent at 55^{o}C for 10 minutes (22-24). HPLC analysis (AMR: 0.008 mM to 0.250 mM) was performed using a Waters 2690 separations module equipped with a Waters 2475 fluorescence detector. The analyte was applied onto a Waters AccQ-Tag column and eluted at 1 mL/min or 0.5 mL/min using a mobile phase system consisting of AccQ-Tag eluent concentrate (A)/ CH_3CN (B) / H_2O (C) at 37^{o}C. The emission and excitation wavelengths were set at 250 and 395 nm, respectively. Two runs per patient sample were carried out on the same day and pre- and post- "PKU camp" plasma analyzed on two separate days.

<u>L-Phe Concentration Determination in DBS by MS/MS:</u>

A 3 mm diameter circle was punched out from the center of DBS on S&S 903 filter paper or QCS and eluted with 100 μL of CH_3OH, containing stable isotope labeled AAs for 20 minutes via sonication (18, 45). After solvent evaporation, AAs were esterified using 3 N *n*-butanolic HCl at 65^{o}C, dried again and redissolved in 80% (v/v) CH_3CN (18, 45). MS/MS analysis (AMR: 0.021 mM to 0.20 mM) was performed on a Micromass Quattro Micro. TIS capillary voltage was held at 3.5 kV, the cone voltage at 35 V and the collision energy at 25 V (the collision gas was Ar). MS/MS analysis used MS/MS scan of a neutral loss of 102 and data analysis performed with Neolynx software. Two runs per patient sample were conducted on the same day and pre- and post- "PKU camp" plasma analyzed on two separate days.

<u>Statistical Analysis of ECA, HPLC, MS/MS and PAA Data:</u>

Intra-day run comparison of L-Phe concentrations in undeproteinized plasma samples measured by ECA were carried out using a Student's t-test for paired means at p = 0.01. Between run comparisons were carried out by computing the standard deviations for the mean L-Phe concentration in each sample in a given run. Pearson correlation coefficients were computed using data collected by ECA, PAA, HPLC and MS/MS methodologies. Bland and Altman plots were used in further comparisons of the ECA, MS / MS and HPLC data to that obtained by PAA.

Microplate ECA with Immobilized Reagents:

An immobilized ECA mixture was prepared by dissolving teleostean gelatin upon heating. ECA components were added to the cooled gelatin mixture. First, 35 μL of gelatin was poured per well of a microplate and dried under a steady stream of air (the final pH of the ECA was 7.0). Thirty five μL of L-Phe buffered at pH 8.6 was added to an ECA–containing well and ΔA_{510} monitored. The final concentrations of ECA reagents were 0.15 mM MTS, 0.075 mM PMS, 0.75 mM NAD^+, 0.13 U/mL PAD, 0.085 mg/μL gelatin, 0.05 mM to 10 mM L-Phe and 2.7 mM potassium phosphate / 21.5 mM triethanolamine buffer. A control assay was performed in the absence of PAD. Initial ΔA_{510} (over the first 300 seconds) was plotted against L-Phe concentration to obtain a calibration curve using Microsoft Excel (2003) of $y = 0.000016 \times x + 0.00008$ with $n = 5$ and $R^2 = 0.98$.

Formulation of Test-Strip for Measuring L-Phe Concentrations

Film Composition and Preparation:

Experiment 1: Effect of pH, Presence of Gelatin, Buffer composition and MTS/PMS Ratio on ECA:

An ECA mixture was prepared by dissolving teleostean gelatin in buffer upon heating. MTS, PMS, L-Phe, NAD^+ were added to the cooled gelatin mixture and stirred vigorously in the presence or absence of Tritonr X detergent. PAD was added to the ECA mixture and absorbance changes at 490 nm were monitored on an HP 8453 diode array spectrophotometer equipped with an HP 8909 temperature-control accessory at 3-second intervals over a period of 300 seconds. The control assay was carried out in the absence of gelatin in 5 mM potassium phosphate / 43 mM triethanolamine (final assay pH of 8.6). The final concentrations of ECA reagents were 0.4 mM MTS, 0.05 or 0.2 mM PMS, 0.375 mM NAD^+, 0.15 U/mL PAD, 0.1 or 0.6 mM L-Phe, 0.11 mg/μL gelatin, 0.0005g/ml Tritonr X and 3.3 mM potassium phosphate / 26.1 mM triethanolamine buffer (pH 7.0) or 5 mM potassium phosphate / 43 mM triethanolamine (pH 7.5). Note the presence of gelatin at the given concentration lowers pH of the ECA mixture by 0.9 units.

Experiment 2: Composition and Preparation of ECA, Filtering / Reflecting (FRL) and Spreading (SL) Layers by Manual Application:

Polyethylene terephthalate (PET) and Fisherfinest Premium microscope slides were used as film supports (Scheme 3 - 6). The ECA layer mixture was prepared by dissolving teleostean gelatin in pH 8.6 buffer by heating, and upon cooling of the solution adding all or some ECA reagents (0.3 mM MTS, 0.15 mM PMS, 1.5 mM NAD^+ and 0.4 to 0.97 U/ml PAD) to 5.6 mM potassium phosphate buffer / 56 mM triethanolamine. The final pH of the ECA mixture was 7.0. Subsequently, the ECA mixture was placed on a solid support (laid flat on the leveling draw-down plate) and spread over the surface with uniform strength using a 4 mil Gardco rod. The film (approximate wet thickness of 102 μm measured with a Gardco depth gauge) was allowed to dry at 25°C in a dust-free hood overnight. The dry thickness in 3 different areas of the same film was measured using a micrometer gauge (n = 9) and found to vary between 9.3 and 22.9 μm, with an average dry thickness of 16.5 μm. Blank ECA layers were produced by excluding all reagents but gelatin, while control ECA layers were made by including all ECA reagents but PAD, the reaction ECA layers contained all the assay reagents. The final amounts of ECA reagents in the volume of ECA layer that comes in contact with 10 μL of analyte are 1.4 mg gelatin, 2.4 nmol MTS, 0.12 nmol PMS, 0.012 μmol NAD^+, 0.0029 to 0.0078 Units PAD, 0.044 μmol potassium phosphate and 0.35 μmol triethanolamine.

FRL was prepared by evenly dispersing 1.2 g of TiO_2 (particle size range of 1 to 5 μm) in 5 ml of 3 % (w/v) cellulose acetate (CA) solution in acetone. The mixture was then diluted to a total volume of 8 ml with a 1:1 mixture of acetone : xylenes. This mixture was then placed on the solid support or ECA layer and spread uniformly over the surface with a 8 mil Bird applicator and 4 or 8 mil Gardco applicator rod . The film was allowed to dry at 25^oC, in a dust-free hood.

SL was prepared by evenly dispersing 0.186 g CA, 0.015 g SSA and 1.8 g of diatomaceous earth in 1.2 : 1 mixture of CH_2Cl_2 : acetone. The slurry was then placed on the solid support or ECA layer or FRL surface and spread out evenly with a 8 mil Bird applicator. The film was allowed to dry at 25^oC, in a dust-free hood.

Experiment 3: Composition and Preparation of ECA, FRL and SL by Spin Coating

PET squares (2.54 × 2.54 cm) or VWR micro-cover glass (2.2 cm in diameter and 0.23 mm in thickness) were used as film supports. Two hundred μL of ECA-containing mixture was placed on the surface of the support and a film layer produced on a WS-400B-6NPP-LITE spin coater via different methodologies. The optimized spin coating method that produced the best results employed a standard acceleration and a 2-step procedure with a 1st step of 500 rpm (30 seconds) followed by the 2nd step of 1500 rpm (3 minutes). The ECA stock solution used to prepare the film contained 0.35 mg/μL of gelatin, 5 mM MTS, 0.625 mM PMS, 10 mM NAD^+, 15 U/ml PAD in 10.5 mM potassium phosphate / 84 mM triethanolamine (pH 7.0). The thickness of ECA layer was measured on a Zygo interferometer and found to be less than 50 nm, which is the LOD (limit of detection) of this particular instrument.

FRL mixture was prepared by dispersing 1.2 g of TiO_2 (particle size of 200 nm and 30 nm) in 5 ml of 3 % (w/v) CA solution in acetone. The mixture was then diluted to a total volume of 8 ml with a 1:1 mixture of acetone : xylenes in the presence or absence of 0.063 % Tritonr X and stirred for 20 to 24 hours. Two hundred μL of FRL mixture was subsequently placed either on ECA layer or solid support and the film formed on a WS-400B-6NPP-LITE spin coater via different methodologies. The best results were obtained with 1.2 g TiO_2 of 200 nm particle size, presence of detergent in FRL aided the wettability of the film but didn't improve the analyte spreading. Several spin coating methods with standard acceleration were employed to make single, double and triple filtering / reflecting layers. Spin speeds of 500, 1000, 1500, 2500 or 5000 rpm were employed with a deposition time of 1 to 1.3 minutes, identical or different spin speeds were used in the formation of a double or triple layer films. The uniformity of single layer films produced with spin speeds of 500, 2000 or 5000 rpm were analyzed using electron microscopy. The number of pinholes was minimized when intermediate spin speed was used. The thickness of one - layer films made at spin speeds of 2000 or 3000 rpm for 1 minute was analyzed on the Tencor Alpha-Step Profilometer. The results showed that uneven films of 2 to 5 μm at faster speeds and 10 to 12 μm at slower speeds were produced, some pinholes on film surface were 20 μm in diameter.

SL was prepared by evenly dispersing 0.375 g CA, 0.015 g SSA and 1.5 g of diatomaceous earth in 1.2 : 1 mixture of CH_2Cl_2 : acetone with or without a small quantity of Tritonr X detergent. The slurry was then placed on the solid support or ECA layer or FRL surface and the film formed on a WS-400B-6NPP-LITE spin coater via different methodologies. The best results were produced with a spin speed of 1000 rpm for 1.3 minutes and standard acceleration.

Experiment 4: Composition and Preparation of ECA, FLR and SL by Solvent Casting

Finally, the most successful ECA layers were prepared using an Aluminum mold (inner diameter of 2.54 cm). Various volumes of ECA mixture (350, 400 or 600 μL) were placed in the mold secured on top of the PET support with vacuum seal grease and allowed to dry under a steady stream of cool air in a dust-free hood at 25^{o}C. The best results were obtained with a 350 μL ECA volume. The concentrations of the reagents in the assay mixture were as follows: 108 mg/ml teleostean gelatin, 1.05 mM MTS, 0.26 mM PMS, 5.4 mM β-NAD^+, 2.3 U/ml PAD and 3.3 mM potassium phosphate/ 26.1 mM triethanolamine buffer (final pH 7.1). The final amounts of ECA reagents in the volume of ECA layer that comes in contact with 10 μL of analyte (considering it spreads to an average diameter of 1.0 cm) are 7.4 mg gelatin, 72.4 nmol MTS, 17.94 nmol PMS, 0.37

μmol NAD^+, 0.16 Units PAD, 0.23 μmol potassium phosphate and 1.8 μmol triethanolamine.

FRL mixture was prepared by dispersing 0.6 g, 0.9 g, 1.2 g 1.5 g, 1.8 g or 2.1 g of TiO_2 (particle size of 1 to 5 μm or 200 nm or 30 nm) in 5 ml of 3 % (w/v) CA solution in acetone. The mixture was then diluted to a total volume of 8 ml with a 1:1 mixture of acetone : xylenes in the presence or absence of 0.063 % Tritonr X. One hundred and fifty, 200, 300, 400 or 600 μL FRL was subsequently poured either onto PET or ECA layer within the well of the mold and allowed to air-dry at 25°C. The best films (minimal cracking or peeling) were obtained using 400 μL of FRL mixture made with 1.2 g TiO_2 of 30 nm particle size.

SL was prepared by evenly dispersing 0.375 g CA, 0.015 g SSA and 1.5 g of diatomaceous earth in 1.2 : 1 mixture of CH_2Cl_2 : acetone. Two hundred, 300, 400 or 500 μL SL was then poured onto PET or ECA layer within the mold and allowed to air-dry at 25°C.

Measurements Carried Using the Portable Ocean Optics Spectrometer Equipment:

The fiber optic cable connected to the halogen light source was placed in the 45° angle slot of the probe holder, while the fiber optic connected to the detector was placed in the 90° angle slot. The integration time was adjusted such that the recorded signal intensity was between 3200 and 3500 intensity counts when the film was placed on the probe holder with PET underside facing the light source and detector. The 'dark' reading was taken at the set integration time when the light source and detector were completely covered. The 'reference' reading was taken when the film was placed in the path of the light source with no analyte added to the surface. Subsequently, 10 μL drop of pH 8.6 buffer or L-Phe (0.5, 1 or 20 mM buffered at pH 8.6) or plasma (diluted with pH 8.6 in a 1:1 ratio) or serum (diluted with pH 8.6 buffer in a 1:1 ratio) was placed on the surface of the ECA or FR or SL layer, the liquid spread over an area approximately 10 mm in diameter in the absence of Tritonr X detergent. In the absence of FRL or SL, a polished

Teflon surface was placed on top of the spreading and % reflectance measured at various time intervals (10 to 30 sec) over a period of 600 seconds in transmittance mode at 490 nm.

In order to investigate the speed with which an aqueous analyte penetrated FRL (prepared in the absence or presence of 0.063 % (v/v) Tritonr X detergent), a 5 or 10 μL drop of 1.2 mM methylene blue was placed on FRL and % reflectance measured at 40 second intervals over a period of 600 seconds at 610 and 670 nm respectively. The presence of detergent in FRL caused irregularity in analyte spreading.

Testing the Sensitivity of the Ocean Optics Detector Cable:

A color pallet of varying intensities (0 to 10 % printed on Epson Styles Color 880 Color Ink Jet printer) was prepared by Charlie Oldham using CoralDRAW (Version 12). The integration time was adjusted as described above for 0 % magenta, 'dark' and 'reference' readings taken in scope mode at the set integration time. The spectra were collected in reflectance mode, whereas the absorbance maxima were at 550 nm.

3 – 4: RESULTS

Selection of Reagents for the Enzymatic-Colorimetric Assay:

SU PAD was chosen as the enzyme for our ECA due to its high degree of specificity for L-Phe as a substrate and its commercial availability (41). Table 3 - 2 compares the specificity, stability, ease of inactivation with inhibitors and other parameters of PAD from *Rhodococcus sp.* M4 strain (*RM*4) and *Sporosarcina ureae* (*SU*) (46). According to the research studies conducted thus far, *SU* PAD is more specific than *RM*4 PAD but is more susceptible to inactivation by various chemicals. Asano *et. al.* reported that *SU* PAD was stable for at least 1 month when stored at 4^{o}C in 10 mM potassium phosphate buffer (pH 7.0), 0.1 M EDTA and 5 mM 2-mercaptoethanol, and for a period of 2 years when stored in crystalline form (41). We investigated the stability of PAD over a 40-day period under different storage conditions (refrigerated or frozen solution, or lyophilized powder). Assay data indicated that loss of activity was minimized when PAD was stored lyophilized in the presence of 50 mM potassium phosphate (pH 7.0) at – 20^{o}C, with no additional stabilizing agents that might interfere with the ECA.

Tetrazolium dyes and Mediators:

Tetrazolium salts are readily reduced chromogenic dyes that generate formazan dyes. These salts are widely used to measure cell proliferation and viability (extra cellular and intracellular dehydrogenase / oxidoreductase activity), in cytotoxicity assays, histochemical procedures and bacteriological screening (respiration) (47). Typically, a tetrazolium dye (MTS, MTT, NBT, XTT or WST-1– 8) is reduced by an electron mediator or directly by NADH or NADPH, formed from a NAD^{+} or $NADP^{+}$ precursor involved in the reaction of the dehydrogenase enzyme and its substrate. Unfortunately some formazan dyes, such as MTT, have poor water solubility and hence cause precipitation during spectrophotometric detection in a certain concentration range.

Table 3 - 2: Comparison of PAD from 2 Different Sources

	PAD from *Rhodococcus sp* M4 strain	PAD from *Sporosarcina ureae*
Substrates	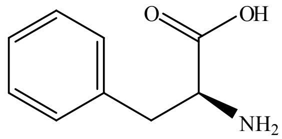 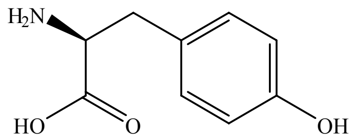 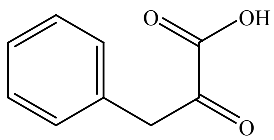 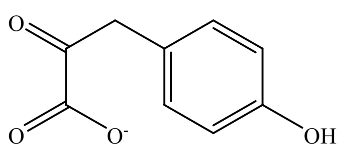 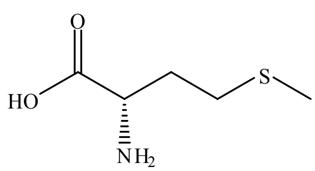 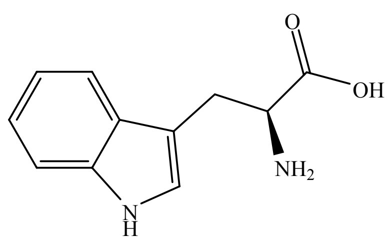 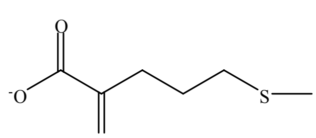 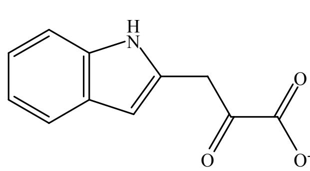 NH_4^+	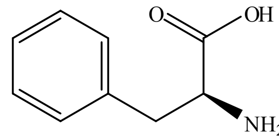 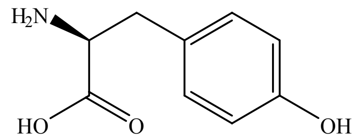 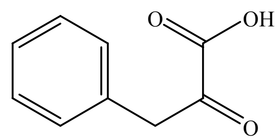 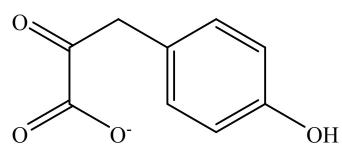 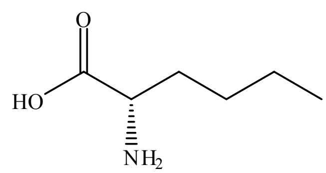 NH_3

Table 3 - 2: Comparison of PAD from 2 Different Sources (Continued)		
Inhibitors	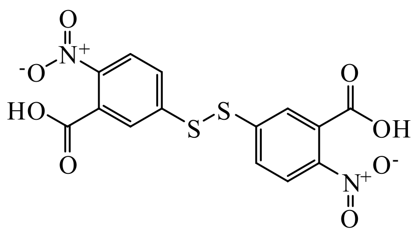 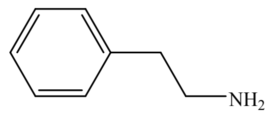 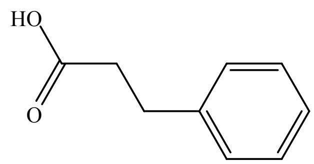 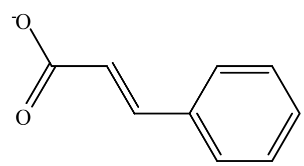	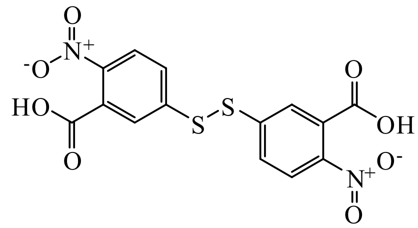 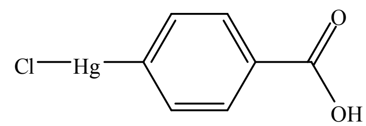 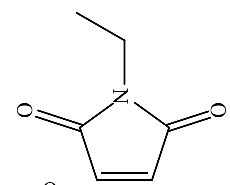 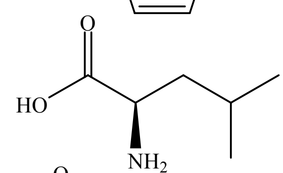 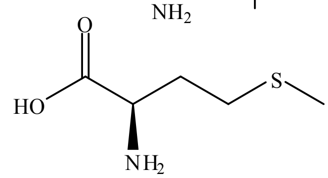 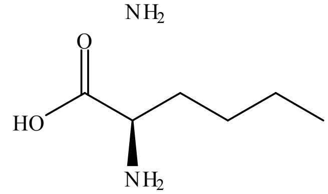 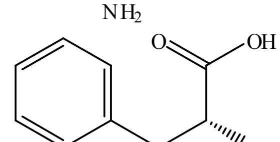 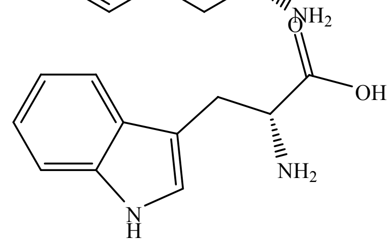 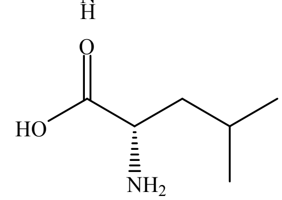 $AgNO_3$; $HgCl_2$

Table 3 - 2: Comparison of PAD from 2 Different Sources (Continued)		
pH	9.3 (reductive amination)	9 to 10.3 (reductive amination) 10.5 to 11.3 (oxidative deamination)
Temperature Optimum	20°C	40°C
Molecular Weight	150 KDa (gel filtration)	305 KDa (sedimentation) 310 and 290 KDa (gel filtration)
Number of Subunits	Tetramer	Unknown

The use of water-soluble dyes (XTT and WST-1) is therefore advantageous. Unlike MTT; XTT, MTS and WST-1 are efficiently reduced by NADH and NADPH in the absence of cells or enzymes but in the presence of electron mediators such as PMS, MPMS (1-methoxy phenazine methosulfate), PES (phenazine ethosulfate) or MB (8-dimethylamino 2,3-benzophenoxazine) and the reduction process involves superoxide (47). Unfortunately, the mechanism of bioreduction of tetrazolium dyes such as MTS has not been fully elucidated (47). The ability of tetrazolium dyes to penetrate plasma membranes without irreparably damaging the cell, is an important parameter in dye selection. Plasma-membrane permeable tetrazolium derivatives (MTT) can undergo reduction intra- and extra-cellularly. On the other hand, plasma membrane-impermeable tetrazolium derivatives (CTC [5-cayno-2,3-ditolyl tetrazolium chloride], WTS-1) are separated from reducing species located in the cell interior, hence their bioreduction can be carried out by plasma membrane associated reductases or long-lived reducing species capable of diffusing out of cells (47, 48). The membrane permeability of MTS has not been investigated, but it would be relevant to the function of ECA, because it is designed to measure extra-cellular levels of plasma L-Phe.

The MTS-PMS dye-mediator combination was found to be optimal for our ECA, which is depicted in Scheme 3 - 5. The regeneration of NAD^+ in the presence of MTS and PMS is facile, occurs in a stoichiometric manner, is accompanied by a distinct color change, and both oxidized and reduced forms of MTS are H_2O-soluble under the ECA conditions. The UV-Visible spectra of MTS and PMS components before and after reduction by NADH are shown in Figure 3 - 1. Upper panel of Figure 3 - 2 shows that PAD-catalyzed conversion of limiting L-Phe concentrations (0.012 mM, 0.06 mM or 0.12 mM) to phenylpyruvate is proportional to L-Phe concentration although the reaction is incomplete after 30 minutes as indicated by the stoichiometry of NADH production (0.008 mM, 0.021 mM or 0.046 mM respectively). Lower panel of Figure 3 - 2 shows

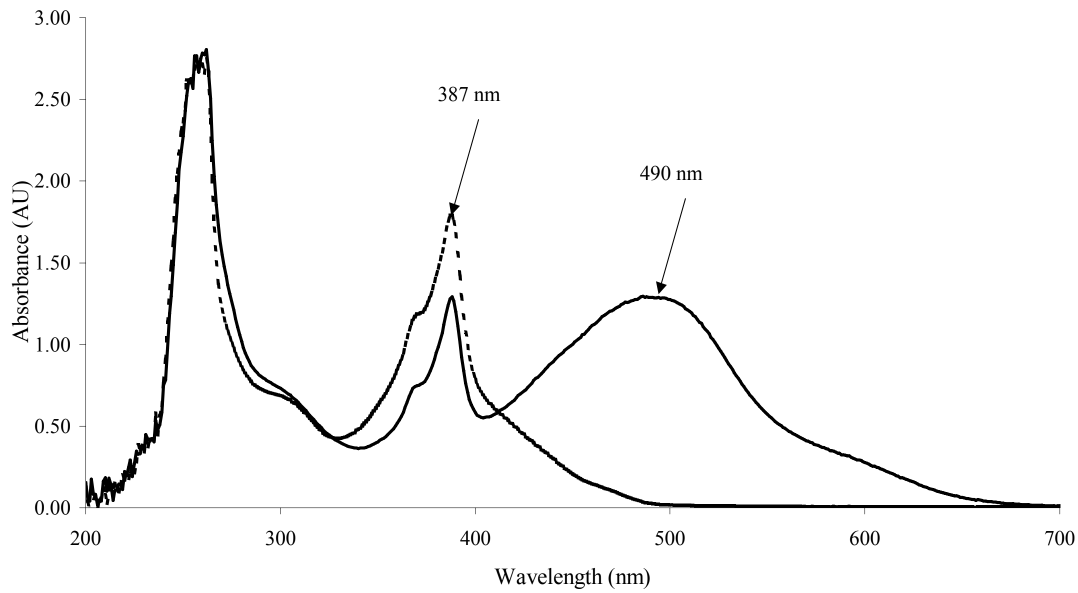

Figure 3 - 1. Overlaid absorbance spectra of 0.06 mM MTS and 0.04 mM PMS in the absence of NADH (- -) and in the presence of 0.06 mM NADH (—) in pH 8.6 buffer.

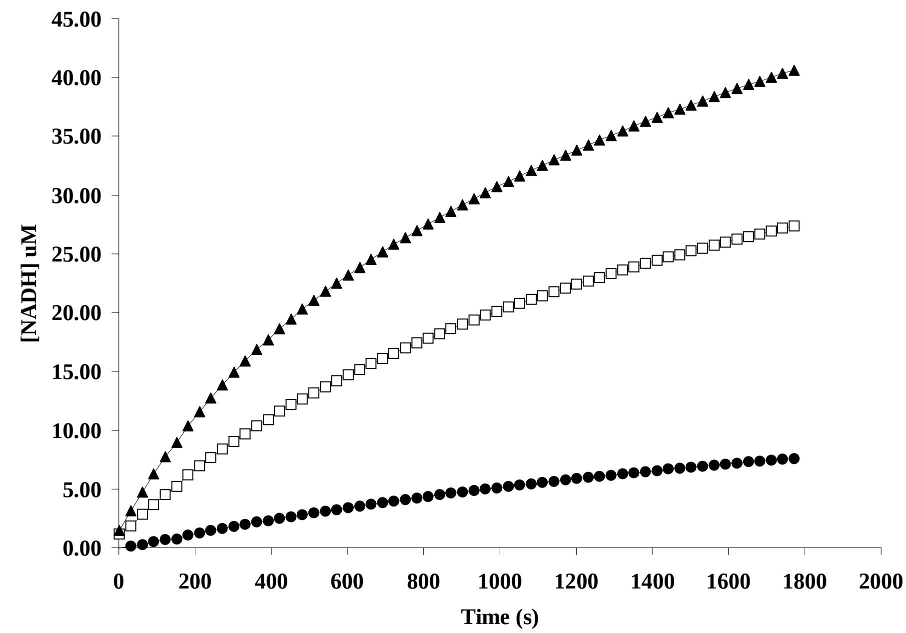

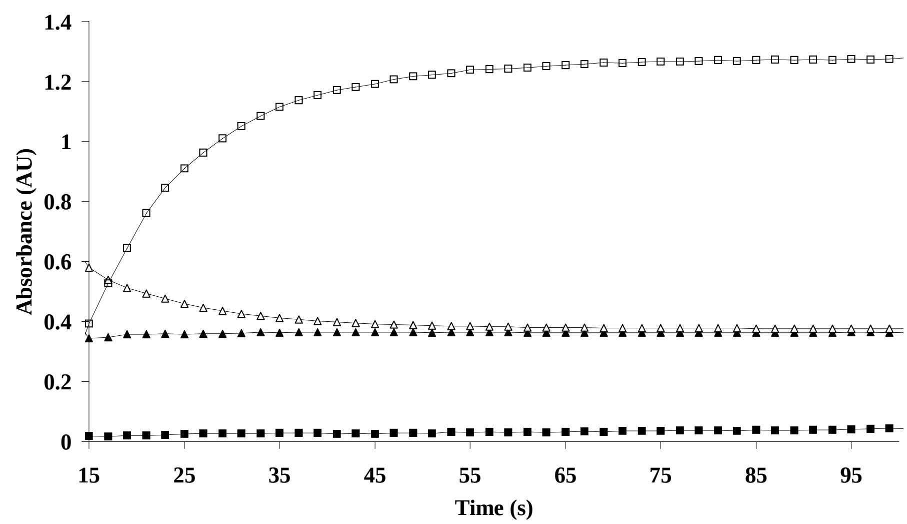

Figure 3 - 2. Upper Panel: Three mL of enzymatic assay contains 0.75 mM NAD^+; 0.012 mM (●), 0.06 mM (□) or 0.12 mM (▲) mM L-Phe and 0.10 U/mL PAD in pH 8.6 buffer. Lower Panel: Three mL of colorimetric assay contains 0.06 mM MTS, 0.04 mM PMS and either 0 mM (340 nm [▲] and 490 nm [■]) or 0.06 mM (340 nm [Δ] and 490 nm [□]) NADH in pH 8.6 buffer.

that 0.06 mM NADH completely reacts with an equivalent amount of MTS in the presence of PMS within 60 seconds, thus demonstrating that the PAD-catalyzed reaction is the rate-determining step in ECA at low L-Phe concentrations.

The effects of changing the concentrations of ECA components were systematically investigated. Within 0 to 0.3 mM L-Phe concentration range, 0.06 mM MTS was found to have no inhibitory effect on PAD activity. In addition, L-Tyr did not interfere with function of ECA; 0.1 mM L-Tyr used is on the high end of concentration range anticipated to be present in plasma of PKU patients. ECA was carried out at pH 8.6 and not pH 10.5 which is optimal for PAD activity, because the rate of spontaneous formazan formation increases with increasing pH (49); at this lower pH, the activity of PAD was reduced by a factor of 2.7.

Blood L-Phe concentration of PKU patients can exceed 1.2 mM, with the reference clinical range for L-Phe at 0.078 to 0.206 mM depending on the age of the individual (50). A linear dependence of the rate of change of absorbance at 490 nm for a broad range of L-Phe concentrations (from 0 to 2400 μM) was obtained, when the concentrations of ECA reagents were adjusted as described in the MATERIALS AND METHODS. The best results were obtained for 0 to 0.3 mM L-Phe concentration range with a regression equation of $y = 0.0017\ (0.0014 \text{ to } 0.0019) + 0.020\ (0.0186 \text{ to } 0.0214) \times x$ ($n = 39$ and $R = 0.98$), which corresponds to a diluted range of 0 to 9 mM L-Phe. The limit of quantitation (LOQ) was determined as described in the experimental section, and found to be 0.069 mM. The accuracy of the curve was tested with standard samples containing known L-Phe concentrations, where % differences between determined and actual concentrations of L-Phe were 1.1 % for 0.11 mM L-Phe and 5.6 % for 0.175 mM L-Phe.

[L-Phe] Determination in Serum and Plasma Samples Using the ECA:

The effect of serum components on ECA was investigated. The presence of serum in ECA, filtered through a 0.45 μm membrane, caused a shift in λ_{max} of the formazan dye from 490 to 520 nm. Experiments were then carried out to investigate the effect of PRP– and serum- spiked L-Phe solutions on ECA. Table 3 - 3 shows that initial ΔA_{520} were identical for serum- and PRP- containing ECAs at L-Phe concentrations of 0.075 mM, 0.125 mM and 0.25 mM. It is therefore evident that additional components present in plasma as compared to serum do not interfere with ECA function under the given reaction conditions.

Whole blood samples were collected from 25 and 22 participants at the beginning and end of "PKU camp", respectively. During the week of camp, the patients were placed on a diet consisting of low Phe protein products enriched with Tyr. PRP was prepared from whole blood and L-Phe concentration in each sample determined by our ECA as described in the MATERIALS AND METHODS. Figure 3 - 3 shows a typical calibration curve used to determine L-Phe concentration in each sample, with typical R values in such graphs ranging from 0.93 (n = 47) to 0.98 (n = 42) with a mean LOQ of 0.07 mM. At least two L-Phe concentration measurements were made in a given run per patient sample, and runs repeated over a number of days. Figure 3 - 4 shows within run variation in mean L-Phe concentrations measured by ECA in pre- and post- "PKU camp" samples (Upper Panel). Mean sample L-Phe concentrations measured in separate runs were compared using Student's t-test for paired means and found to be statistically equivalent at $p = 0.01$ in all but one inter-run comparison. Overall average L-Phe concentrations at the beginning and end of "PKU camp" for each participant were subsequently determined, and correlation with the diet the subjects were placed on depicted in Figure 3 - 4 (Lower Panel). It is evident that for most PKU patients with elevated L-Phe levels, a decrease in L-Phe was observed after a one-week camp.

Table 3 - 3: Effect of Serum and Plasma on ECA Compared Rate of Change of Absorbance (AU/sec)				
	[L-Phe] = 0 μM	[L-Phe] = 75 μM	[L-Phe] = 125μM	[L-Phe] = 250μM
Serum	0.0011	0.0023	0.0030	0.0036
Plasma	0.0013	0.0022	0.0029	0.0036

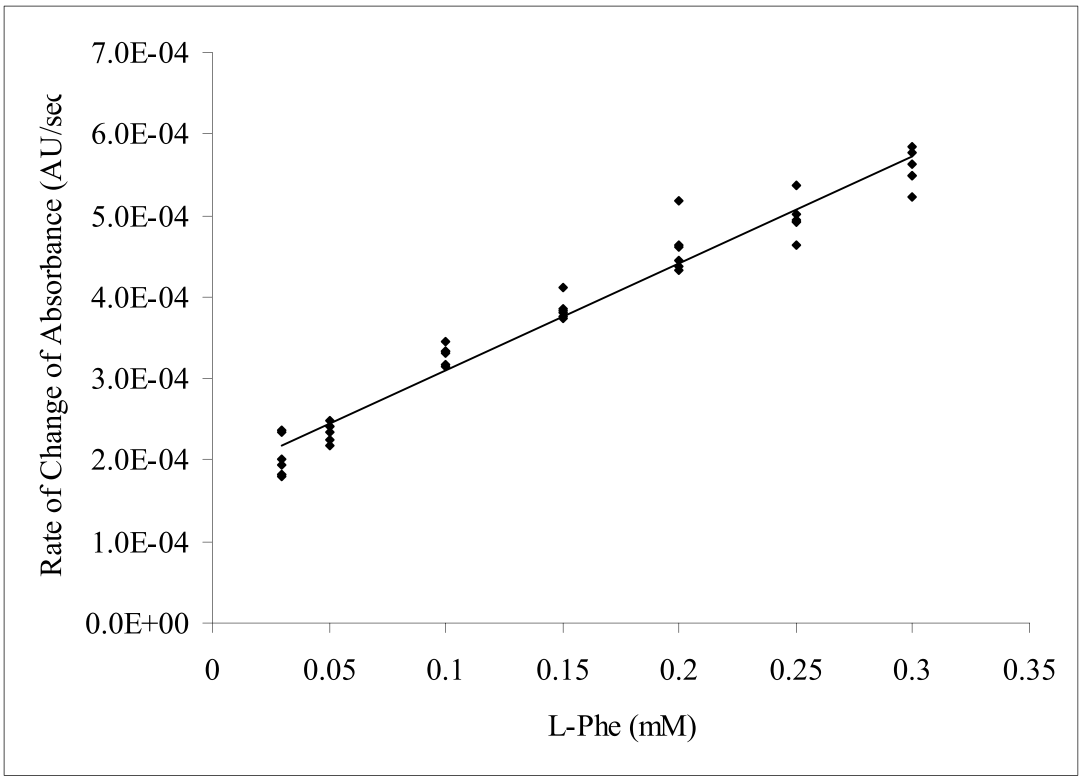

Figure 3 - 3. A calibration curve used to determine plasma L-Phe concentration of PKU patients obtained as described in the experimental section. The regression equation for the calibration curve is $y = 0.0013\ (0.0012 \text{ to } 0.0014) \times x + 0.00018\ (0.00016 \text{ to } 0.00019)$ with $n = 42$, $R = 0.98$, $S_R = 0.000024$ and LOQ = 0.06 mM.

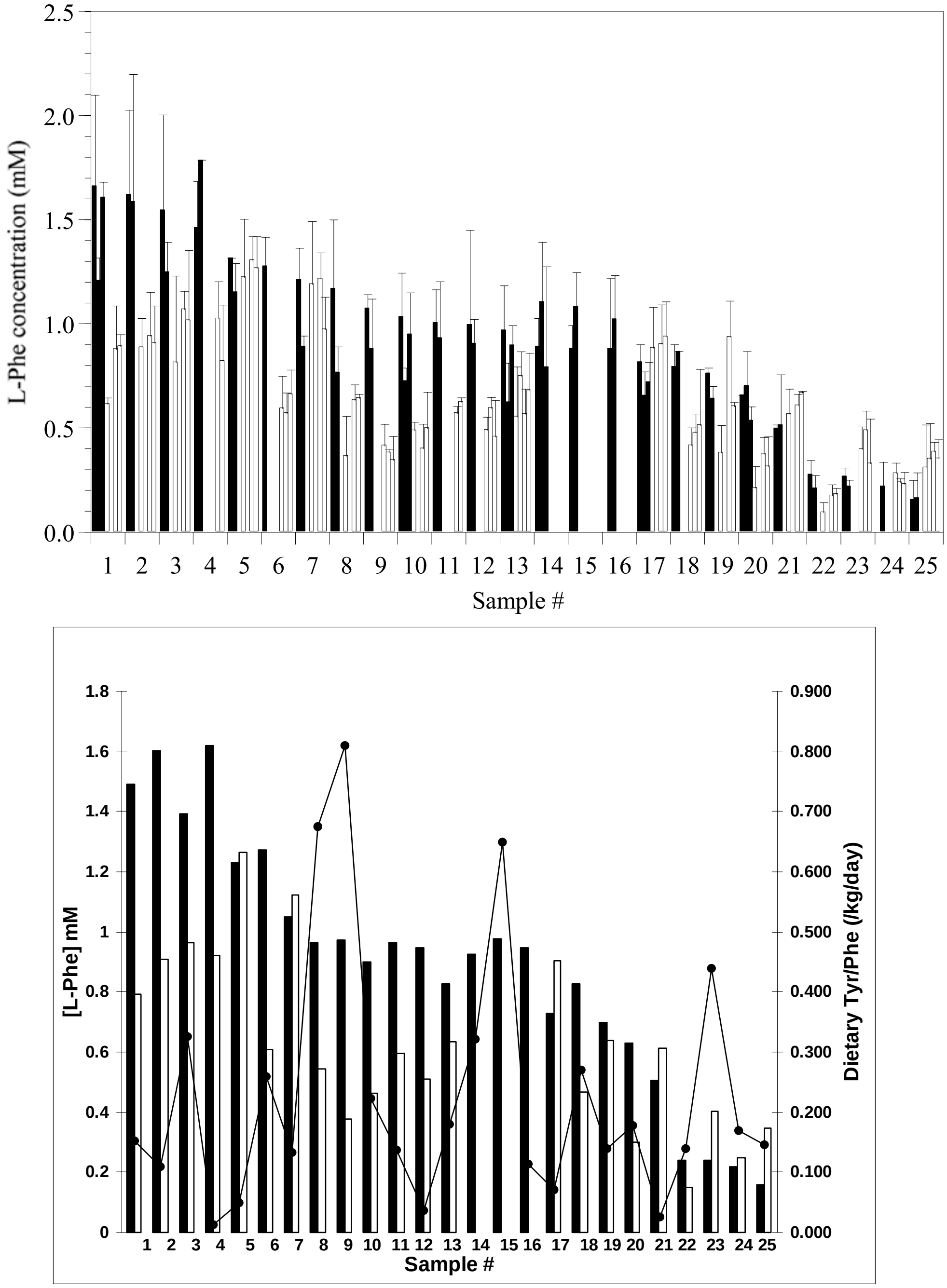

Figure 3 - 4. Upper Panel: Inter- and intra- run comparison of mean plasma L-Phe concentrations measured by ECA, each bar represents run average per sample measured at the beginning (■) and end (□) of "PKU camp". Lower Panel: Average L-Phe concentrations in pre- (■) and post- (□) PKU camp samples. Dietary Tyr/Phe per kg of weight a day fed to each subject at the beginning of "PKU camp" is represented by ─.

Comparison of our ECA to Other Techniques Used to Monitor PKU:

Three other techniques were used to measure L-Phe levels in plasma and DBS samples from "PKU camp" participants: PAA, HPLC and MS/MS. PAA was conducted on deproteinized plasma samples, while HPLC and MS/MS analyses were performed on derivatized DBS eluates as described in the MATERIALS AND METHODS section. Table 3 - 4 and Figure 3 - 5 show that the ECA results correlated reasonably well with the data obtained by PAA with a Pearson correlation coefficient $R = 0.951$ at $n = 47$ and $p < 0.0001$. R values within a similar range were obtained when L-Phe concentrations determined by PAA were compared with results of HPLC and MS/MS analyses with $R = 0.976$, and $R = 0.988$, respectively. Tables 3 - 5 and 3 - 6 show that ECA results collected with the pre-'PKU' camp plasma samples had a higher Pearson correlation coefficient with PAA data of 0.961 than post-'PKU' camp data with R values of 0.926.

ECA-, HPLC- and MS/MS- measured L-Phe concentrations were then compared with values determined by PAA using Bland and Altman plots. Figure 3 - 6 shows that L-Phe concentrations measured by PAA are on average 0.065 mM lower than values measured by ECA and on average 0.14 mM and 0.10 mM higher than those measured by MS/MS and HPLC analyses. Higher ECA-determined L-Phe values could be the result of minimizing the manipulations carried out on the patient sample in comparison to PAA, HPLC and MS/MS methods, which involve plasma deproteinization or DBS eluate derivatization and if needed deproteinization (50, 51). In addition, Figure 3 - 6 shows that differences between individual L-Phe values determined by either HPLC or MS/MS and PAA are smaller in the L-Phe concentration range of 0 to 0.80 mM. A similar trend, which correlated L-Phe concentration range and differences in values measured by ECA and PAA was not observed. Bland and Altman plots also show that the majority of the points are within $2 \times SD \pm d$ range, where SD represents the standard deviation of the mean difference (d) between L-Phe concentrations measured by PAA and either HPLC, MS/MS or ECA.

Table 3 - 4: Combined Pre- and Post- “PKU camp” Data

Pearson Correlation Coefficients ($n = 47$, $p < 0.0001$)

	PAA	HPLC	MS/MS	ECA
PAA	1.000	0.976	0.988	0.951
HPLC	0.976	1.000	0.980	0.905
MS/MS	0.988	0.980	1.000	0.937
ECA	0.951	0.905	0.937	1.000

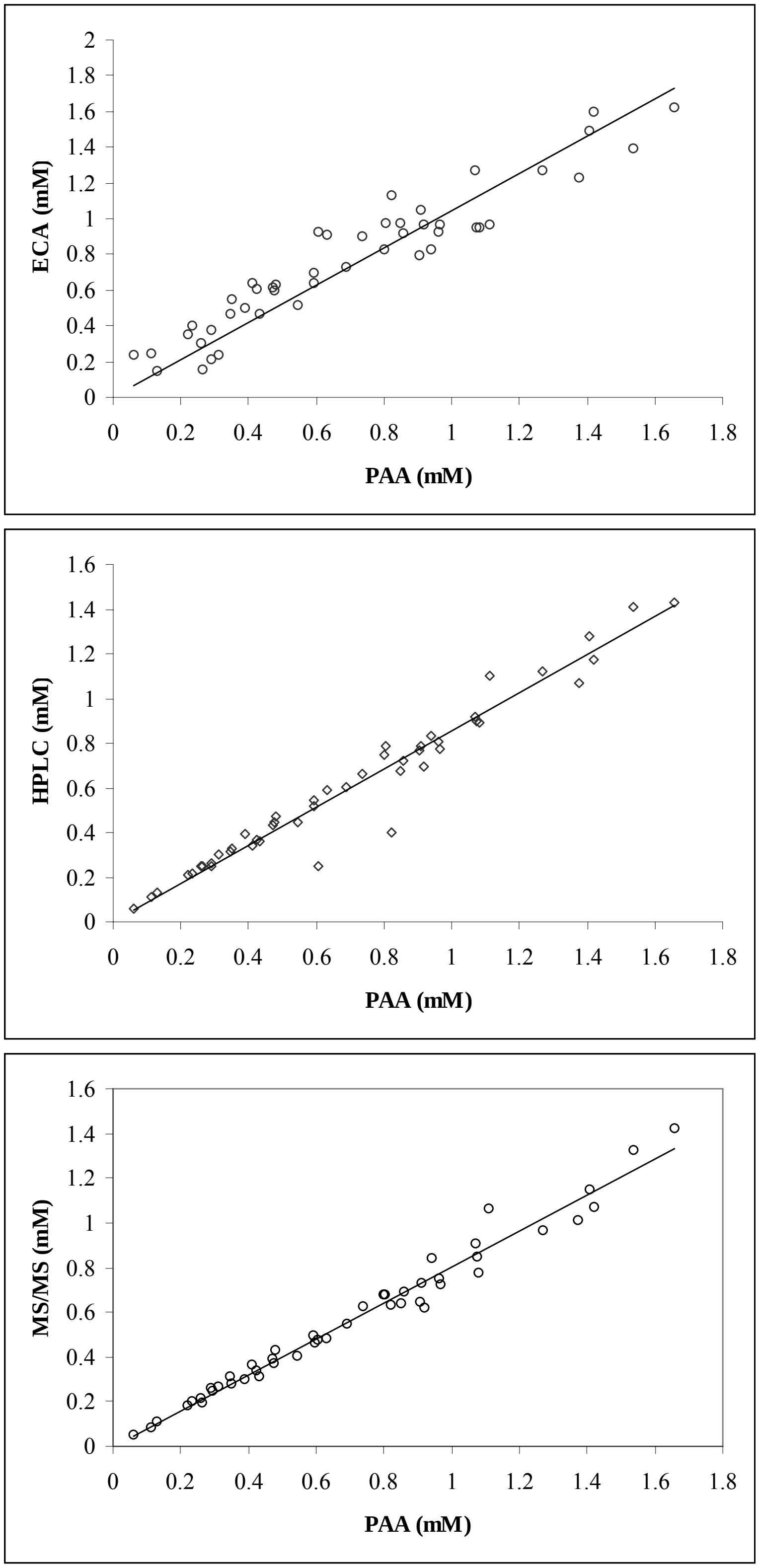

Figure 3 - 5: Correlation plots of HPLC ,MS/MS-, ECA- measured L-Phe values as compared to PAA data.

Table 3 - 5: Pre - "PKU camp" Data Pearson Correlation Coefficients (n = 47, p < 0.0001)				
	PAA	**HPLC**	**MS/MS**	**ECA**
PAA	1.000	0.988	0.983	0.961
HPLC	0.988	1.000	0.995	0.948
MS/MS	0.983	0.995	1.000	0.936
ECA	0.961	0.948	0.936	1.000
Table 3 - 6: Post -"PKU camp" Data				
	PAA	**HPLC**	**MS/MS**	**ECA**
PAA	1.000	0.922	0.991	0.926
HPLC	0.922	1.000	0.915	0.784
MS/MS	0.991	0.915	1.000	0.940
ECA	0.926	0.784	0.940	1.000

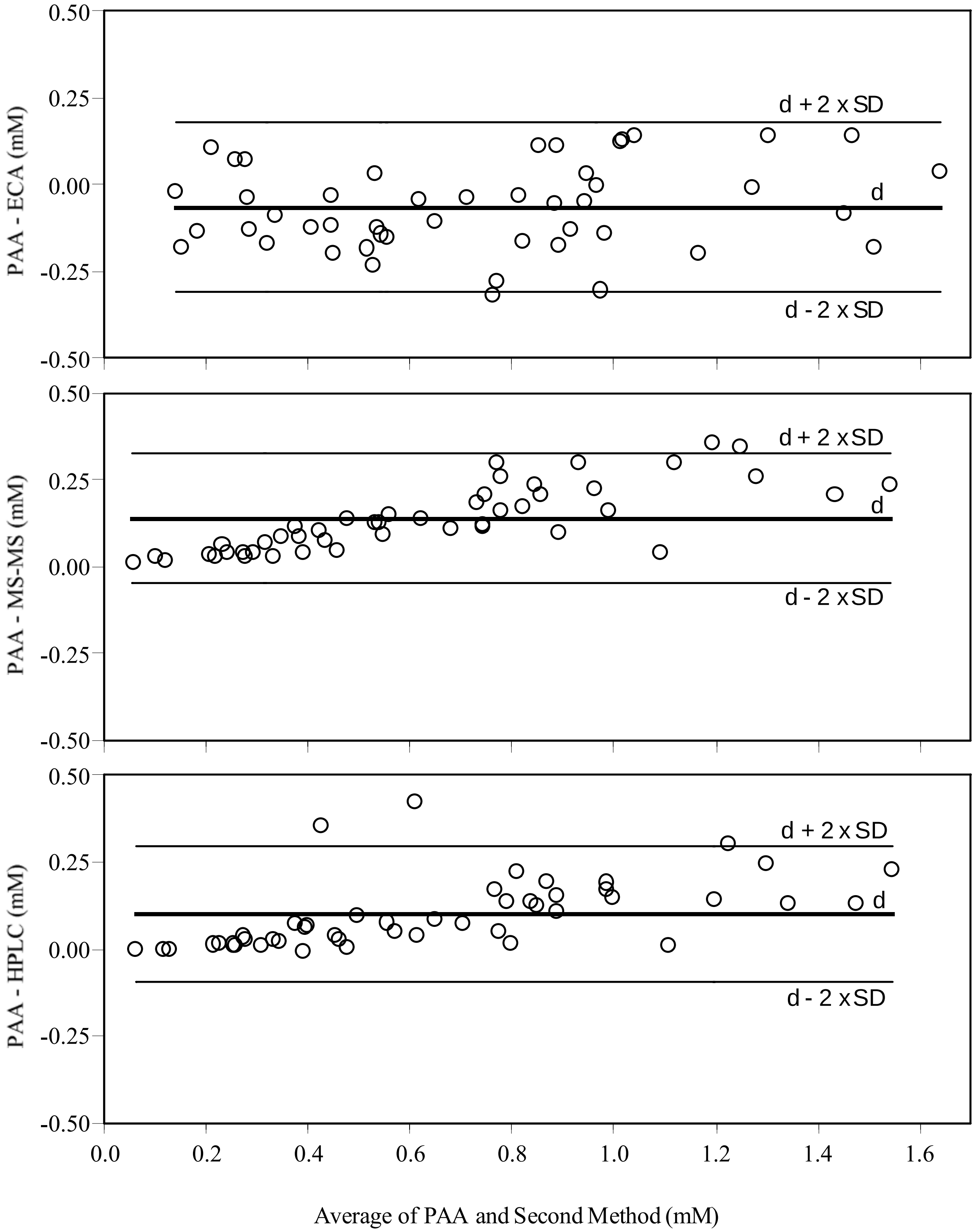

Figure 3 - 6. Bias plots of HPLC-, MS/MS-, ECA- measured L-Phe values as compared to PAA data.

Towards Home-Monitoring of L-Phe for PKU Patients:

A home-monitoring device for PKU patients would likely entail a multi-layer format, where the first layer filters out blood cells from the sample, the next layer contains immobilized ECA reagents, which enable spectrophotometric detection of plasma L-Phe concentration. Initial studies showed that ECA components function as expected when immobilized. A typical reagent mixture was prepared as described in the MATERIALS AND METHODS section, a solution of L-Phe (buffered at pH 8.6) added to the dry ECA mixture buffered at pH 7.0 and ΔA_{510} monitored. Figure 3 - 7 shows a calibration curve, based on preliminary results, for a broad L-Phe concentration range.

The effects of pH, presence of gelatin, Tritonr X detergent and MTS/PMS ratio were investigated via a spectrophotometric assay as documented in Table 3 - 7. It was found that the presence of 0.0005 g/ml detergent or lower PMS concentration had no statistically significant effect on the results of ECA at pH 8.6 in the absence of gelatin with 0.1 and 0.6 mM L-Phe. On the other hand, ΔA_{490} decreased when the composition of buffer was varied such that the final pH of the ECA in the presence of gelatin was 7.0 instead of 7.5.

Preliminary experiments have been carried out to make multi-layer films comprising ECA (ECA reagents in a gelatin matrix), filtering / reflecting (TiO_2 particles of various sizes embedded in a cellulose acetate binder) and spreading layers (diatomaceous earth in a cellulose acetate binder) on a glass or PET solid support. Several methodologies have been employed to prepare these layers: manual application with Gardco Wire-Wound rods and Bird Type applicators, solvent casting and spin coating.

In the case of ECA films, manual application with Gardco rods did not produce uniform films; however the appropriate thickness (low μm range) was obtained. On the other hand, spin coating via a two-step spin speed deposition technique produced more uniform, but very thin, ECA films of less than 50 nm in thickness. Both of these film

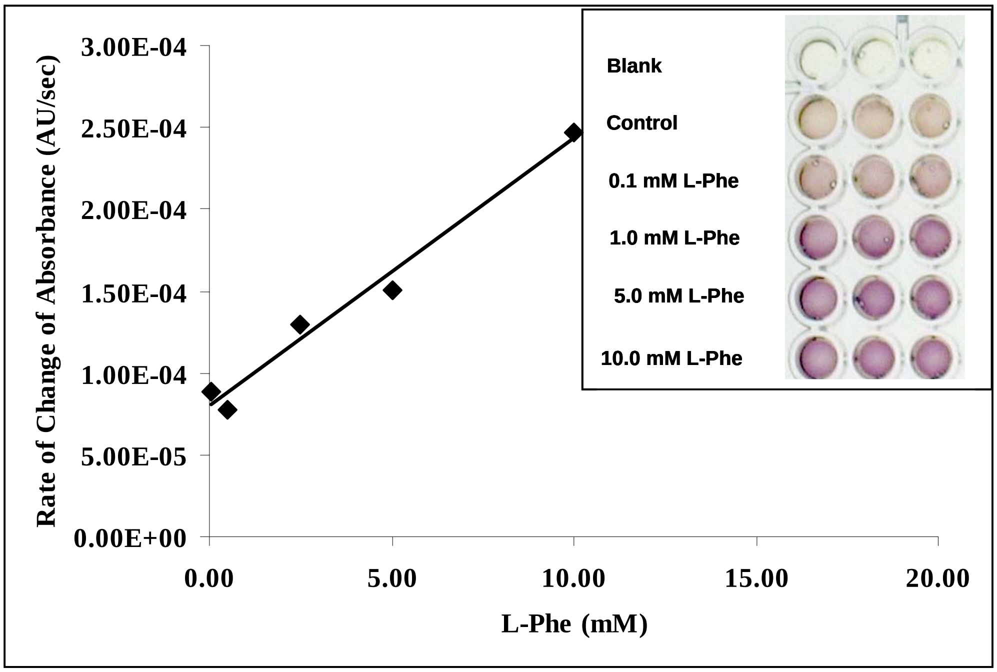

Figure 3 - 7. A calibration curve for 0 to 10 mM L-Phe range obtained with immobilized ECA as described in the MATERIALS AND METHODS. The regression equation for the calibration curve is $y = 0.000016 \times x + 0.00008$ with $n = 5$ and $R^2 = 0.98$. Inset is a digital image of the microplate containing immobilized mixtures with only gelatin (blank), all reagents and no PAD (control) and all ECA components with 0 to 10 mM L-Phe (rows 3 to 6).

Table 3 - 7: Investigation of Immobilized ECA

	pH 8.6 No Gelatin 0.4 mM MTS 0.2 mM PMS 0.375 mM NAD^+ 0.15 U/ml PAD	pH 8.6 No Gelatin 0.4 mM MTS **0.05 mM PMS** 0.375 mM NAD^+ 0.15 U/ml PAD	pH 8.6 No Gelatin 0.4 mM MTS 0.2 mM PMS 0.375 mM NAD^+ 0.15 U/ml PAD **0.0005 g/ml Tritonr X**	**pH 7.5** **0.11 mg/μl Gel** 0.4 mM MTS 0.2 mM PMS 0.375 mM NAD^+ 0.15 U/ml PAD	**pH 7.0** **0.11 mg/μl Gel** 0.4 mM MTS 0.2 mM PMS 0.375 mM NAD^+ 0.15 U/ml PAD
ΔA_{490} 0.1 mM L-Phe	0.0019	0.0017	0.0016	-	-
ΔA_{490} 0.6 mM L-Phe	0.0052	0.0055	0.0053	0.0015	0.00083

preparation methods inherently waste ECA reagents. Some ECA reagents (such as MTS) have limited solubility in aqueous buffer at very high concentrations, and the Ocean Optics instrumentation used for reflectance measurements within the ECA layer has limited detection capabilities, hence the requirement for thicker ECA films. Such thicker films were made by solvent casting, where a detectable signal could be measured with the Ocean Optics portable equipment in the presence of the analyte. Optimal films were made with 350 μl of ECA mixture as described in the MATERIALS AND METHODS.

In the case of filtering / reflecting layers (FRL) made by manual application, the best films were produced when 1.2 g of TiO_2 (particle size range of under 5 μm) was suspended 3 % (v/v) binder and applied onto the ECA layer with a 8 mil Bird applicator. The films made in this manner weren't analyzed by optical microscopy and the thickness could not be measured with a micrometer gauge due to the sensitivity of this layer to metal contact.

Spin-coating methodology was next used to make FRL films, where the optimal TiO_2 particle size, the time and extent of stirring of the FRL mixture, the presence of Tritonr X detergent and various spin coating methods (varied spin speeds, time of deposition, the number of steps in method and the number of depositions) were investigated in relation to the quality of the films produced. Although greater degree of uniformity was obtained with spin coating vs. manual application, the desired thickness of FRL films wasn't achieved via spin coating, and the porosity of the layer was non-uniform. The pore size on some of the best films produced using TiO_2 of 200 nm particle size, standard acceleration and a single deposition method with a spin speed of 2000 or 3000 rpm for 1 minute still had pore sizes of more than 10 μm, which means that this layer would not be capable of filtering out blood cells. Film characterization (pore size and thickness) was carried out on the Tencor Alpha-Step Profilometer and an Optical Microscopy instrument. Further optimization of FRL films produced by spin coating is required.

Spreading layer (SL) films were primarily made using the 8 mil Bird applicator rod and an extensive investigation to make such layers by either spin coating or solvent casting method was not carried out.

Preliminary experiments to investigate that these 2 or 3 layer films can detect 0.5 to 20 mM L-Phe have been carried out, but the results obtained were not easily reproducible, primarily due to issues related to the non-uniformity of the films. Figure 3 - 8 shows that a 3-layer film prepared by manual application functions as expected, when a 10 μl drop of 20 mM L-Phe (pH 8.6) was placed on the SL surface. However, the initial rate of change of absorbance is not linear.

The films made by solvent casting were next used in further investigations. The production of ECA films via solvent casting was successfully accomplished. On the other hand, FRL films made via solvent casting tended to peel and crack upon drying when poured over the ECA films made by the same methodology. The best results were obtained when 400 μl of 1.2 g of TiO_2 (30 nm particle size) suspended in 3 % (v/v) cellulose acetate (CA) was used to make the film and was subsequently air-dried. The most consistent and reproducible measurements were obtained when a polished Teflon surface was used in place of a FRL, since the latter still needs further optimization. Figure 3 - 9 shows that ECA layer made via solvent casting could detect a 1 mM L-Phe concentration (pH 8.6), as the initial rate of change of absorbance observed at 490 nm is higher than that observed for the same volume of pH 8.6 buffer. A calibration curve for a range of L-Phe concentrations could not be obtained under the given experimental conditions due to the low reproducibility associated with these experiments. The poor measurement to measurement reproducibility with the same ECA film could be attributed to low instrument sensitivity, uneven distribution of L-Phe over the surface of the film once covered with a Teflon surface and non-uniform thickness.

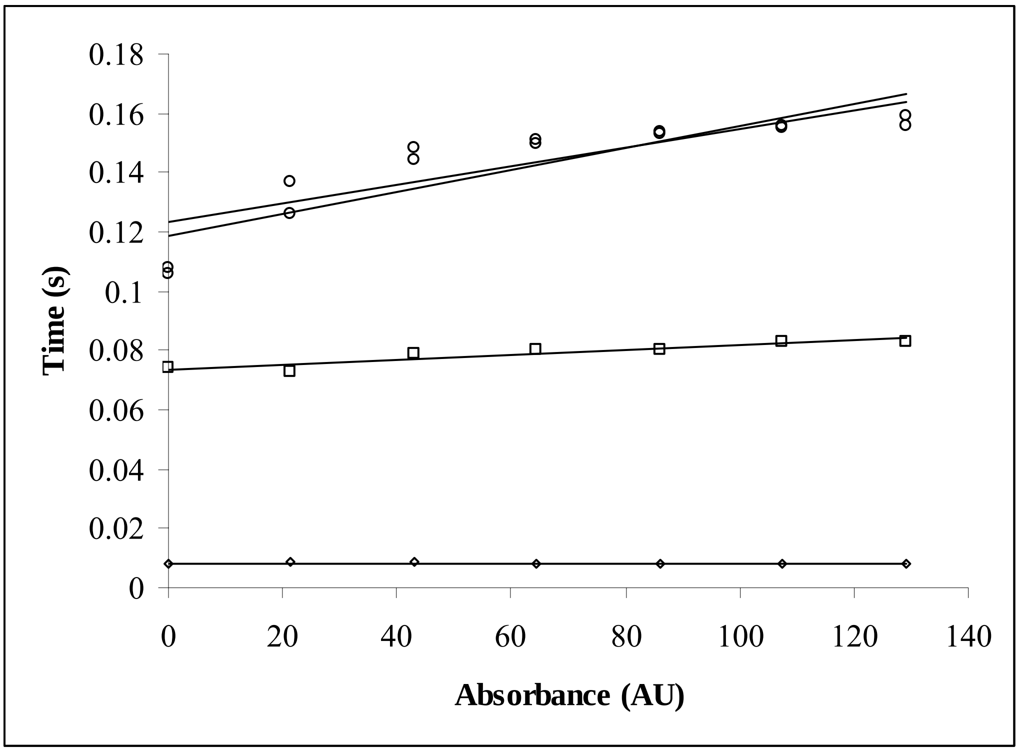

Figure 3 - 8. Change of Absorbance at 490 nm measured with the Ocean Optics spectrometer when a 10 µl drop of 20 mM L-Phe (pH 8.6) was placed on the surface of a 3-layer film, where ECA layer was made with a 40 mil Gardco applicator, and FRL and SL with a 8 mil Bird applicator as described in experiment 2. Lines marked with: ◊ represent data collected with Blank ECA/ FRL/ SL film; □ represent data collected with control ECA/ FRL/ and SL film and ○ represent data collected with reaction ECA/ FRL/ SL film.

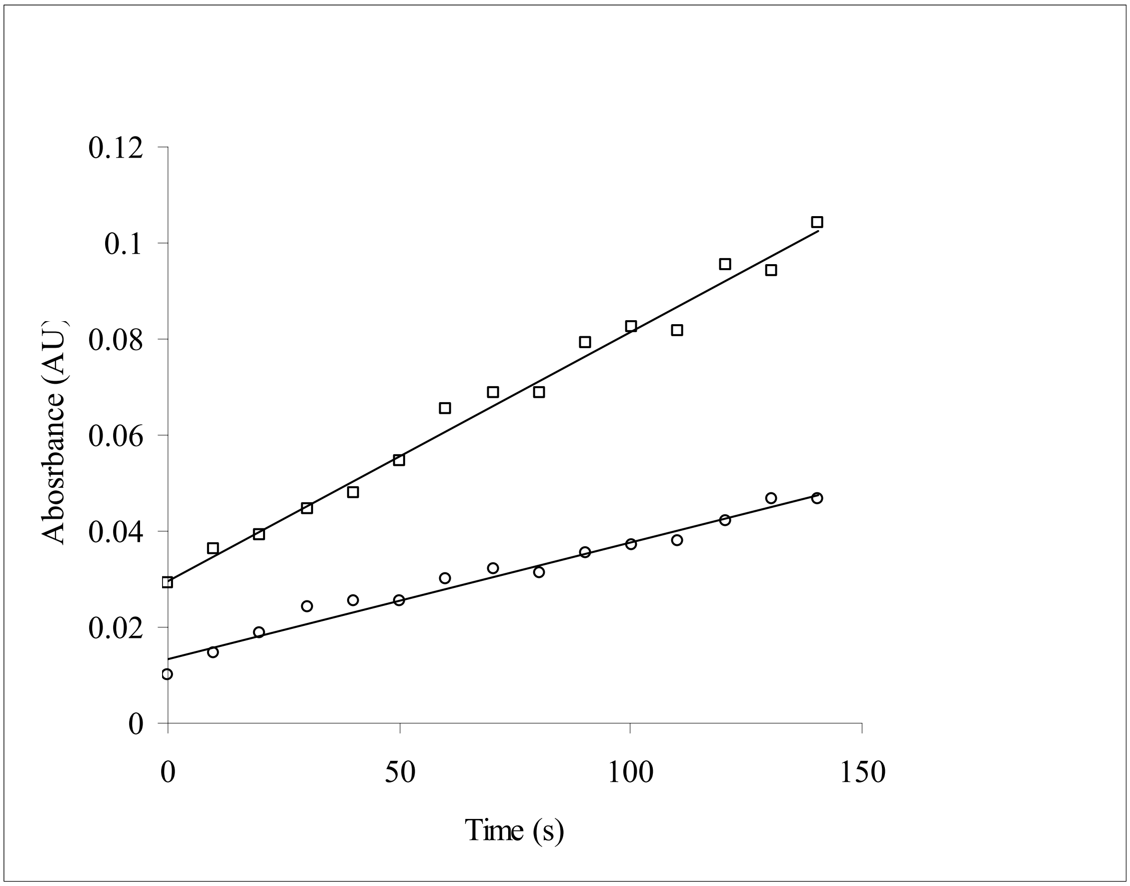

Figure 3 - 9. Change of Absorbance at 490 nm measured with the Ocean Optics spectrometer when a 10 μl drop of 1 mM L-Phe (pH 8.6) represented by □ or 10 μl drop of pH 8.6 buffer represented by ○ was placed on the surface of an ECA film prepared by solvent casting as described in experiment 3. A polished Teflon surface was used as the reflecting surface.

3 – 5: DISCUSSION

The generally accepted goal of treatment for PKU is normalization of L-Phe and L-Tyr plasma levels and thus prevention of the severe symptoms associated with PKU. Blood L-Phe levels in newborns should be brought within normal levels 3 weeks after their birth, hence the requirement for PKU neonatal screening (10). If left untreated, the accumulation of high plasma L-Phe concentrations causes disruptions in protein metabolism and impaired brain development and function in PKU patients. The direct cause of the severe symptoms associated with PKU is unknown but major contributing factors are: AA imbalance; elevated plasma and tissue L-Phe; transport inhibition of AAs across the blood brain barrier; white matter abnormalities; delays in the development of cerebral cortex; and interference with myelination (11, 52).

The frequency of monitoring plasma L-Phe concentrations in PKU patients of different age groups varies from state to state in USA. Plasma L-Phe level is measured once a week in patients less than 1 year of age, once a month during adolescence and 6 months to a year in adults (10). Women with a PAH deficiency must be careful to bring L-Phe levels under 0.3 mM during conception and gestation (53, 54). Abnormalities that result from fetal exposure to elevated maternal plasma L-Phe concentrations include congenital heart disease, intrauterine and postnatal growth retardation, microcephaly and mental retardation (53, 54). The Maternal PKU Collaborative Study reports that even at maternal plasma L-Phe concentrations of 0.12 to 0.36 mM, 6 % of infants are born with microcephaly and 4 % with postnatal growth retardation (54). If maternal plasma L-Phe concentrations are higher than 0.9 mM, the risk increases to 85 % for microcephaly, 51 % for postnatal growth retardation and 26 % for intrauterine growth retardation.

Currently, the most common approach used to keep L-Phe levels under control in PKU patients is the use of modified protein products, which provide required amounts of L-Phe and L-Tyr (55). The response to dietary therapy is monitored via measurement of plasma L-Phe concentrations to ensure the efficacy of the diet. Recent recommendations by NIH specify that dietary restriction should be continued and monitored indefinitely (10). Studies have shown that adults who have abandoned L-Phe-restricted diets tend to have reduced attention span and slow information processing abilities and motor reaction time (10). Tetrahydrobiopterin monotherapy is used as an experimental dietary approach that has shown much promise in patients with certain mutations in PAH gene, who exhibit a mild to moderate PKU phenotype, the treatment has often resulted in a progressive relief or withdrawal from the Phe restricted diet of treated subjects (56-59). Another experimental approach for treatment of PKU is gene therapy, where an epidermal transduced skin patch is used to handle the excess L-Phe in blood plasma (60, 61). Phenylalanine ammonia lyase (PAL) treatment, where by L-Phe is enzymatically degraded to harmless metabolites such as ammonia and trans-cinnamic acid, the latter of which is excreted in urine as hippurate, is yet another alternative to lower L–Phe plasma levels in PKU patients, (62).

The ECA developed in our laboratory is based on coupling the enzymatic oxidation of L-Phe to phenylpyruvate with a tetrazolium dye reduction to a formazan product via an electron mediator PMS and the cofactor NAD^+. As opposed to previous work on ECAs, our assay uses MTS that produces a water-soluble formazan product. Previous investigators have used INT or MTT, which upon oxidation yield formazan products not readily soluble in aqueous media (21, 22, 24, 27).

A second advantage of our methodology is that much less sample preparation is required than in previously developed ECAs. For example, DBS samples had to be eluted and / or deproteinized with H_2O / alcohol or trichloroacetic acid (TCA) / perchloric acid (PCA) / SSA for an extensive period prior to measuring L-Phe level in the sample (22, 24, 25, 27, 28, 29, 31, 32). Similarly, plasma samples were deproteinized prior to use in other ECAs (21, 23, 26, 30). In the procedures described here, the sample preparation is limited to removal of blood cells via centrifugation, and material losses resulting from extensive analyte manipulation are therefore minimized. In addition, for

DBS specimens, analyte recovery depends on blood hematocrit, blood spot size and preparation, duration of elution and elution conditions, filter paper type and the portion of filter paper used in analysis, thus further complicating the determination of L-Phe in comparison with the direct measurement of plasma L-Phe (50, 51). Furthermore, quantitation of AAs from biological matrices without derivatization is advantageous because it eliminates the need for extra reagents and minimizes analysis errors introduced by derivative stability, side reactions, yield issues and reagent interference. It should be noted that some of the previously developed ECAs required pre-equilibration of the L-Phe-containing sample with the enzyme / cofactor mixture for approximately 30 minutes prior to addition of other ECA reagents as shown in Table 3 - 1. The assay methodology described in this chapter does not require a pre-equilibration step prior to spectrophotometric measurement.

Our ECA-measured L-Phe concentrations were compared with PAA-measured values obtained with the same but deproteinized plasma samples collected pre- and post-'PKU' camp. A Pearson correlation coefficient of 0.956 was obtained. Similar Pearson correlation coefficients of 0.976 and 0.988, respectively, were obtained when L-Phe values measured by PAA were compared with those determined by HPLC and MS/MS analyses carried out on derivatized DBS eluates.

The agreement between PAA and ECA or HPLC or MS/MS was further investigated using Bland and Altman plots. PAA-measured L-Phe concentrations are on average 0.065 mM lower than ECA-measured values, which could be due to losses incurred during the deproteinization procedure. PAA-measured L-Phe concentrations are on average 0.14 mM and 0.10 mM higher than values obtained by MS/MS and HPLC, respectively, which may be a result of analyte losses incurred during elution and derivatization of DBS eluates. Fifty seven percent of the L-Phe measurements exhibit differences below 0.14 mM and 0.1 mM, respectively, when MS/MS and HPLC results were compared with PAA data in the 0 to 0.8 mM L-Phe concentration range. A similar trend was not observed when ECA results were compared with PAA measurements, which indicates a greater consistency of ECA in its ability to measure plasma L-Phe regardless of the concentration range. It should be noted that the majority of measured L-Phe differences lie within the $d \pm 2 \times SD$ range of the bias plots.

Considering the current consensus in the literature regarding the need for monitoring L-Phe concentration in plasma of PKU patients over their entire life spans, the necessity for a robust and efficient home-monitoring methodology is quite evident. The need for ongoing monitoring of plasma L-Phe levels is underscored by the measurements carried out in this study, which show the overall mean L-Phe concentration amongst participants at the beginning of "PKU camp" is 0.92 mM, which is higher than it should be. At the end of camp the average L-Phe concentration was reduced by approximately 0.29 mM. Hence PKU patients would derive a significant benefit from a methodology, which would enable them to measure plasma L-Phe levels at home. Convenient monitoring on a day-to-day basis would provide a correlation of diet and body chemistry of PKU patients, which could increase the patient's understanding of the condition and improves his or her motivation for effective dietary management of PKU.

In summary, we report here ECA-determined L-Phe concentrations are indeed comparable to PAA-measured values for a broad range of plasma L-Phe levels, based on Pearson correlation coefficient of 0.951 and the Bland and Altman analysis. Preliminary studies have also been carried to investigate the feasibility of making multi-layer films for L-Phe quantitation. Thus far, the ECA reagents were shown to function in an immobilized format in a gelatin matrix and a linear response could be obtained for a 0 to 10 mM L-Phe range. The preparation and formulation of FRL and SL films still requires further effort before they could be used in the multi-layer format of the home-monitoring device.

3 – 6: References

1. Scriver CR, Kaufman S. (2001) The hyperphenylalaninemias. In: Scriver CR, Beaudet AL, Sly SW, Valle D (eds) Childs B, Kinzler KW, Vogelstein B (assoc eds) The Metabolic and Molecular Bases of Inherited Disease, 8 ed. McGraw-Hill, New York, Ch. 77.

2. Erlandsen H, Patch MG, Gamez A, Straub M, Stevens RC. Structural studies on phenylalanine hydroxylase and implications toward understanding and treating phenylketonuria. Pediatr 2003;112:1557-65.

3. Erlandsen H, Fusetti F, Martinez A, Hough F, Flatmark T. Crystal structure of the catalytic domain of human phenylalanine hydroxylase reveals the structural basis for phenylketonuria. Nat Struc Biol 1997;4:995-1000.

4. Erlandsen H, Bjorgo E, Flatmark T, Stevens CR. Crystal structure and site-specific mutagenesis of pterin-bound human phenylalanine hydroxylase. Biochem 2000;39:2208-17.

5. Fitzpatrick PF. (2000) The aromatic amino acid hydroxylases. In: Purich (ed) Advances in enzymology, v 74. Interscience Publishers, New York, 235-94.

6. Anderson OA, Flatmark T, Hough E. (2002) Crystal structure of ternary complex of the catalytic domain of human phenylalanine hydroxylase with tetrahydrobiopterin and 3-(2-thienyl)-L-alanine, and its implications for the mechanism of catalysis and substrate activation. J Mol Biol; 320:1095-108.

7. Waters PJ. How PAH gene mutations cause hyper-phenylalaninemia and why mechanism matters: insights from in vitro expression. Human Mutation 2003;21:357-69.

8. Scriver CR, Clow, LL. Phenylketonuria: epitome of human biochemical genetics. N Engl J Med 1998;303:1336.

9. Scriver CR. Whatever happened to phenylketonuria? Clin Biochem 1995;28:137-144.

10. National Institutes of Health Consensus Development Panel. National Institutes of Health Consensus Development Conference Statement: phenylketonuria: screening and management. Pediatr. 2000;108:972-82.

11. Surtees R, Blau N. The neurochemistry of phenylketonuria. Eur J Pediatr 2000;159:S109-13.

12. Pietz J, Kreis R, Rupp A, Mayatepek E, Rating D, Boesch C, Bremer HJ. Large neutral amino acids block phenylalanine transport into brain tissue in patients with phenylketonuria. J Clin Invest 1999;103:1169-78.

13. Moller HE, Ullrich K, Weglage J. In vivo proton magnetic resonance spectroscopy in phenylketonuria. Eur J. Pediatr 2000;159:S121-5.

14. Guthrie R, Susi A. A simple phenylalanine method for detecting phenylketonuria in large populations of newborn infants. Pediatric 1963;32:338-43.

15. McCaman NW, Robins E. Fluorometric method for determination of phenylalanine in serum. J Lab Clin Med 1962;59:885-90.

16. Rivero A, Allué JA, Grijalba A, Palacios M, Merlo SG. Comparison of two different methods for measurement of phenylalanine in dried blood spots. Clin Chem Lab Med 2000;38:773-6.

17. Slocum RH, Cummings JG. Amino acid analysis of physiological samples. In: Hommes FA, ed. Techniques in diagnostic human biochemical genetics. New York: Wiley-Liss, 1991:87-126.

18. Ceglarek U, Muller P, Stach B, Buhrdel P, Joachim T, Kiess W. Validation of the phenylalanine/tyrosine ratio determined by tandem mass spectrometry: sensitive newborn screening for phenylketonuria. Clin Chem Lab Med 2002;40:693-7.

19. Chace DH, Millington DS, Terada N, Kahler SG, Roe CR, Hofman LF. Rapid diagnosis of phenylketonuria by quantitative analysis for phenylalanine and tyrosine in neonatal blood spots by tandem mass spectrometry. Clin Chem 1993;39:66-71.

20. Dale Y, Mackey V, Mushi R, Nyanda A, Maleque M, Ike J. Simultaneous measurement of phenylalanine and tyrosine in phenylketonuric plasma and dried blood by high-performance liquid chromatography. J Chromat B 2003;788:1-8.

21. Wendel U, Hummel W, Langenbeck U. Monitoring of phenylketonuria: A colorimetric method for the determination of plasma phenylalanine using L-phenylalanine dehydrogenase. Anal Biochem 1989;180:91-4.

22. Wendel U, Koppelkamm M, Hummel W, Sander J, Langenbeck U. A new approach to the newborn screening for hyperphenylalaninemia: use of L-phenylalanine dehydrogenase and microtiter plates. Clin Chim Acta 1990;192:165-70.

23. Wendel U, Koppelkamm M, Hummell W. Enzymatic phenylalanine estimation for the management of patients with phenylketonuria. Clin Chim Acta 1991;201:95-8.

24. Dooley KC. Enzymatic method for phenylketonuria screening using phenylalanine dehydrogenase. Clin Biochem 1992;25:271-5.

25. Taylor RP, Smith IC, Standing SJ. Rapid automated enzymatic measurement of phenylalanine in plasma and blood spots. Clin Chim Acta 1993;218:207-14.

26. Villaseca MA, Farre C, Ramon F. Phenylalanine determined in plasma with use of phenylalanine dehydrogenase and a centrifugal analyzer. Clin Chem 1993;39:129-31.

27. Campbell RS, Hollifield RD, Varsani H, Milligan TP, Brearly G, Price CP. Development of an enzyme-mediated assay for phenylalanine in blood spots. Ann Clin Biochem 1994;31:140-6.

28. Keffler S, Denmeade R, Green A. Neonatal screening for phenylketonuria: evaluation of an automated enzymatic method. Ann Clin Biochem 1994;31:134-9.

29. Randall EW, Lehotay DC. An automated enzymatic method on the Roche COBAS MIRA S for monitoring phenylalanine in dried blood spots of patients with phenylketonuria. Clin Biochem 1996;29:133-8.

30. Fingerhut R, Stehn M, Kohlschutter A. Comparison of four different phenylalanine determination methods. Clin Chim Acta 1997;264:65-73.

32. Rivero A, Allue JA, Grijalba A, Palacios M, Merlo SG. Comparison of two different methods for measurement of phenylalanine in dried blood spots. Clin Chem Lab Med 2000;38:773-6.

34. Schulze A, Mayatepek E, Hoffmann GF. Evaluation of 6-year application of the enzymatic colorimetric phenylalanine assay in the setting of neonatal screening for phenylketonuria. Clin Chim Acta 2002;317:27-37.

35. Huang T, Warsinke A, Kuwana T, Scheller FW. Determination of L-Phenylalanine based on an NADH-detecting sensor. Anal Chem 1998;74:991-7.

36. Schultz CL, Moini M. Analysis of underivatized amino acids and their D/L enantiomers by sheathless capillary electrophoresis/electrospray ionization-mass spectrometry. Anal Chem 2003;75:1508-13.

37. Qu J, Wang Y, Luo G, Wu Z, Yang C. Validation quantitation of underivatized amino acids in human blood samples by volatile ion-pair reversed phase liquid chromatography coupled to isotope dilution tandem mass spectrometry. Anal Chem 2002;74:2034-40.

38. Langenbeck U, Baum F, Mench-Hoinowski A, Luthe H. Predicting the phenylalanine blood concentration from urine analyses. An approach to noninvasive monitoring of patients with phenylketonuria. J Inherit Metab Dis 2005;28:855-61.

39. May, SW, Shunnarah, RD, Odlham, CD, DeSilva, V. World Patent Number 091376 (2004). Medical Device for Monitoring Blood Phenylalanine Levels.

40. Przybylowicz, EP, Millikan, AG. United States Number 3,992,158 (1976). Integral Analytical Element.

41. Asano Y, Nakazawa A, Endo K. Novel Phenylalanine Dehydrogenase from Sporosarcina ureae and Bacillus sphaericus. J Biol Chem 1987;262:10346-54.

42. Cohen SA, Michaud DP. Synthesis of a fluorescent derivatizing reagent, 6-aminoquinolyl-N-hydroxysuccinimidyl carbamate, and its application for the analysis of hydrolysate amino acids via high-performance liquid chromatography. Analyt Biochem 1993;211:279-87.

43. Vollmer DV, Jinks DC, Guthrie R. Isocratic reverse-phase liquid chromatography assay for amino acid metabolic disorders using eluates of dried blood spots. Analyt Biochem 1990;189:115-21.

44. Cohen SA, de Antonis KM. Applications of amino acid derivatization with 6-aminoquinlyl-N-hydroxysuccinimidyl carbamate. Analysis of feed grains, intravenous solutions and glycoproteins. J Chromat A 1994;661:25-34.

45. Rashed MS, Ozand PT, Bucknall MP Diagnosis of inborn errors of metabolism from blood spots by acylcarnitine and amino acids profiling using automated electrospray tandem mass spectroscopy. Pediat Res 1995;38:324-31.

46. Brenda, The Comprehensive Enzyme Information System. Retrieved on April 28, 2007, from http://www.brenda.uni koeln.de/php/result_flat.php4?ecno=1.4.1.20&organism.

47. Dobrucki JW, Bernas, T. The role of plasma membrane in bioreduction of two tetrazolium salts, MTT, and CTC. Arch Biochem Biophys 2000;380:108-16.

48. Tan AS, Berridge, MV. Superoxide produced by activated neutrophils efficiently reduces the tetrazolium salt, WST-1 to produce a soluble formazan: a simple colorimetric assay for measuring respiratory burst activation and for screening anti-inflammatory agents. J Immunol Meth 2000;238:59-68.

49. Debnam PM, Shearer G. Colorimetric Assay for Substrates of $NADP^+$-Dependent Dehydrogenases Based on Reduction of a Tetrazolium Dye to Its Soluble Formazan. Anal Biochem 1997;250:253-5.

50. Chace DH, Adam BW, Smith JS, Alexander RJ, Hillman SL, Hannon WH. Validation of accuracy-based amino acid reference materials in dried-blood spots by tandem mass spectrometry for newborn screening assays. Clin Chem 1999;45:1269-77.

51. Adam BW, Alexander JR, Smith SJ, Chace DH, Loeber JG, Elvers LH et al. Recoveries of phenylalanine from two sets of dried-blood spot reference materials: prediction from hematocrit, spot volume, and paper matrix. Clin Chem 2000; 46:126-8.

52. Moller HE, Ullrich K, Weglage J. In vivo proton magnetic resonance spectroscopy in phenylketonuria. Eur J Pediatr 2000;159:S121-5.

53. Koch R, Hanley W, Levy H, Matalon R, Rouse B, Trefz F et al. Maternal Phenylketonuria: An International Study. Mol Gen Met 2000;71:233-9.

54. Jardim LB, Palma-Dias R, Silva LC, Ashton-Prolla P, Giugliani R. Maternal hyperphenylalaninemia as a cause of microcephaly and mental retardation. Acta Peadiatr 1996;85:943-6.

55. MacDonald A. Diet and compliance in phenylketonuria. Eur J Pediatr 2000;159:S136-41.

56. Perez-Duenas B, Vilaseca MA, Mas A, Lambruschini N, Artuch R, Gomez L, et al. Tetrahydrobiopterin responsiveness in patients with phenylketonuria. Clin Biochem 2004;37:1083-90.

57. Muntau AC, Roschinger W, Habich M, Demmelmair H, Hoffmann B, Sommerhoff CP, Roscher AA. Tetrahydrobiopterin as an alternative treatment for mild phenylketonuria. N Engl J Med 2002;347:2122-32.

58. Weglage J, Grenzebach M, von Teeffelen-Heithoff A, Marquardt T, Feldmann R, Denecke J et al. Tetrahydrobiopterin responsiveness in a large series of phenylketonuria patients. J Inherit Metab Dis 2002;25:321-2.

59. Matalon RKR, Michaels-Matalon K, Moseley K, Surendran K, Tyring S, Erlandsen E et al. Biopterin responsive phenylalanine hydroxylase deficiency. Genet Med 2004;6:27-32.

60. Christensen R, Kolvraa S, Blaese RM, Jensen TG. Development of a skin-based metabolic sink for phenylalanine by over expression of phenylalanine hydroxylase and GTP cyclohydrase in primary human keratinocytes. Gene Ther 2000;7:1971-8.

61. Christensen R, Guttler F, Jensen TG. Comparison of epidermal keratinocytes and dermal fibroblasts as potential target cells for somatic gene therapy of phenylketonuria. Mol Genet Metab 2000;76:313-8.

62. Sarkissian CN, Shao Z, Blain F, Peevers R, Su H, Heft R, Chang TMS et al. A different approach to treatment of phenylketonuria: phenylalanine degradation with recombinant phenylalanine ammonia lyase. Proc Natl Acad Sci USA 1999;96:2339-44.